An optimality principle governing human walking

Gustavo Arechavaleta-Servin

École Doctorale Systèmes

Thèse

pour obtenir le grade de

Docteur de l'Université de Toulouse

délivré par l'Institut National des Sciences Appliquées de Toulouse

Spécialité: Systèmes Informatiques

An optimality principle governing human walking

Gustavo Arechavaleta Servin

Préparée au Laboratoire d'Analyse et d'Architecture des Systèmes
sous la direction de M. Jean-Paul Laumond

Jury

Mme. Tamar Flash	Rapporteur
M. Thierry Pozzo	Rapporteur
M. Alain Berthoz	Examinateur
M. Michel Courdesses	Examinateur
M. Jean-Paul Laumond	Directeur de Thèse

Abstract

This work seeks to analyze human walking at the trajectory planning level from an optimal control perspective. Our approach emphasizes the close relationship between the geometric shape of human locomotion in goal-directed movements and the simplified kinematic model of a wheeled mobile robot. This kind of system has been extensively studied in robotics community. From a kinematic perspective, the characteristic of this wheeled robot is the *nonholonomic* constraint of the wheels on the floor, which forces the vehicle to move tangentially to its main axis. In the case of human walking, the observation indicates that the direction of the motion is given by the direction of the body (due to some anatomical, mechanical body constraints...). This coupling between the direction θ and the position (x,y) of the body can be summarized by $tan\theta = \frac{\dot{y}}{\dot{x}}$. It is known that this differential equation defines a non integrable 2-dimensional distribution in the 3-dimensional manifold $R^2 \times S^1$ gathering all the configurations (x,y,θ). The controls of a vehicle are usually the linear velocity (via the accelerator and the brake) and the angular velocity (via the steering wheel). The first question addressed in this study can be roughly formulated as : where is the "steering wheel" of the human body located ? It appears that the torso can be considered as a kind of a steering wheel that steers the human body. This model has been validated on a database of 1,560 trajectories recorded from seven subjects.

In the second part we address the following question : among all possible trajectories reaching a given position and direction, the subject has chosen one. Why ? The central idea to understand the shape of trajectories has been to relate this problem to an optimal control scheme : the trajectory is chosen according to some optimization principle. The subjects being viewed as a controlled system, we tried to identify several criteria that could be optimized. Is it the time to perform the trajectory ? the length of the path ? the minimum jerk along the path ?... We argue that the time derivative of the curvature of the locomotor trajectories is minimized. We show that the human locomotor trajectories are well approximated by the geodesics of a differential system minimizing the L_2 norm of the control. Such geodesics are made of arcs of clothoids. The clothoid is a curve whose curvature grows with the distance from the origin. The accuracy of the model is supported by the fact that 90 percent of trajectories are approximated with an average error < 10cm.

In the last part of this work we provide the partition of the 3-dimensional configuration space in cells : 2 points belong to a same cell if and only if they are reachable from the origin by a path of the same type. Such a decomposition is known as the synthesis of the optimal control problem. Most of the time when the target changes slightly the optimal trajectories change slightly. However, some singularities appear at some critical frontiers between cells. It is noticeable that they correspond to the strategy change for the walking subjects. This fundamental result is another poof of the locomotion model we have proposed.

Acknowledgements

Fist of all, I would like to express a deep sense of gratitude to Jean-Paul Laumond, my advisor for the past four years, for allowing me to taste the rigor of science as well as for the wonderful conversations we had during succulent meals at his residence. Thank you for your unending patience and wise counsel. I would like to thank Prof. Alain Berthoz, Halim Hicheur, Quang-Cuong Pham and Anh Troung with whom this thesis has been a collaboration.

I would like to thank Prof. Michel Courdesses, Philippe Soueres, Florent Lamiraux, Wael Suleiman and Efrain Lopez-Damian for tolerating my all too many math questions. I have benefited greatly from the advice and humor of my office-mates Claudia, Thierry, Olivier and recently Aurelie. I also thank the RIA and more specially Gepetto's people for the nice discussions and support materials. My gratitude goes to the directors of the LAAS-CNRS, Malik Ghallab, and Raja Chatila for giving me the opportunity for my graduate studies. Also, and very importantly, to Conacyt for their financial support during my graduate studies in Toulouse, France.

I would like to thank Prof. Tamar Flash and Prof. Thierry Pozzo for the review of this thesis. Their comments and suggestions have inestimable value for me.

I would like to thank Claudia and Jose-Miguel for their valiant effort in proof-reading this thesis. Thank you Thierry for the French and tennis tutoring. I would like to thank too many friends : America, Berenice, Miguel, Luis, Akin, Nacho, Jib, DeChivolosTamales.com, among others, for the nice moments and discussions about everything and nothing...

Finally, I also want to deeply thank all my family for their support and for visiting Maggie and I from the other side of the Atlantic Ocean. Thank you mama, Miriam, Arnold, Mariana, Tia Ana, Mickey, Emilio, Sra Chela, Monica, Alex and Pedro.

This thesis is dedicated to Maggie, my beloved wife, in recognition for her tremendous help, patience, and encouragement during these foundational years of our lives that I will never forget.

Table des matières

1 Introduction

The study of sensorimotor control in biological systems has been a major source of inspiration in the always improving quest to better design autonomous machines. This has led roboticists to expand enormously their interaction with the life science community over the last decades. As a result, many exciting developments and novel applications have arisen from the humanoid, the biomedical, and the biomechatronics research areas (among others). Roboticist's traditional emphasis has been on applying the principles underlying complex behaviours of biological systems to implement sophisticated robotic interfaces. On the flip side, neuroscientists are interested in the tools emerging from the computational approach developed by roboticists to formalize the knowledge acquired by experimentation in terms of mathematical models. As a consequence of this neurophysiological perspective, appropriate experimental protocols must be defined to exhibit the behaviour under study. In much the same way, the motivation of the work presented here aims to apply a computational approach in the area of movement neuroscience (for a review, see [Wolpert and Ghahramani 2000]).

The pioneer work of Bernstein to identify the strategies of biological motor control (or control law), suppose a categorization of control models [Bernstein 1967]. The first class of models focuses on open-loop control which plan and execute the motion, ignoring the role of sensory feedback information. The second class of models focuses on closed-loop control to predict and correct deviations away from the current motion execution by online sensory feedback. In addition to what has been stated, and following the Bernstein's approach, different motor levels of description must be taken into account to accomplish a motor task (even in simple tasks like arm motion between two different spatial positions) : dimensionality (the number of degrees of freedom of the mechanism), redundancy, and the apparently existence of an infinite number of solutions. This has motivated the experimental study of motor patterns in order to find motor invariants in the generation of biological movements. Consequently, many theories of motor

FIG. 1.1 – *Step trace. Photograph by Marey (1830 - 1940). Copyright : Cinémathèque française*

commands are based on optimal control perspective : find a natural optimal performance, like energy consumption, to predict averaged body or limbs' trajectories.

1.1 Problem statement

The walking of people in the snow or in the sand leave traces (see Figure 1.1). The placement of a body on a 2-dimensional space requires three parameters : two for the position of the body and one for its direction (with respect to a given frame of the world). The trace left by the walking of a man is made of the history of the various *positions* he traversed. It is printed in a 2-dimensional space. The information about the *direction* of the body seems a priori missing. However it can be logically deduced by considering that the direction of the body at a given instant of the trajectory is the direction tangent to the trace at the corresponding *position*. Looking at the trace derivative of the body position gives the body direction. This is a consequence of the fact the man is walking forward. Such a coupling between position (x,y) and direction θ is a differential coupling defined by

$$\dot{y}\cos\theta - \dot{x}\sin\theta = 0 \tag{1.1}$$

This means that the tangent vectors at any point of an admissible trajectory necessary belongs to a 2-dimensional vector space spanned by the vector fields :

$$\begin{pmatrix} \cos\theta \\ \sin\theta \\ 0 \end{pmatrix} \text{and} \begin{pmatrix} 0 \\ 0 \\ 1 \end{pmatrix} \tag{1.2}$$

In that vector space, sideway steps are not allowed. The *control space* of the human walking is 2-dimensional. However it is a well-known fact that the man can walk everywhere he wants ! Its *reachable space* is 3-dimensional. The differential equation 1.1 is not integrable. The corresponding system is not holonomic : a *nonholonomic* system is a system whose reachable space dimension is strictly greater than its control space dimension. The underlying hypothesis is that the simple differential Equation 1.1 contains enough information to build a human locomotion model. This means that such a model can be derived from a top-down approach, by exclusively looking at the shape of locomotor trajectories and by ignoring all the body biomechanical motor controls generating the motions.

The goal of this work is to find the underlying locomotion principle explaining the shape of locomotor trajectories. Let us state the problem in more accurate manner.

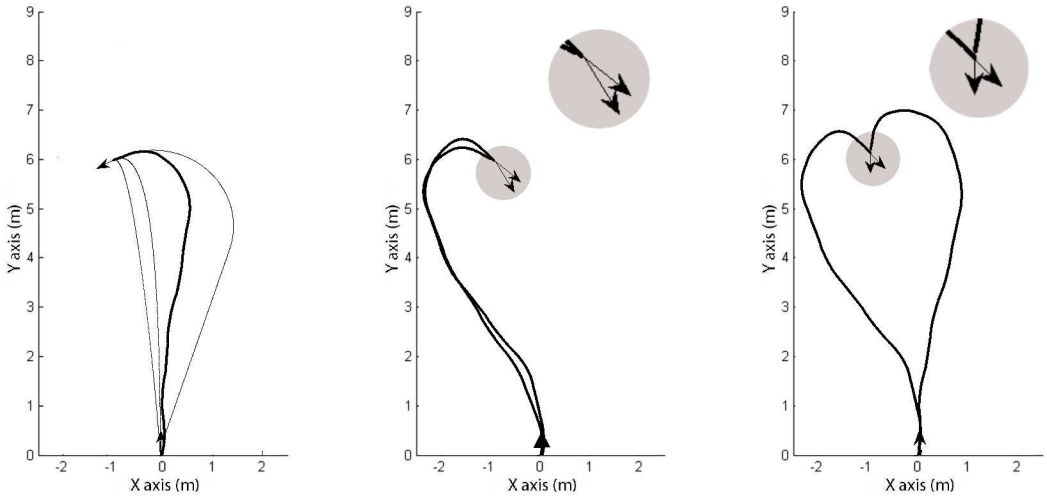

(a) (b) (c)

FIG. 1.2 – *(a) among four "possible" trajectories reaching the same goal, the subject has chosen the bold one. Why ? (b) and (c) show some examples of real trajectories with the same final position. The final directions are almost the same. (b) a subject performed two very close trajectories. (c) the same subject performed two completely different trajectories. How to explain this strategy change ?*

Ask somebody to enter a large empty room by a door and to leave it by another one. The resulting motion is an intentional motion motivated by a well defined goal. A lot of trajectories solve possibly the task. The subject will choose one of them. Why that one instead of all the other possible ones (see Figure 1.2.a) ? Would anybody else choose the same trajectory ? If we change a little bit the position and the direction of the goal, how is the initial trajectory reshaped ? How is this reshaping smooth ? For instance, let us consider the real study cases illustrated in Figures 1.2.b and 1.2.c. In both figures both goals are at the same position. Their respective directions differ by a small margin. In the case of Figure 1.2.b a subject has chosen two very close trajectories. In the case of Figure 1.2.c the same subject has chosen two completely different strategies. How to explain this strategy change ?

In this document we address all these questions via the study of a single optimal control problem :

1. We show that the human locomotion trajectories are well approximated by the trajectories of a nonholonomic system optimizing the derivative of the curvature. Such trajectories are piecewise made of elementary clothoid arcs.
2. We provide an optimal control synthesis (i.e. a complete description of all the finite possible sequences of such elementary arcs). Such sequences may be phrased as, for instance, "Start turning left while increasing the curvature during time τ_1, then decrease the curvature during time τ_2 and finally increase the curvature during time τ_3". These combinations generate "words" that account for the locomotion strategy used by the subjects according to the placement of the 3-dimensional goal.

1.2 Contributions of this work

This work is mainly and above all, a multidisciplinary research effort between robotics and neuroscience domains. The collaboration benefits from the sharing of common investigation tools such as optimal control theory.

Our work is devoted to analyze the steering of human locomotion at the trajectory planning level. As a consequence of this neurophysiological perspective, an appropriate experimental protocol has been defined. We have implemented an original protocol to record intentional trajectories generated by seven subjects in an empty room. We then performed a statistical analysis to validate that human locomotor trajectories contain stereotyped properties in terms of both path geometry and velocity profiles. These results suggest that common planning strategies govern the formation of locomotor trajectories in goal-directed tasks.

The existence of stereotyped behaviors validates the second stage of our study, which represents the first contribution of our work : the consideration of the differential coupling between the position and the direction of the human body while walking.

Such coupling is the underlying hypothesis to propose a nonholonomic system accounting for human forward locomotion. Nonholonomy is a concept from mechanics that has been very fruitful in mobile robotics in the past twenty years. As a consequence, we made use of available techniques for steering nonholonomic wheeled robots.

The next stage of the study, which represents the second contribution of our work, has been the application of optimal control methods to understand the shape of human locomotor trajectories. We made several hypothesis to finally find a model together with a cost function that approximates the walking trajectories. To characterize their geometric shapes, we made use of analytical and numerical optimal control approaches for nonlinear systems. We argue that walking trajectories are made of pieces of clothoid arcs.

The last stage of our study, which represents the global contribution of our work, has been to provide the numerical synthesis of the proposed control model. In other words, we computed the partition of the system reachable space (3-dimensional) according to the sequences of the concatenation of clothoid arcs. The objective of the numerical synthesis is to determine the motion patterns of human walking by a family of words.

1.3 Document organization

The structure of this document is as follows :

In Chapter 2 we present a general overview of computational movement neuroscience from an optimal control perspective, which serve as basis of this work. We describe some techniques to deal with the optimal steering of nonholonomic systems.

In Chapter 3 we present the experimental protocol as well as the statistical analysis we performed to show that general principles govern the motion strategy. This statistical study confirms the validity of the subsequent parts of our study.

Chapter 4 depicts the modeling of the human forward locomotion and the study of the choice of the body frame accounting for the nonholonomic hypothesis.

Having a control model of human locomotion, we describe in Chapter 5 the strategy for explaining the geometric shape of walking trajectories by means of optimal control tools. This part of our work illustrates mainly our strategy to compute the optimal trajectories of the control model according to a given cost function.

The aim of Chapter 6 is the numerical computation of the synthesis of the human forward locomotion. This part of our study describes a numerical algorithm to find the families of trajectories according to words. In particular we explored singular situations known as cut-locus in SubRiemannian geometry appearing in the human locomotion strategy.

Chapter 7 concludes and gives various comments of ongoing research.

1.4 Publications

The following publications are associated to this thesis :

1. ARECHAVALETA, G., LAUMOND, J.-P., HICHEUR, H., AND BERTHOZ, A. The nonholonomic nature of human locomotion. *To appear in Autonomous Robots*. Short version appeared in *Proceedings of the IEEE/RAS-EMBS International Conference on Biomedical Robotics and Biomechatronics*. Pisa, Italy, 2006.
2. ARECHAVALETA, G., LAUMOND, J.-P., HICHEUR, H., AND BERTHOZ, A. An optimality principle governing human walking trajectories. *To appear in IEEE Transactions on Robotics*. Short version appeared in *Proceedings of the IEEE/RAS International Conference on Humanoid Robots*. Genoa, Italy, 2006.
3. LAUMOND, J.-P., ARECHAVALETA, G., TRUONG, T.-V.-A., HICHEUR, H., PHAM, Q.-C., AND BERTHOZ, A. 2007. The words of the human locomotion. *In 13th International Symposium of Robotics Research*. Hiroshima, Japan.
4. HICHEUR, H., PHAM, Q.-C., ARECHAVALETA, G., LAUMOND, J.-P., AND BERTHOZ, A. 2007. The formation of trajectories during goal-oriented locomotion in humans I. *In European Journal of Neuroscience, vol. 26*.
5. PHAM, Q.-C., HICHEUR, H., ARECHAVALETA, G., LAUMOND, J.-P., AND BERTHOZ, A. 2007. The formation of trajectories during goal-oriented locomotion in humans II. *In European Journal of Neuroscience, vol. 26*.

Note : during my PhD, work has been done on digital actors animation. For coherence purpose this work is not included in this document.

1. ARECHAVALETA, G., ESTEVES, C., AND LAUMOND, J.-P. 2004. Planning fine motions for a digital factotum. In *Proceedings of the IEEE/RSJ International Conference on Intelligent Robots and Systems*. Sendai, Japan, 822-827.

2. ESTEVES, C., ARECHAVALETA, G., AND LAUMOND, J.-P. 2005. Motion planning for human-robot interaction in manipulation tasks. In *Proceedings of IEEE International Conference on on Mechatronics and Automation*. Niagara Falls, Canada, 1766-1771.

3. FERRÉ, E., LAUMOND, J.-P., ARECHAVALETA, G., AND ESTEVES, C. 2005. Progresses in assembly path planning. In *Proceedings of International Conference on Product Lifecycle Management*. Lyon, France, 373-382.

4. LAUMOND, J.-P., FERRÉ, E., ARECHAVALETA, G., AND ESTEVES, C. 2005. Mechanical part assembly planning with virtual mannequins. In *Proceedings of IEEE International Symposium on Assembly and Task Planning*. Montréal, Canada.

5. ESTEVES, C., ARECHAVALETA, G., PETTRÉ, J., AND LAUMOND, J.-P. 2006. Animation planning for virtual characters cooperation. *ACM Transaction on Graphics (TOG) 25, 2* (April), 319-339.

2

Walking versus rolling

This chapter aims to provide an overview of the available optimal control approaches for modeling the behavior of the human motor system as well as the behavior of wheeled robots. We first comment, in Section 2.1, an interesting set of problems of computational motor control. The computational approach allows to relate some common research issues between robotics and neuroscience communities such as redundancy (see Section 2.2) and motion patterns (see Section 2.3). In Section 2.4, we discuss the interest of applying optimal control algorithms to the understanding of voluntary movements. These techniques are able to treat the formation of the hand (see Section 2.5) and locomotor (see Section 2.6) trajectories. The optimal motions of a wheeled robot are computed by the same kind of methods. As explained in Section 1.1, the human walking may be affected by nonholonomic constraints. Indeed, wheeled robot's determining characteristic lies in its nonholonomic constraint. In Section 2.7 we explain two important notions of control theory related to mobile robotics (i.e. controllability and nonholonomy). In Section 2.8, we comment the implications of these notions for planning optimal motions of wheeled robots. The application of these tools to mobile robotics is the starting point of our study on the human forward locomotion modeling by means of an optimal control approach. The last objective of this chapter is to introduce the analytical (see Section 2.9) and the numerical (see Section 2.10) optimal control methods used in this work.

2.1 Introduction : computational motor control

The current state of our biological motor system arises as a consequence of adaptation of our species throughout evolutionary history. It seems likely that long before our ancestors owned the attributes for sophisticated cognition, language, or abstract reasoning, they performed motor tasks with respect to

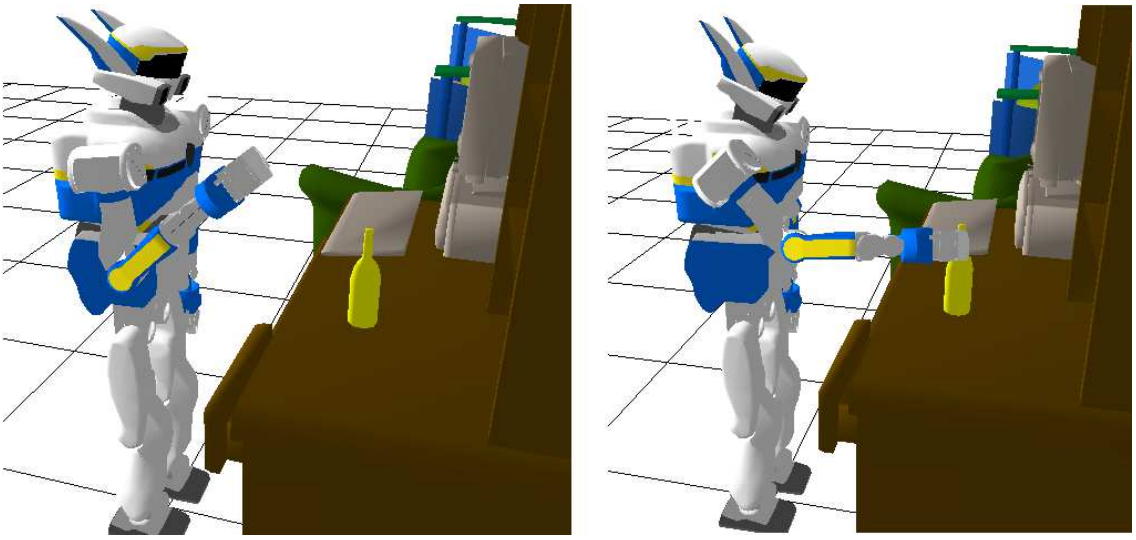

FIG. 2.1 – *The robot perceive its environment by using its sensory devices. The sensory data contributes to formulate motor plans. The robot uses the plans as a basis for performing the sequence of actions to achieve the motor task.*

places and objects in the physical world.

The human motor system is mainly composed of peripheral and central parts. The first part includes muscles and sensory nerve fibers among others. The interaction of those muscles generates biomechanical events leading to movement. The second part includes the central nervous system and a wide variety of components. For instance, the spinal cord includes the proprioceptive system and central pattern generators for rhythmic movements as well as those components involved in walking and running. It is undeniable that the various components of the human motor system work together as an integrated neural network. However, the understanding of the complex and sophisticated integrative motor activities remain partially unknown. The following sections are not intended to survey the major components of the central nervous system and their interaction (for a review see [Wise and Shadmehr 2002]). Rather than describing the components of the human motor system, we discuss the interest of the computational motor control approaches to the understanding of voluntary movements.

Motor functions are closely related to sensory and motor information. The sensory signals and motor commands could adopt a variety of forms and may refer to different levels of organization : from cellular to behavioral and cognitive levels [Grillner et al. 2005]. The central nervous system has to manage the respective processes allowing motor and sensory data to be related [Wolpert 1997].

In robotics we find similar problems relating sensory and motor information in order to give the robots some degree of autonomy. Autonomy means that robots have to decide a sequence of actions to accomplish motor tasks within the same physical world [Chatila 1995]. For this purpose, a robot must be capable to perceive its environment by using its sensory devices. The sensory data contributes to formulate motor plans. The plans are then used as a basis for performing the desired actions, which include everyday actions such as changing its current posture to reach and grasp a glass of water (see Figure 2.1).

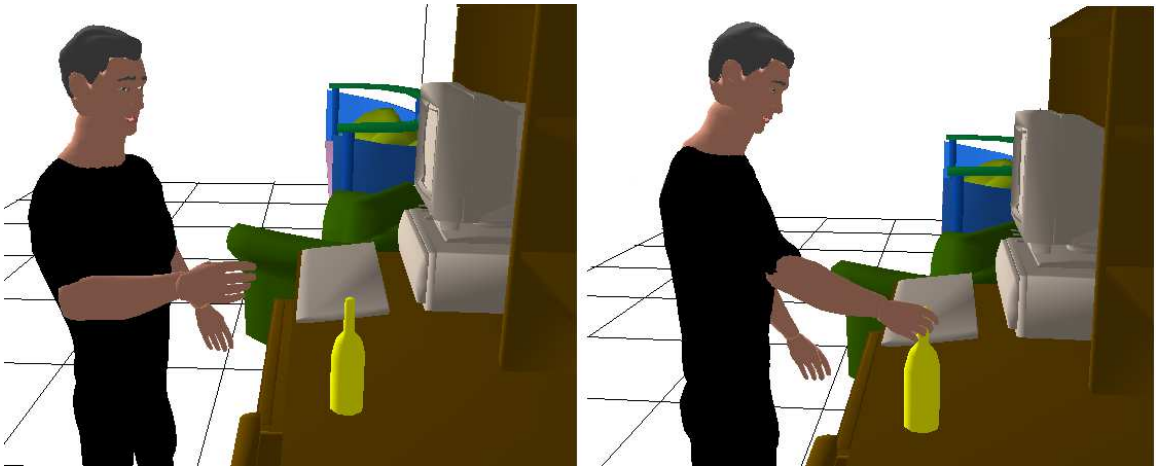

FIG. 2.2 – *After [Wolpert 1997], the human motor system uses an inverse model to generate the required muscle activation patterns according to the acquired sensory data regardless of the sensory feedback. The spatial features of the target allow the computation of the sequence of actions in the task space. During the movement execution, the human motor system uses a forward dynamic model to predict locally how the system will behave ignoring the delay of the sensory signals. Then, a forward sensory model is needed to reduce the uncertainty both in sensory and motor data relative to the movement execution.*

In computational movement neuroscience, the main stages of the sensorimotor loop are known as *internal models* : *the inverse model*, *the forward dynamic model* and *the forward sensory model*. A key distinction between the robotic and the human motor system is the restricted access to the state variables. The notion of *internal model* refers to the assumption that the state of the human motor system is not directly measurable. Thus, the state estimation is done by tracking the behavior of the system inputs and outputs (see Figure 2.2).

The *inverse models* generate the required muscle activation patterns according to the acquired sensory data regardless of the sensory feedback [Kawato et al. 1987]. This means that the spatial features of the target allow the computation of the sequence of actions in the task space. These models suppose that the set of muscle activations that drives the controlled system to a given target is computed in advance. The solution of this problem is called an *inverse dynamic problem* (see [Hollerbach and Flash 1982]). Then, the motion is performed by applying the sequence of motor commands until the movement is completed without any kind of feedback. Consequently, these models are related to the open-loop control scheme.

The aim of the *forward dynamic models* is the prediction of how the system will behave knowing the current input and its dynamics. In other words, it compute an estimate of the near future state of the system as output. At each instant of time, a sensory signal provides the information about the current state of the system. Then, the estimated state can be compared to the target location and in the case of discrepancies an error signal is used to correct the behavior of the controlled system. Thus, this type of models are related to closed-loop control scheme. However, as these type of models do not take into consideration the delay of the sensory signals, the prediction is not very accurate. For instance, a prediction of the current arm's posture can be obtained from vision and proprioceptive information but as there is some delay and noise in the signal that reaches the central nervous system (see [Bays and Wolpert 2007]), the prediction won't be accurate.

In order to close the sensorimotor loop, a *forward sensory model* is needed to reduce the uncertainty both in sensory and motor data relative to the movement execution. However, a non-sensory feedback can be considered by the fact that the current state of the controlled system is obtained through a *forward model* integrating efferent and afferent signals without delay (see [Wolpert 1995])[1]. The underlying idea of the *forward models* is that the nervous system progressively learns to estimate the behavior of the motor plan for a given command.

The interpretation of the above three considered *internal models* is not fully accepted in the motor control community. Some researchers point out that contrary to the *internal forward model* concept, what is usually called *inverse model* should be skipped [Todorov 2004]. One of the main reasons is that the borders between open and closed loop control notions are still debated : one could be contained within the other as a special case. For instance, in [Desmurget and Grafton 2000] the authors propose an hybrid model for goal-directed movements in which both control schemes are integrated as a single control process. First, an inverse model is used to plan the whole motion from the initial to the final states. Then, a sensory feedback loop is performed near to the final location in order to correct the possible errors between the current and the final states.

Moreover, there exist other sensorimotor paradigms such as the equilibrium point approach [Bizzi et al. 1992; Feldman and Latash 2005], the synergetics theory applied to motor coordination [Haken et al. 1985; Kelso 1997] and the more recent adaptive control approach [Schaal and Schweighofer 2005] validated in [Schaal et al. 2004].

For these reasons, it is not surprising to find that the main research topics of computational sensorimotor control such as planning, control, and learning share some mathematical tools that have been extensively used in Robotics[2]. These include dynamical system theory, differential geometry, optimal control theory, kalman filter, bayesian theory, among others. This chapter is focused on some of the common tools from optimal control.

2.2 Motor redundancy

As it has been already stated by Bernstein [Bernstein 1967], the number of degrees of freedom that compose the human body is closely related to the complexity of motor coordination.

A redundant system can be viewed as a mapping from a control space with dimension q onto a task space with dimension n, with $n < q$. Such a mapping is not one-to-one. As a consequence performing a given task can be done by an infinite number of trajectories. In robotics, it is a well known practice to benefit from the system redundancy to optimize some criteria (see for instance [Siciliano and Slotine 1991; Khatib 1987; Yoshikawa 1984] and for an overview see [Nakamura 1991]).

The human body is a highly redundant system. For most tasks (e.g., walking, grasping) we get $n << q$. Since pioneering works like those of Bernstein [Bernstein 1967] we know that the central nervous system does not explore the entire q-dimensional manifold each time a task has to be performed. For

[1] The efference concept means the totality of motor impulses necessary for a movement, and whenever the efference is produced it leaves an image of itself somewhere in the central nervous system. This image is called the efference copy.

[2] We should keep in mind that in robotics we develop control models to build autonomous robots while in computational motor control we develop control models to understand the biological motor systems.

instance, when we are walking the rhythmic motions of the arm follow the same rhythmic motions of the legs. Such synchronization of motions reduces the dimension of the motor space to be explored. Humans learn by discovering motion patterns that reduce the dimension of the motor space. They tend to build a control space with lower dimensions than their motor space (see [Berthoz 1997], 149-166). The challenge of modern computational neuroscience is to propose control space models that can be generic enough to account for large classes of tasks [Jordan and Wolpert 1999; Wolpert and Ghahramani 2000; Todorov and Jordan 2002; Guigon et al. 2007]. Among the developed approaches, differentail geometry (e.g., [Flash and Handzel 2007]) and optimal control (e.g., [Todorov 2004; Jordan and Wolpert 1999]) play today a central role in such researches. The study we present in this work gives another lighting of the optimal control interest different from one dealing with redundant systems.

2.3 Motor invariants

Even though the human body is highly redundant, the execution of motor tasks have invariant features. The existence of motor invariants has been reported in many experimental studies related to arm movements [Morasso 1981; Abend et al. 1982; Lacquaniti et al. 1983; Bullock and Grossberg 1988; Flash and Handzel 2007] and human locomotion [Vieilledent et al. 2001; Hicheur et al. 2005; Hicheur et al. 2007]. These studies suggest that the nervous system choice a common motor pattern among an infinite number of motor solutions. Actually, there exist experimental evidences on the study of the spinal cord of frogs and rats suggesting a vocabulary of a finite number of *motor primitives* (e.g., [Mussa-Ivaldi and Bizzi 2000]). The *motor primitives* represent words. Thus, it is of great interest to understand how the central nervous system combines the repertoire of words to generate complex movements.

The research efforts to provide some elements of the underlying nature of motor patterns can be classified in two general categories [Wolpert 1997]. The first one accounts for kinematics, in particular the relationship between the relative position of limb segments with respect to the target, the position and direction of end effectors relative to each limb segment and the successive derivatives of those quantities [Flash and Hogan 1985; Pham et al. 2007]. The second one accounts for dynamics that include forces, torques and moments in order to produce motor commands [Uno et al. 1989]. The fundamental element linking both categories is the optimization theory [Pontryagin et al. 1964] : the motor control is based on optimal principles [Todorov 2004]. In other words, the desired movements are optimal movements that maximize or minimize a cost function. The cost function may take the form of effort, smoothness, accuracy, duration,... [Nelson 1983].

To understand the motor control strategies, the human arm trajectory formation has been studied extensively. Nevertheless, human locomotion also represents an active area of study involving different research domains like neurophysiology, biomechanics, and robotics.

2.4 Optimal control in movement neuroscience

This section concentrates on the computational view point of voluntary control of two types of movements : forelimb reaching and locomotion. Voluntary movements translate tasks into plans. To

implement those plans the patterns of force are needed. In contrast to these type of movements, there exist innate behaviors and reflex responses. All of them are controlled by the motor system. Reflexes and voluntary movements are closely related. However, there are studies suggesting that reflexes play only an indirect role in voluntary actions.

Generally stated, the motor system permits the selection of movements from a large variety of learned skills by generating a motor plan and coordinating the forces needed to achieve a given target.

Different hypotheses, like the maximization of the smoothness [Flash and Hogan 1985; Todorov and Jordan 1998], have been used for characterizing the production of motor behavior. In [Viviani and Flash 1995] the authors proposed a modified minimum jerk model accounting for the *"power law"*. The studies on the known *"power law"* were previously introduced in [Lacquaniti et al. 1983] for drawing and hand-writing movements. On elliptical pre-defined locomotor paths the same principle [Vieilledent et al. 2001] has been validated. This law states that the velocity varies in proportion to the one-third power of the radius of curvature. However, in [Viviani and Cenzato 1985] it is showed that, for hand movements, the power law locally varies according to the geometric shape of the path. The authors suggested the existence of a segmentation strategy for the movement generation (i.e. the path geometry is composed by a sequence of elementary units). Then, in [Richardson and Flash 2002] is suggested that the hypothesis of the segmented control in the central nervous system given by the piecewise constant gain factor previously proposed in [Viviani and Cenzato 1985] cannot provide sufficient evidence. This is because the segmentation features can be extracted from the geometric shape of the path. Moreover, it has been demonstrated that the *"one-third power law"* does not describe such relationship for more complex pre-defined locomotor paths [Hicheur et al. 2005]. Nevertheless, this principle has been successful and widely accepted as an important invariant for some classes of trajectories even if no physical reason relating speed and curvature exists. Moreover, other studies suggest that the power law seems to be a by-product of a more complex behavior. For instance, in [Todorov and Jordan 1998] is argued that the power law is a consequence of an underlying motor strategy to generate smooth trajectories. In [Schaal and Sternad 2000] is suggested that the power law is a by-product of smooth trajectories that not necessary implies a fundamental principle in motor planning (e.g., by applying a strong enough low-pass filter the power law emerges). In [Gribble and Ostry 1996] is suggested that biomechanics contributes significantly to the emergence of the power law. The explanation in [Flash and Handzel 1996; Pollick and Sapiro 1997] is that the power law is a consequence of the constant affine velocity.

The minimum torque-change model [Uno et al. 1989] is also a smoothness optimization principle in which dynamics is involved. This model predicts also straight line hand trajectories that correspond to the hand trajectories observed experimentally. The minimum variance model has been proposed for both eye and arm movements [Harris and Wolpert 1998]. This model suggests that the neural control signal is corrupted by noise. The predicted velocity profiles of eye and arm trajectories account for the speed-accuracy compromise stated by the Fitts' law [Fitts 1954].

Recently an optimization approach based on stochastic optimal feedback control has been proposed [Todorov and Jordan 2002]. This approach attempts to relate motor coordination, motor planning and sensory uncertainty as a unified framework for sensorimotor control. This approach is based on three important assumptions. First, the hypothesis of the signal-dependent noise in the motor system. Second,

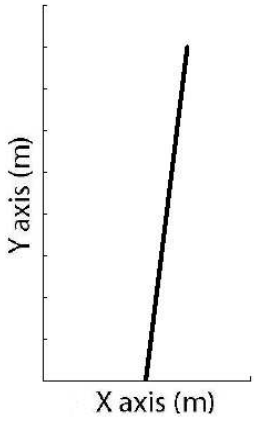

FIG. 2.3 – *Optimizing the jerk between two given positions on the plane, the predicted path is a straight line segment.*

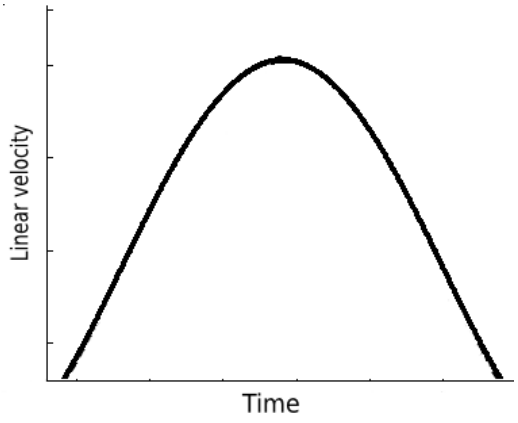

FIG. 2.4 – *The velocity profile has a bell-shape when minimizing the jerk cost function for planar movements.*

the state of the system is only observable by means of delayed and noisy sensors. Third, an effort penalty term associated to the task.

Most recent is the computational motor control model proposed in [Guigon et al. 2007]. This model is mainly focused on the kinematic redundancy of the arm. The authors suggest that four principles govern the human motor control. First, the separation principle which states that dynamic and static forces in goal-directed movements are computed separately by the motor system. Elasticity and gravity are labeled as static forces while inertial and velocity-dependent are classified as dynamic forces. Second, the model assumes the existence of an optimal controller dedicated for dynamic forces based on an optimal feedback control (the current implementation of the model omits the static controller and the state estimator). Third, it supposes that the movement is performed by minimizing the control effort. This criterion depends on the circumstances to perform a given task. Finally, the model stipulates a relationship between the duration of the movement and the required effort to execute the movement.

Even if these models capture many aspects of observed hand trajectories and the minimum variance model also predicts eye trajectories, they have not been applied, in our knowledge, for locomotor planning (see [Arechavaleta et al. 2006b; Pham et al. 2007]).

2.5 Hand movements

A wide range of experimental studies on the formation of arm trajectories show that the hand moves smoothly with a symmetric velocity pattern. Moreover, it is surprising that even if the kinematic structure of the arm is composed by rotational joints, the end-effector follows a straight line path (see Figure 2.3) and a bell-shape velocity profile (see Figure 2.4). This observation suggests that the movement of the forelimb segments depends primarily on the computation of the hand kinematics in the task space. In [Flash and Hogan 1985] the authors proposed a model to predict such kind of hand motions. The underlying idea is to find the optimal trajectories of a point (x, y) by minimizing the following squared jerk cost

$$J = \int_0^T \left(\left(\frac{d^3x}{dt^3} \right)^2 + \left(\frac{d^3y}{dt^3} \right)^2 \right) dt \tag{2.1}$$

where $\frac{d^3x}{dt^3}$ and $\frac{d^3y}{dt^3}$ represent the third-order derivatives of the position and T is the duration of the movement. Applying analytical methods the solution of this optimization problem is

$$\begin{aligned} x(t) &= a_5t^5 + a_4t^4 + a_3t^3 + a_2t^2 + a_1t + a_0 \\ y(t) &= b_5t^5 + b_4t^4 + b_3t^3 + b_2t^2 + b_1t + b_0 \end{aligned} \tag{2.2}$$

$x(t)$ and $y(t)$ are 5th-degree polynomials. This model assumes that an inverse kinematic algorithm exists to map the hand position to the appropriated joint angles.

It is shown in [Richardson and Flash 2002] that the minimum jerk cost function is a particular version of the minimum squared derivative (MSD) principles expressed as

$$J = \int_0^T \left(\left(\frac{d^nx}{dt^n} \right)^2 + \left(\frac{d^ny}{dt^n} \right)^2 \right) dt \tag{2.3}$$

where n corresponds to nth-derivative of each coordinate. In [Richardson and Flash 2002] the authors point out that only $n = 3$ is in agreement with the experimental data.

Rather than the kinematic models of the arm, in [Uno et al. 1989] the authors suggest a different model accounting for dynamics of the forelimb movements. The proposed model minimizes the following cost function

$$J = \int_0^T \left(\left(\frac{d\tau_1}{dt} \right)^2 + \left(\frac{d\tau_2}{dt} \right)^2 \right) dt \tag{2.4}$$

where $\tau_1(t)$ and $\tau_2(t)$ are the torques applied to each rotational joint at instant t. The authors used a simplified model of the planar arm dynamics represented with a two degrees of freedom manipulator.

In addition to these smoothness maximization models, a different approach has been proposed in [Harris and Wolpert 1998] to predict successfully not only the hand but also the eye trajectories. The authors suggest that a stochastic component should be considered. The key feature of the minimum variance model is the assumption of the signal-dependent noise in the neural commands. This model attempts to explain the relationship between the variability and the accuracy of the movement relative to the final position.

An alternative optimization framework has been proposed in [Todorov and Jordan 2002]. The authors point out the importance of the optimal stochastic feedback control scheme to relate variability and redundancy in motor control. This approach has been validated for a linear model of the arm.

Finally, arm movements have been also predicted by the model proposed in [Guigon et al. 2007]. This model is based on the separation principle as well as the principles stated in [Todorov and Jordan 2002]. Contrary to the models presented above, this model uses more complicated kinematic structures of the arm. Indeed, the authors compute optimal point-to-point trajectories of two, four, and seven degrees of freedom arms.

In summary, based on optimization theory there exist different models and costs for achieving

the prediction of hand movements. In addition to the computational hand models, the important role and the representation of the gravitational force during drawing arm movements have been studied (see [Papaxanthis et al. 1998]). The authors suggest that gravity should not be only considered as a *mechanical* parameter in the motor plan but as a component represented by the central nervous system at different levels of the sensorimotor transformation in the whole motor process.

2.6 Goal-directed locomotion

Goal-directed locomotion has been investigated with respect to how different *sensory inputs* are dynamically integrated [Grillner et al. 2005]. This has facilitated the elaboration of locomotor commands that allow reaching a desired body position in space [Berthoz and Viaud-Delmon 1999]. Visual, vestibular and proprioceptive inputs have been analyzed during both normal and blindfolded locomotion to study how humans could continuously control their trajectories (see [Glasauer et al. 2002; Kennedy et al. 2003] and for a review, see [Hicheur et al. 2005]). The interaction between the relative motion of the head, the torso and the eyes has also been studied [Grasso et al. 1998]. The important role of the head reference frame for the steering of locomotion along curved paths is investigated in [Hicheur and Berthoz 2005]. Since the visual and vestibular systems are located at the level of the head which is directly linked with the neck's proprioceptive sensors, a top-down control of locomotion has been suggested and validated in various studies (see [Grasso et al. 1996; Pozzo et al. 1995; Pozzo et al. 1990]). These experimental studies emphasize that the head serves as an inertial guidance device for the steering of locomotion thanks to its stabilization and anticipatory mechanisms. In [Imai et al. 2000], the authors introduce a gravito-inertial acceleration (GIA) vector that represents the sum of linear accelerations acting on the head. The authors use this vector to characterize the interaction of the body, head and eyes along straight and curved paths. However, which principles govern the generation (or planning) of body trajectories has received little attention.

Recently the hypothesis that common principles govern the generation (or planning) of hand and whole body trajectories has been tested [Vieilledent et al. 2001; Hicheur et al. 2005]. In particular, a strong coupling between path geometry (curvature profile) and body kinematics (walking speed) is observed with some quantitative differences between two types of movements [Hicheur et al. 2005]. These experimental observations have been discussed within the framework of the simplifying control strategies that may govern the steering of locomotion in humans. However, these studies are limited to pre-defined paths. In our research, as we explain in Chapter 3, we investigate human forward locomotion in a less restrictive situation : only beginning and end are known, but not the path to reach the goal (see [Hicheur et al. 2007]).

Most recent is the study developed in [Pham et al. 2007] to test whether the family of smoothness maximization models MSD accounts not only for hand movements but also for human locomotion. The experimental protocol designed by the authors is detailed in the next chapter. *Grosso modo*, the task given to the subjects was "walking through a distant doorway" where the initial and final positions and directions were imposed and the initial and final velocities were greater than zero (see Figure 2.5). Within these circumstances, the authors show that only $n = 3$ (minimum jerk) and $n = 4$ (minimum snap) can

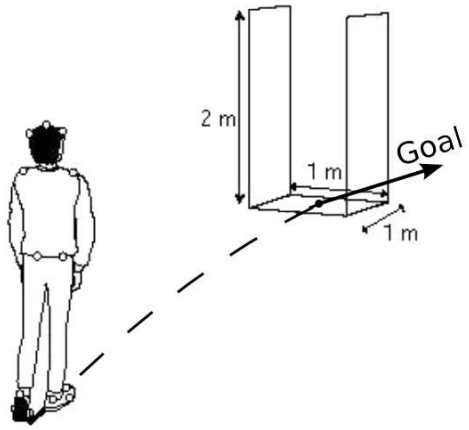

FIG. 2.5 – *The formation of trajectories during human goal-directed locomotion.*

predict locomotor trajectories. For paths with more complex geometric shapes than those used in [Pham et al. 2007], the minimum jerk cost function is also tested. The details and results are given in Chapter 5.

2.7 Some useful notions of control theory

In order to know whether a system is able to move for any pair of points in its state space, it is necessary to study the controllability properties of the control system. A precise statement of this concept is given in the first part of this section. Now, let us consider that the structure of the mechanism contains a kinematic constraint. The following question must be asked : Is the constraint integrable ? The second part of this section is devoted to provide the answer and its consequence. In particular, we are interested in control systems of the form

$$\dot{q} = B(q)u, \quad B(q) = g_1(q), ..., g_m(q) \tag{2.5}$$

where q of R^n which belongs to a manifold[3] M and $B(q) \in R^{n\times m}$ is a smooth m-dimensional distribution (i.e. at each point $q \in M$ the vectors' family $g_1(q), ..., g_m(q)$ generates a linear subspace $\triangle(q)$ on the tangent space T_qM). Each g on R^n represents a smooth map which assigns to each q of R^n a tangent vector $g(q) \in T_qM$. The distribution is said to be *regular* if the dimension of $\triangle(q)$ does not vary with q. This control system will serve as basis to introduce the notions of controllability and nonholonomy.

2.7.1 Controllability and existence of optimal trajectories

The notion of controllability of a control system means that any state q of M can be reached from any other one (see [Sussmann 1990; Laumond et al. 1998]). The Lie bracket of two vector fields is given by

[3] A manifold (resp. smooth manifold) is a topological space such that every point $q \in M$ has an open neighborhood homeomorphic (resp. diffeomorphic) to an open ball of R^n where n is the dimension of M

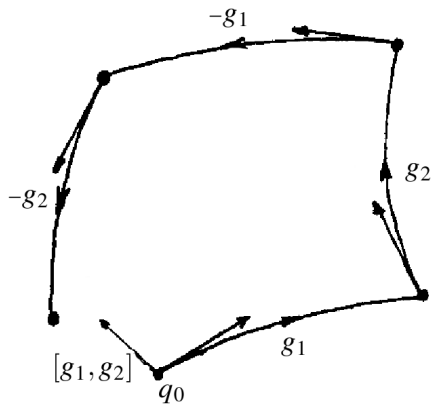

FIG. 2.6 – *A geometric representation of the Lie bracket. If we follow g_1 and then g_2, we do not get the same result as if we had followed g_2 and then g_1.*

$$[g_1,g_2] = \frac{\partial g_2}{\partial q} g_1 - \frac{\partial g_1}{\partial q} g_2 \tag{2.6}$$

The result of this differential operation gives another vector field $[g_1,g_2]$. If $[g_1,g_2] \neq 0$ then it means that g_1 and g_2 do not commute (see Figure 2.6). If $[g_1,g_2]$ is not a linear combination of $g_1(q),...,g_m(q)$ then $[g_1,g_2]$ represents a *new direction which the system can move*. The fundamental properties of the Lie bracket are the skew-symmetry and the Jacobi identity :

$$[g_1,g_2] = -[g_2,g_1] \quad \textit{and} \quad [[g_1,g_2],g_3] + [[g_2,g_3],g_1] + [[g_3,g_1],g_2] = 0 \tag{2.7}$$

The set of vector fields with the Lie bracket is a *Lie algebra* denoted by $LA(g_i)$. The *Lie algebra* of vector fields $g_1(q),...,g_m(q)$ plays an important role in the study of controllability properties of a system (i.e. all linear combinations of vector fields $g_1(q),...,g_m(q)$). By applying the lie algebra rank condition (LARC [Sussmann 1990]), it can be proved that the System 2.5 is controllable. Actually, it is controllable if the rank of the controllability lie algebra is n (i.e. the smallest lie algebra containing $g_1(q),...,g_m(q)$). More precisely, if $LA(g_i) = T_qM$ which implies that the dimension of $LA(g_i) = n$ then the System 2.5 accounts for the accessibility property (i.e. the set of all reachable states by a trajectory from q_0 in $\tau \leq T$). In addition, if the system is symmetric (i.e. every trajectory of the system followed backwards is also a trajectory) and M is connected then the system is said to be *completely controllable*.

Although the following chapters use this terminology, we do not intend to repeat the precise definitions detailed in [Sussmann 1990; Brockett 1976]. All we need to know here is that the existence of a trajectory between any two states involves the rank condition. Nevertheless, the existence of a trajectory does not mean that there exist *optimal* feasible trajectories given any two states. Ensuring the existence of an optimal solution is done by the Fillipov's existence theorems (see [Cesari 1983]). The following theorem is sufficient for our purpose :

Let q_0 and q_f be two points in M. The following hypothesis must be satisfied to ensure the

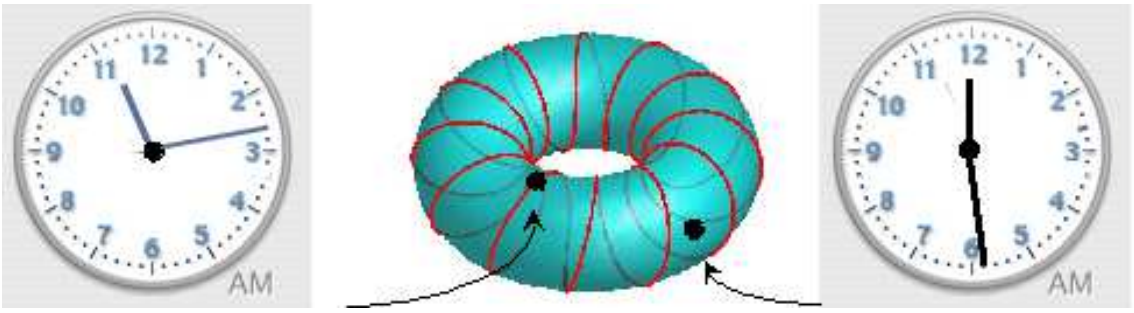

FIG. 2.7 – *The velocity of the long arrow is 12 times faster than the velocity of the small one. Such a coupling is clearly integrable. This means that the reachable space of both arrows is only 1-dimensional (the line on the torus). The time displayed by the watch of the left side corresponds to a point on the torus line. The "time" displayed by the watch on the right picture will never happen !*

existence of an optimal solution. (H_1) The vector fields g_i are locally Lipschitz. (H_2) The control set U is a compact convex subset of R^m. (H_3) There exists an admissible trajectory from q_0 to q_f. (H_4) The system is complete, in the sense that for every control function $u(.)$ and every initial condition $q_0 \in M$, there exists a trajectory which is defined in the whole interval $[\tau_0, \tau_1]$ and satisfies $q_0 = q(\tau_0, u)$.

2.7.2 Holonomic versus nonholonomic systems

Let $\triangle$ be a distribution of dimension m on M. If M can be decomposed into leaves (submanifolds), and $\triangle(q)$ is the tangent space T_qM to the leaf passing through q, then $\triangle$ is said to be *integrable*. If $m = n$ then q is able to move anywhere in M. If $m < n$ then $\triangle(q)$ is a linear subspace of T_qM at q. But if $\triangle(q)$ can be integrated to locally reduce the dimension of M to m, then the system is called *holonomic*. In the opposite case (i.e. it is not possible to integrate $\triangle(q)$), the system is called *nonholonomic*.

The integrability of a differential coupling defined by a distribution $\triangle$ is related to the dimension of the *reachable space* of the associated system.

Let us consider the watch depicted in Figure 2.7. It is a mechanical system made of two rotating arrows. The control space is 2-dimensional. It can be represented as a torus. The velocity of the long arrow is 12 times faster than the velocity of the small one. There is a differential coupling between both arrows. Such a coupling is clearly integrable. This means that the *position* of the small arrow depends on the *position* of the long arrow. The *reachable space* of the arrow positions is not 2-dimensional. It is only 1-dimensional. The system is said to be *holonomic*.

Let us consider now the familiar example of a wheel rolling on a plane. The position is defined by the coordinates of contact relative to the plane. The direction of the wheel is defined by the coordinate of contact relative to a given axis. The rolling constraint implies that the Equation 1.1 must hold at every point along a path. Saying that Equation 1.1 is nonholonomic we mean that it is a function which cannot be integrated to give an equivalent position constraint.

The study of nonholonomic systems has generated works in the community of pure mathematics (e.g., [Bellaiche and Risler 1996]), control theory (e.g., [Li and Canny 1993]) and robotics (e.g.,

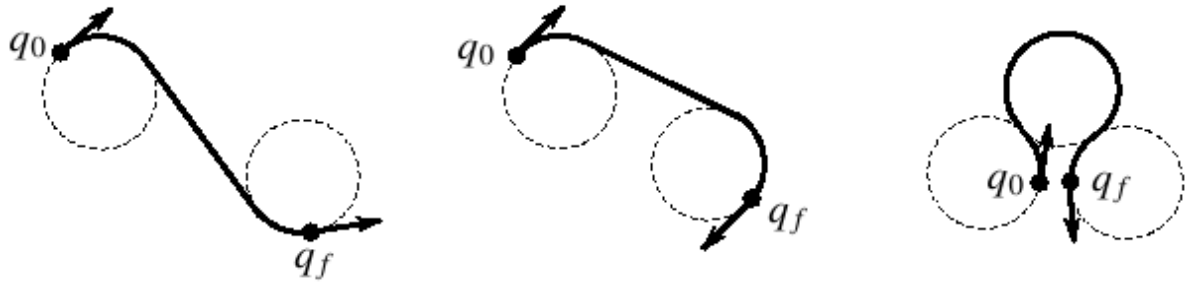

FIG. 2.8 – *Examples of Dubins shortest paths.*

[Laumond et al. 1998]). Checking whether a distribution is integrable or not is done by the Frobenius theorem, a classical tool from differential geometry [Varadarajan 1984]. Actually, it is sufficient to check that the Lie brackets of the basis elements are contained in the finite dimensional distribution (i.e. if the distribution is closed under the lie bracket). In our work, we shall be mainly interested in the case of nonintegrable (i.e. nonholonomic) distributions (see Chapter 4).

2.8 Optimal control in mobile robotics

The optimal solution for a general nonholonomic system is unknown. Nevertheless, one of the rare exceptions for the minimum time problems is the characterization of the C^1 shortest paths of bounded curvature joining two points in the plane with given tangent angles. In this case the cost function is given by $J = T - 0$. In [Dubins 1957] the author proves that there exists a unique optimal path which is a concatenation of at most three pieces ; every piece is either a straight line segment or an arc of circle of fixed radius (see Figure 2.8).

In [Reeds and Shepp 1990] the authors solve a similar problem when the cusps are allowed. They obtain the list of all possible optimal paths contained in forty eight types. Each of them is a finite concatenation of pieces. Each piece is either a straight line or an arc of a circle (see Figure 2.9). In [Sussmann and Tang 1991] but also in [Boissonnat et al. 1992] the same two problems are revisited. The authors provide, by using the Maximum Principle of Pontryagin, new proof of Reeds-Shepp's result. Based on these results, the computation of the complete synthesis for the shortest paths for Reeds-Shepp and Dubins models has been achieved (see [Souères and Laumond 1996] and [Pecsvaradi 1972] respectively and some extensions of them [Balkcom and Mason 2002], [Balkcom et al. 2006]).

For more difficult models, as the mathematical model considered in Chapter 5, work has been done in [Boissonnat et al. 1994; Kostov and Degtiariova-Kostova 1995] to find the shortest path connecting two given points in the plane when the initial and final tangent angles and curvatures are also specified. Using the Maximum Principle of Pontryagin they proved that any extremal path is a C^2 concatenation of line segments in one and the same direction and arcs of clothoids all of finite length. The clothoid is a curve, whose curvature grows linearly with the distance from the origin (see Chapter 5). However, when studying the possible variants of concatenation of such pieces they obtain that if an extremal path contains but is not reduced to a line segment, then it contains an infinite number of concatenated arcs of

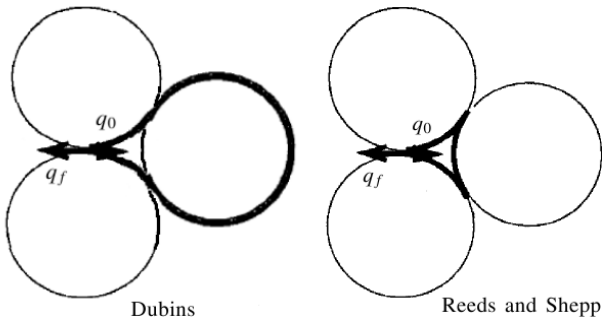

FIG. 2.9 – *The difference between the geometric shape of a Dubins and a Reeds-Shepp's shortest paths joining the same two points.*

clothoids. Consequently, optimal paths have an infinite number of switching points.

2.9 Some optimal control tools

Since the Greeks we know that the straight line segment is the shortest path (i.e. minimum length) joining two points in the Euclidean space. However, such minimum length criterion could be replaced by any other cost function to be optimized (e.g., minimum time). More than that, we may realize that the two n-dimensional points belong on an n-dimensional manifold M. Thus, the shortest path cannot always be a straight line segment. It turns out that the shortest path joining two points on M is a geodesic segment. A familiar example is the shortest path joining two far points on the surface of the Earth. Usually during a flight the passengers have access to see on the onboard screen the path followed by the airplane. In this case, the path *globally* looks like a geodesic segment. But if we decide to take a bicycle instead of an airplane, we may have the impression that *locally* a good approximation of the path followed by the bicycle is a straight line[4].

For our purpose, a *"point"* represents the coordinates of a given system of ordinary differential equations

$$\dot{q} = f(q,u) \tag{2.8}$$

where q of R^n which belongs to M is the state variable and $u \in R^m$ the control input. In other words, the *"point"* q defines the state of the system at each instant of time. Now let us state the following problem : given any two states $q_0, q_f \in R^n$, we want to characterize, among all the control laws steering the system from q_0 to q_f, one (if exist) minimizing the functional :

$$J = \int_0^T L(q(\tau,u),u(\tau))d\tau \tag{2.9}$$

where $L(q,u)$ is a function continuously differentiable with respect to its arguments. Here, we focus on point-to-point optimal control problems (i.e. we do not discuss the area of transversality conditions).

[4]even if we do not reach the destination...

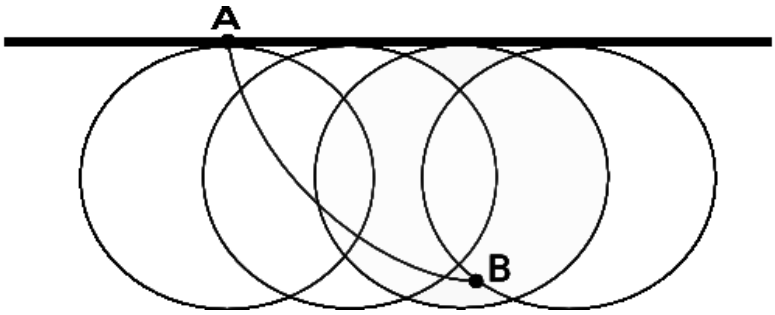

FIG. 2.10 – *The Brachystochrone cycloid.*

There exist at least two distinctive components of an optimal control problem. First, the functional 2.9 to be minimized subject to endpoint constraints. Second, the dynamical constraints 2.8 to be satisfied. As we have mentioned above, even though the cost function is completely trivial (i.e. $L \equiv 1$) for the minimum time problems in wheeled robots, the dynamics f makes the problem difficult to solve.

We may now introduce the control formulation of Hamilton's equations to state the necessary conditions for optimality that lead toward the Pontryagin's maximum principle (PMP). We define the Hamiltonian function H as

$$H(q,u,\psi) = < \psi, f(q,u) > + L(q,u) \tag{2.10}$$

where ψ is the adjoint state associated to q and $< .,. >$ is the inner product of R^n. Then we can define the following system of equations :

$$\begin{array}{rcl} \dot{q} & = & \frac{\partial H}{\partial \psi}(q,\psi) \\ \dot{\psi} & = & -\frac{\partial H}{\partial q}(q,\psi) \\ \frac{\partial H}{\partial u} & = & 0 \end{array} \tag{2.11}$$

with boundary conditions $q(0) = q_0$ and $q(T) = q_f$.

2.9.1 Pontryagin's maximum principle

The birth of optimal control theory is controversial (for a historical perspective see [Sussmann and Willems 1997]). Some mathematicians argue that it was born in 1697 when Johann Bernoulli formulated the so-called Brachystochrone[5] problem stated as follows

> *"If in a vertical plane two points A and B are given, then it is required to specify the orbit AMB of the movable point M, along which it, starting from A, and under the influence of its own weight, arrives at B in the shortest possible time. [...] In order to avoid a hasty conclusion, it should be remarked that the straight line is certainly the line of shortest distance between A and B, but it is not the one which is traveled in the shortest time."*

[5]From the Greek words $\beta\rho\alpha\chi\iota\sigma\tau o\varsigma$: shortest, and $\chi\rho o\nu o\varsigma$: time. It is well known that the solution of this problem is a cycloid segment (see Figure 2.10)

On the contrary, other mathematicians suggest that optimal control was born in 1958 when the PMP was announced in the International Congress of Mathematicians. Leaving out the fascinating historical events since the Bernoulli's problem, there is no doubt that the PMP constitutes a generalization of Euler-Lagrange formalism of the calculus of variation.

Notice that we have already introduced the Hamiltonian formalism, but we have not yet added a minor component needed to state the PMP. This component is a new ψ-variable ψ_0 which is called the *"abnormal multiplier"*. Now, we can rewrite the Hamiltonian equation as

$$H(q,u,\psi) =< \psi, f(q,u) > +\psi_0 L(q,u) \tag{2.12}$$

Finally we state the **PMP** as

For the problem of minimizing a functional 2.9 subject to a dynamical constraint 2.8 and endpoint constraints $q(0) = q_0$ and $q(T) = q_f$, with the parameter u belonging to a set U, the variable q taking values in R^n and the time interval $[0,T]$ fixed, a necessary condition for a function $\tau \rightarrow u^*(\tau)$ on $[0,T]$ and a corresponding solution $\tau \rightarrow q^*(\tau)$ of 2.8 to solve the minimization problem is that there exists a function $\tau \rightarrow \psi^*(\tau) \in R^n$ and a constant $\psi_0 \geq 0$ such that $(\psi^*(\tau), \psi_0) \neq (0,0)$ for all $\tau \in [0,T]$ and

$$H(q^*(\tau), u^*(\tau), \psi^*(\tau)) = min_{u \in U}(H(q^*(\tau), u(\tau), \psi^*(\tau))) \tag{2.13}$$

For a minimization problem with a variable time interval (i.e. T is not fixed in advance) and assuming that f and L do not depend on time, the extra requirement is

$$H(q^*(\tau), u^*(\tau), \psi^*(\tau)) \equiv 0 \tag{2.14}$$

In particular, the statement 2.14 applies to minimum time problems (i.e. $L \equiv 1$). It should be emphasized that PMP establish a set of necessary, but not sufficient, conditions for optimality. In addition, PMP does not provide a precise methodology to extract concrete information to characterize the optimal control law for nonlinear systems. Furthermore, the *existence* of an optimal solution cannot be guaranteed by the PMP alone.

Remark : The convention $\psi_0 \leq 0$ corresponds to the maximum principle, while the convention $\psi_0 \geq 0$ corresponds to the minimum principle.

2.9.2 The least-squares optimal control problem

In [Sastry and Montgomery 1992] the authors obtained an interesting result studying the structure of the optimal controls for steering a nonlinear control system without drift. Let us consider the dynamical system 2.5 together with a cost function

$$J = \frac{1}{2}\int_0^T <(u(\tau), u(\tau))> d\tau \tag{2.15}$$

which corresponds to the least squares optimal control problem. Given two configurations $q_0, q_f \in R^n$,

find a set of control inputs $u(\tau) \in R^m, \tau \in [0,T]$, which minimizes the cost J and steers the system from q_0 to q_f. Thus, the Hamiltonian function H is defined as

$$H(q,u,\psi) = \frac{1}{2}u^t u + \psi^t \sum_{i=1}^{m} g_i(q)u_i \tag{2.16}$$

The normal optimal control are obtained by minimizing the Hamiltonian as

$$u_i^* = -\psi^t g_i(q) \tag{2.17}$$

and the optimal Hamiltonian is given by

$$H^*(q,\psi) = -\frac{1}{2}\sum_{i=1}^{m}(\psi^t g_i(q))^2 \tag{2.18}$$

Hence, the optimal control system satisfies the Hamiltonian equations :

$$\begin{array}{rcl} \dot{q} & = & -\sum_{i=1}^{m} g_i(q)(\psi^t g_i(q)) \\ \dot{\psi} & = & \sum_{i=1}^{m} \frac{\partial g_i}{\partial q}(\psi^t g_i(q)) \end{array} \tag{2.19}$$

with boundary conditions $q(0) = q_0$ and $q(T) = q_f$. The interesting result is obtained by differentiating the optimal controls of Equation 2.17, that is :

$$\dot{u}_i = -\dot{\psi}^t g_i(q) - \psi^t \frac{\partial g_i}{\partial q}\dot{q} \tag{2.20}$$

Then, by using the Hamiltonian equation for $\dot{\psi}_k$ given by

$$\dot{\psi}_k = -\sum_{i=1}^{m} \psi^t \frac{\partial g_i}{\partial q_k}u_i \tag{2.21}$$

the following differential equation is satisfied :

$$\dot{u}_i = \sum_{j=1}^{m} \psi^t [g_i, g_j]u_j \tag{2.22}$$

where $[g_1, g_2]$ is the Lie bracket of two vector fields. This fact establishes that the norm of the optimal input is constant for all τ, that is

$$\|u(\tau)\|^2 = \|u(0)\|^2 \tag{2.23}$$

2.10 Numerical approach to optimal control

In general, it is difficult to find the solution of the optimal steering of nonholonomic systems, the only possibility is to rely on numerical methods[6]. We describe here the method developed by Fernandes,

[6]Few special cases similar to ours have been solved analytically : they deal with the computation of the shortest paths for Dubins's car [Dubins 1957], Reeds and Shepp's car [Reeds and Shepp 1990], and some extensions of them [Boissonnat et al. 1992], [Balkcom and Mason 2002], [Balkcom et al. 2006].

Gurvits, and Li [Fernandes et al. 1994].

Let us consider the dynamical System 2.5 together with the cost function given by 8.9. Denoting by $\{e_k\}_{k=1}^{\infty}$ an orthonormal basis for $L_2([0,T])$ and considering a continuous and piecewise C^1 control law u defined over $[0,T]$, we may write a function $u \in L_2([0,T])$ in terms of a Fourier basis :

$$u = \sum_{k=1}^{\infty} (\alpha_k e^{i\frac{2k\pi t}{T}} + \beta_k e^{-i\frac{2k\pi t}{T}})$$

Then u can be approximated by truncating its expansion up to some rank N. The new control law u and the objective function J is then expressed as

$$u = \sum_{k=1}^{N} \alpha_k e_k \Longrightarrow J \simeq \frac{1}{2} \sum_{k=1}^{N} \alpha_k^2$$

where $e_k \in \{e^{i\frac{2p\pi}{T}}, p \in Z\}$ and $\alpha = (\alpha_1, \alpha_2, ..., \alpha_N) \in R^N$ is to be determined. The configuration $q(T)$ is the solution at time T applying the control law u. Clearly, $q(T)$ appears as a function $f(\alpha)$ from R^N to R^n. In order to steer the system to q_f, an additional term must be added to the cost function :

$$J(\alpha) = \frac{1}{2} \left(\sum_{k=1}^{N} \alpha_k^2 + \gamma \| f(\alpha) - q_f \|^2 \right)$$

where $q(T) = f(\alpha)$ and γ is a tuning parameter during the optimization. It is proved that the solution of the new finite-dimensional problem converges to the exact solution as N and γ go to infinity [Fernandes et al. 1994].

The new optimization problem becomes : given a fixed time T and q_0, q_f find $\alpha \in R^N$ such that the cost function $J(\alpha)$ is minimized. In other words, this approach will give us near-optimal paths. Because $f(\alpha)$ is in most of the cases not known, we should use numerical integration to obtain $f(\alpha)$ and its Jacobian $\frac{\partial f}{\partial \alpha} \in R^{n \times N}$.

Let us now give a description of the Newton's method to compute a solution of this numerical optimization problem.

For a twice continuously differentiable scalar function $I(x) \in R^n$, the necessary conditions for x^* to be a minimum of I are :

- the gradient of I in x^* : $I_x(x^*) = \left(\frac{\partial I}{\partial x_1}(x^*), ..., \frac{\partial I}{\partial x_n}(x^*) \right) = 0$, and
- the Hessian of I in x^* : $I_{xx}(x^*) = \left(\frac{\partial^2 I}{\partial x_i \partial x_j}(x^*) \right)_{1 \leq i,j \leq n}$ must be a positive definite matrix.

For nonlinear functions, the iterative optimization procedure requires a starting point x_0 to be a reasonable estimate of the solution. Starting at x_0, the algorithm generates a sequence of iterates until a good approximation of a solution is reached. Otherwise it stops when no more progress can be made. At each iteration the algorithm uses information about the function I to decide how to move from the current iteration to the next one with a lower function value. That is, $I(x_{n+1}) \leq I(x_n)$. Hence, the algorithm chooses a direction p_n and an appropriate step length λ in order to decide how far to move along p_n. The iteration is given by $x_{n+1} = x_n + \lambda_n p_n$. Among all possible directions, the steepest-descent direction $p_n = -\lambda I_x(x_n)$ is the one along which I decreases most rapidly. According to the first-order expansion of I, it follows that such direction is orthogonal to the contours of the function I (see Figure 2.11). It

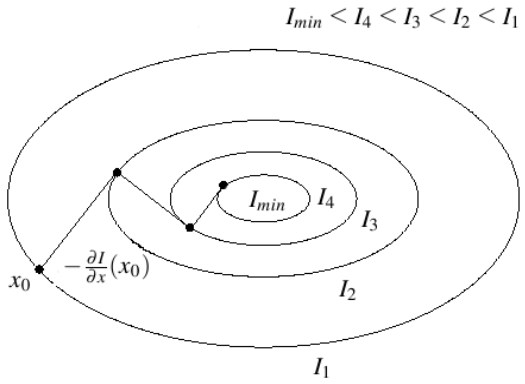

FIG. 2.11 – *The steepest-descent direction requires calculation of the gradient. Such direction is orthogonal to the contours of the function I.*

requires calculation of the gradient but not of second derivatives. There exist a variety of ways to choose the parameter λ. A small value of λ produces an unacceptable slow rate of convergence. In contrast, a too large λ may overshoot the minimum. A simple condition to select λ is that it provides a reduction in I. Considering the second-order expansion of I, we obtain the Newton direction. Unlike the steepest descent direction, Newton's method use the unit step $\lambda = 1$ which produces a fast rate of convergence in just a few iterations. However, the Newton direction needs the computation of the Hessian I_{xx} and when this matrix is not positive definite its inverse does not exist. Otherwise the search direction has the form :

$$p_n = -I_{xx}^{-1}(x_n) I_x(x_n) \tag{2.24}$$

In quasi-Newton methods, I_{xx} is replaced by a positive and invertible matrix that approximates it.
To minimize the nonlinear function $J(\alpha)$ using this technique, we compute

$$\frac{\partial J}{\partial \alpha}|_{\alpha_n} = \alpha_n + \gamma A^t (f(\alpha_n) - q_f) \tag{2.25}$$

and

$$\frac{\partial^2 J}{\partial \alpha^2}|_{\alpha_n} = I + \gamma A^t A + \gamma \sum_{i=1}^{n} \left(f_i(\alpha_n) - q_i^f \right) H_i \tag{2.26}$$

where

$$A = \frac{\partial f}{\partial \alpha}|_{\alpha_n} \in R^{n \times N} \quad and \quad H_i = \frac{\partial^2 f_i}{\partial \alpha^2}, \quad i = 1, ..., n \tag{2.27}$$

are the Jacobian of f and the Hessians of the compoment functions of f respectively. Then, the iteration is given by

$$\alpha_{n+1} = \alpha_n - \mu [\rho I + A^t A]^{-1} [\rho \alpha_n + A^t (f(\alpha_n) - q_f)] \tag{2.28}$$

where $\rho = 1/\gamma, 0 < \mu < 1$ and $(\rho I + A^t A)$ is the positive definite matrix that replaces the computation of the Hessians.

Now, we will address the problem of computing $f(\alpha)$ and $A(\alpha)$ by solving a differential equation that has to be incorporated into the statement of the algorithm. Thus, let us rewrite the System 2.5 such that

$\forall(\tau,\alpha) \in [0,T] \times [0,+\infty[$

$$\frac{\partial q}{\partial \tau}(\tau,\alpha) \quad = \quad \sum_{i=1}^{m} u_i(\tau,\alpha) B_i(q(\tau,\alpha)) \tag{2.29}$$

the columns $B_i(q(\tau,\alpha))$ are the control vector fields. By differentiating 2.29 we get :

$$\frac{\partial^2 q}{\partial \tau \partial \alpha}(\tau,\alpha) = X(\tau,\alpha) Y(\tau,\alpha) + B(\tau,\alpha)\mathbf{e}(\tau,\alpha) \tag{2.30}$$

where $Y(\tau,\alpha) = \frac{\partial q}{\partial \alpha}(\tau,\alpha)$ and $\mathbf{e}(\tau,\alpha) = \frac{\partial \mathbf{u}}{\partial \alpha}(\tau,\alpha)$ are vector-valued functions. $X(\tau,\alpha)$ is the following $n \times n$ matrix :

$$X(\tau,\alpha) \quad = \quad \sum_{i=1}^{m} (u_i(\tau,\alpha) \frac{\partial B_i}{\partial q}(q(\tau,\alpha))) \tag{2.31}$$

and $B(\tau,\alpha)$ is a $n \times m$ matrix. Therefore, the System 2.30 is in fact the linearized system of 2.5 about $\tau \to q(\tau,\alpha)$.

Using the above equations, $f(\alpha)$ and $\frac{\partial f}{\partial \alpha}$ are obtained by evaluating 2.5 and 2.30 at $\tau = T$ respectively. This numerical approach is used in Chapter 5 to compute optimal trajectories.

3
Methodology

The purpose of the current chapter is to describe the specifications of the experimental protocol that has been implemented to record human locomotor trajectories. In particular, we designed a goal-directed task to validate the existence of stereotyped behaviors. In Section 3.1, we recall the objectives of our study in order to introduce the methodology we followed for the generation of locomotor trajectories. Then, in Section 3.2 we describe the protocol, the characteristics of subjects in the experiments and the methods used to extract the data from the body and head coordinate frames. In Section 3.3, we focus on the statistical study to exhibit the geometric and the kinematic features of human walking. We dedicate a short note on the so called one-third power law that has been tested with our data basis of locomotor trajectories (see Section 3.4). Finally in Section 3.5 we comment the stereotyped behavior of human locomotion that serves as the basis of the next stage of this work.

3.1 Our approach

Our approach aims at explaining the shape of the locomotor trajectories *via* optimal control. By nature the validation of the control model we are looking for should be done by comparing the trajectories simulated from the proposed model with a set of observed trajectories. We first have to find a control system that "reasonably" accounts for the human locomotion. Then we have to find an optimal cost that "reasonably" accounts for the shape of the trajectories. "Reasonably" means that we want a human locomotion model that applies as closely as possible to a set of observed data : the "proofs" will come from statistical analysis. Our approach underlies several questions :

1. Does everybody obey the same locomotor strategy ? To answer the question, we should build a data basis of trajectories performed by several subjects having to reach a same goal. Then we should

prove the existence of stereotyped behaviors.

2. A data basis of trajectories being given, we should find a control model with an associated optimal cost. The inputs of a standard optimal control problem are a model and an associated cost function. The outputs are the optimal trajectories. Here we assume that the observed trajectories are optimal and we should find the corresponding system (model and cost). This problem is then viewed as an *inverse* optimal control problem.

The current chapter focuses on the first item. Of course the data basis should not be made of a single trajectory. All the possible goals have a priori to be considered. The task is obviously impossible from the experimental point of view. This is why the experimental protocol considers a sampling of the reachable space.

We follow a methodology based on an accessibility domain geometric study of forward locomotor trajectories. We exclude from the study the goals located behind the starting position and the goals requiring side walk steps. Nevertheless, any goal in an empty space, even one located behind the starting position, may be reachable by a forward walk. However, this is not the "natural" way to do so. A human would not intentionally walk all around the room to reach a point that is right behind them. This important assumption is related to the accessibility space of a control system. Here we reasonably assume that the accessibility domain of the forward locomotion is a kind of a 3-dimensional cone approximated by sampling the reachable space we consider in the protocol (see Section 3.2).

3.2 Trajectory data basis : protocol and apparatus

The idea is to sample the 3-dimensional reachable space into a set of goals to be reached. It involves only three parameters : two for the body position and one for the body direction (with respect to an external frame). We restrict the study to the natural forward locomotion with nominal speed. The model we study should be valid for all possible intentional goals reachable by a forward walk.

3.2.1 Subjects and materials

To examine the geometric properties of human locomotor paths, trajectories were recorded in a large gymnasium in seven normal healthy males who volunteered for participation in the experiments. Their ages, heights and weights ranged from 26 to 29 years, from 1.75 to 1.80 meters, and from 68 to 80 kilograms respectively.

We used motion capture technology to record the trajectories of body movements. Subjects were equipped with 39 light reflective markers located on their head and bodies. The 3D positions of the light reflective markers were recorded using an optoelectronic Vicon motion device system (Vicon V8, Oxford metrics) composed of 24 cameras. The sampling frequency of the markers was 120 Hz. It is important to mention that we do not apply any kind of filter to raw data in our analysis (see Figure 3.1).

Only nine markers have been directly used for this analysis. Three reflective markers were fixed on a helmet (200 g). The helmet was placed so that the midpoint between the two first markers was aligned with the head yaw rotation (naso-occipital) axis. We also used other two reflective markers located at each shoulder and finally four markers located on the bony prominences of the pelvis.

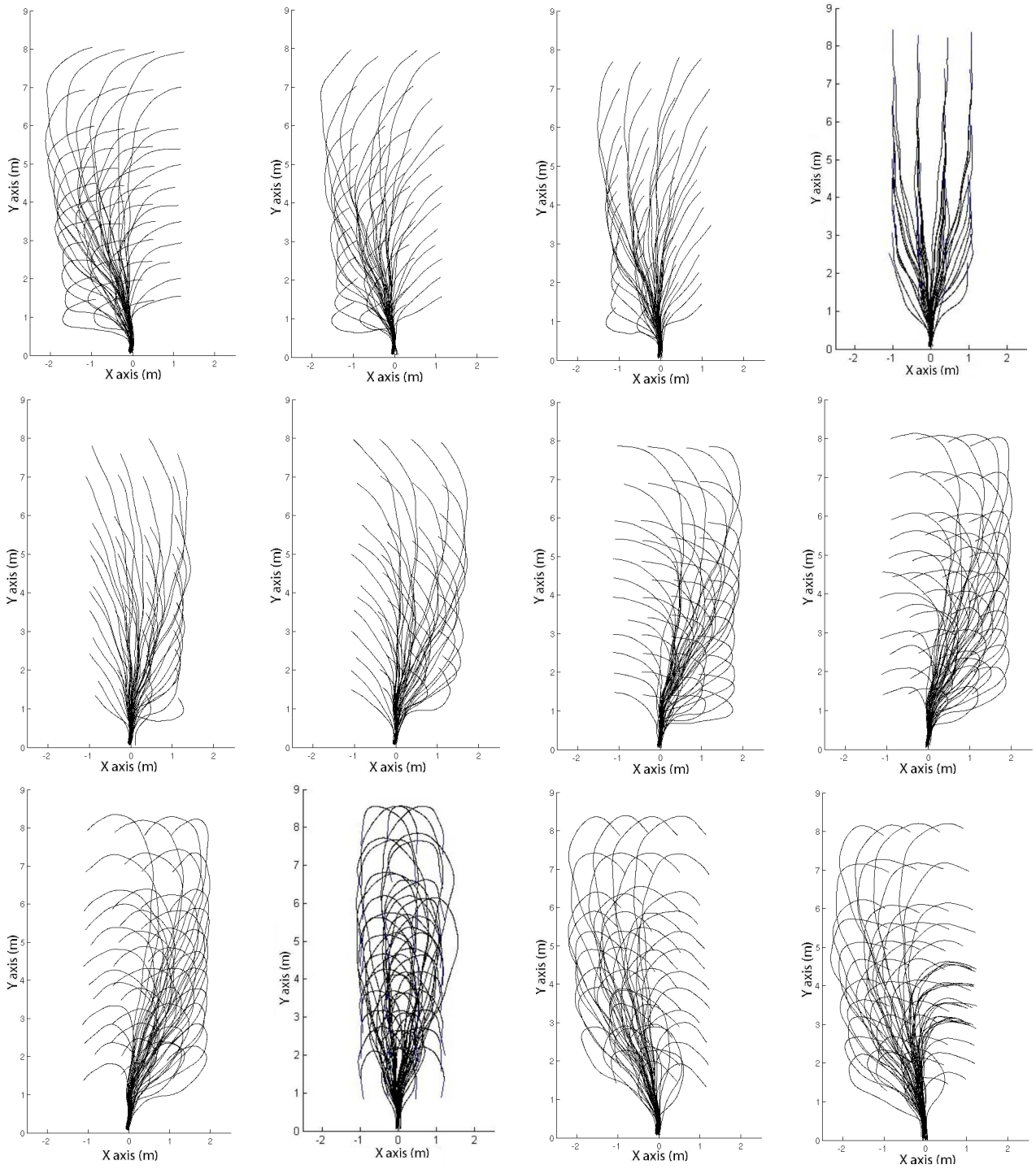

FIG. 3.1 – *The 480 recorded trajectories performed by one subject. The trajectories are those of the torso. At each figure the final direction is fixed. From top to bottom and from left to right, the final direction varied from -π to π in intervals of $\frac{\pi}{6}$.*

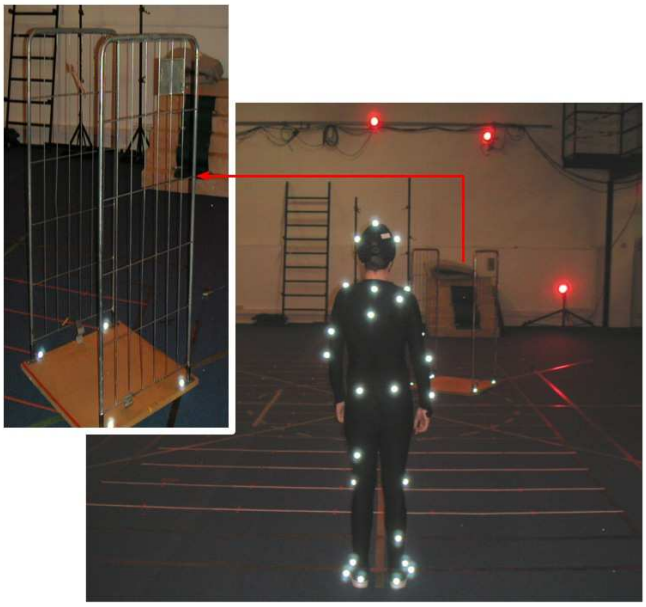

FIG. 3.2 – *The porch and the room used in the experiments. We sampled a region of the gymnasium with 480 points defined by 40 positions on floor (within a 5m by 9m rectangle) and 12 directions each. The starting position was always the same while the goal was randomly selected. One subject performed all the 480 trajectories while other 6 performed only a subset of them chosen at random.*

In order to specify the position of the subject on the plane we established a relationship between the laboratory's fixed reference frame and the trajectory's reference frame which can be computed using either head, torso or pelvis markers as we explain in Chapter 4. Hence, the configuration A of the subject is described as a 3-vector (x_a, y_a, φ_a).

3.2.2 Protocol

The aim of the experimental protocol was to validate whether subjects, in a free environment, perform stereotyped trajectories in terms of geometric and kinematic attributes.

In the experiment, subjects walked from the same initial configuration A_{init} where the initial direction was approximately orthogonal to the horizontal axis of the laboratory to a randomly selected final configuration A_{final} represented by the doorway. The target consisted of a porch which could be rotated around a fixed point to indicate the desired final direction (see Figure 3.2). The subjects were instructed to cross over such porch (from A_{init} to A_{final}) without any spatial constraints relative to the path they might take. Subjects were allowed to choose their natural walking speed in order to perform the task. They were not asked to stop walking after entering the door because such instruction could influenced their behavior few steps before reaching the porch (see Figure 3.3).

To be more precise, when the subjects were asked to go through a distant doorway without any instructions on speed or accuracy, they had several possibilities for planning and executing the sequence of movements allowing them to reach the goal. The only constraints were the initial position and direction that were always the same and the final position and direction given by the doorway (see Figure

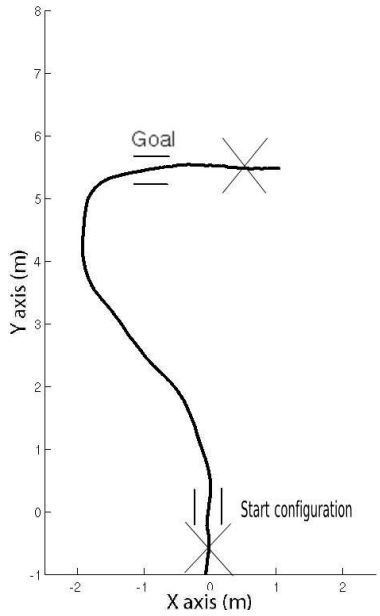

FIG. 3.3 – *To exclude the positive and negative acceleration effects at the beginning and at the end of trajectories, the first and the last steps of the subject's trajectories are not considered in this study.*

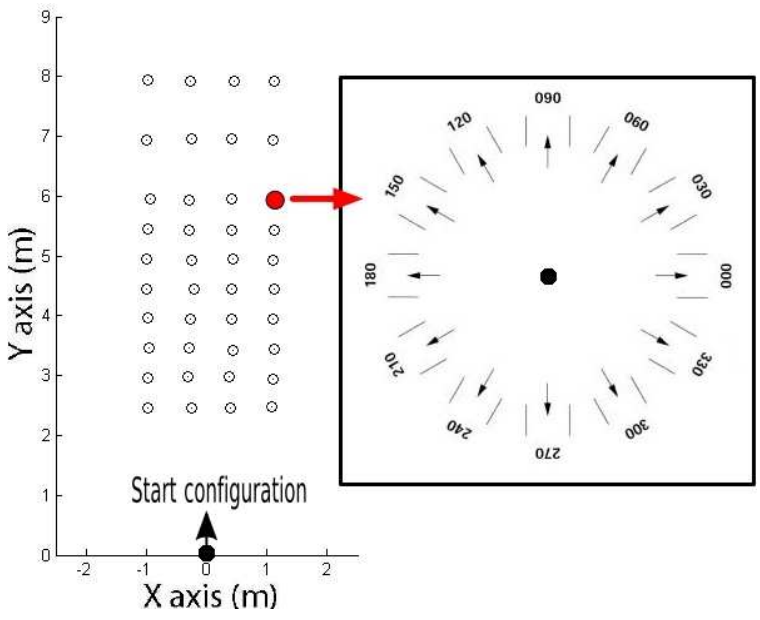

FIG. 3.4 – *It shows all the final configurations considered for the first subject. All the pictures are displayed in the same frame*

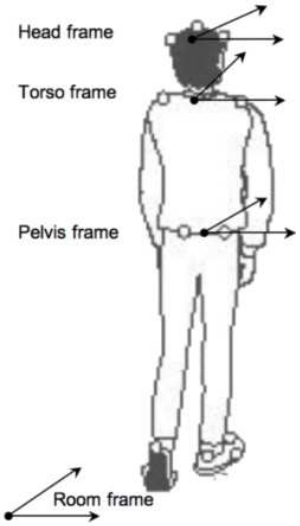

FIG. 3.5 – *Definition of the local frames. The position and the direction of the frames are deduced from the motion capture markers located respectively above the ears, on the shoulders and on both sides of the hip.*

3.4). Surprisingly, we observed that in such simple goal-directed task the subjects reproduced similar trajectories.

The final direction varied from -π to π in intervals of $\frac{\pi}{6}$ at each final position. In order to exclude the positive and negative acceleration effects at the beginning and at the end of trajectories, the first and the last steps of the subject's trajectories are not considered in this study. The subjects started to walk straight ahead one meter before the initial configuration A_{init} and stopped two meters after passing through the porch. Thus, the initial and final linear velocity were never zero.

The experiment was carried out in seven sessions. The first subject was asked to perform 480 different trajectories in two sessions (corresponding to 40 positions $\times$ 12 directions).

The six other subjects were asked to perform 180 different trajectories during the next six sessions. Each subject performed 3 trials for a given configuration of the porch A_{final}. Therefore, they walked 180 trajectories with only 60 different final configurations. It means that they have done a subset of the recorded trajectories executed by the first subject.

The length of the trajectories performed by the first subject ranged between 2 and 10 meters. The length of trajectories performed across the other six subjects and trials ranged from 1.96 to 2.12 meters for the nearest targets and from 6.48 to 6.50 meters for the furthest targets.

3.2.3 Global, head, torso and pelvis coordinate frames

While walking, the body generated trajectories in the space relative to the laboratory's reference frame *LRF*. To describe the movement of the body, a local reference frame was defined (see Figure 3.5). Several experimental studies have shown the important role of the head in the steering of locomotion (e.g., [Pozzo et al. 1990]). The torso has also been used in the study of the head anticipation in human navigation (e.g., [Hicheur et al. 2005]) and linear locomotion [Hirasaki et al. 1999]. The pelvis is

frequently used in humanoid robots and character animation for planning their motions (e.g., [Yoshida et al. 2005; Esteves et al. 2006]). Thus, in our study three body coordinate frames were used for the head RF_H, the torso RF_T and the pelvis RF_P respectively. The origins of RF_H, RF_T and RF_P and their directions have been determined from the markers' coordinates. However, the way in which the central nervous system may use different kinematic coordinates to encode the direction of movement is still an open question (e.g., [Soechting and Flanders 1994]).

To calculate the origin x_H,y_H of RF_H, we used the markers located on the back and the forehead. The direction φ_H of RF_H is easily identified according to the segment whose endpoints are the back and the forehead markers. Therefore, the desired direction is merely the rigid body transformation of RF_H onto LRF.

The midpoint of the shoulder markers and the direction orthogonal to the shoulder axis correspond to the origin x_T,y_T and the direction φ_T of RF_T respectively. Finally, to find the origin x_P,y_P and the direction φ_P of RF_P, four markers are used, left and right-front, left and right-back. These markers are located on the bony prominences of the pelvis.

3.2.4 Data processing

Numerical computation is performed to obtain the walking velocity profile. Each recorded trajectory is represented as a sequence of discrete points on the plane. We computed the linear v and angular ω velocities at each point such that

$$\begin{aligned} \dot{x}(\tau) &\leftarrow \tfrac{x(\tau+\Delta\tau)-x(\tau-\Delta\tau)}{2\Delta\tau} \\ \dot{y}(\tau) &\leftarrow \tfrac{y(\tau+\Delta\tau)-y(\tau-\Delta\tau)}{2\Delta\tau} \\ v(\tau) &\leftarrow \sqrt{\dot{x}^2(\tau)+\dot{y}^2(\tau)} \end{aligned} \tag{3.1}$$

$$\omega(\tau) \leftarrow \frac{\varphi(\tau+\Delta\tau)-\varphi(\tau-\Delta\tau)}{2\Delta\tau} \tag{3.2}$$

where $x(\tau)$, $y(\tau)$ and $\varphi(\tau)$ are the configuration parameters of the body along the trajectory. Therefore, these parameters describe the motion of any of the three RF_H, RF_T or RF_P local frames. We computed the desired tangential direction $\theta(\tau)$ along the path as

$$\theta(\tau) \leftarrow tan^{-}1\left(\frac{\dot{y}(\tau)}{\dot{x}(\tau)}\right) \tag{3.3}$$

It should be pointed out that $\varphi(\tau)$ has been calculated from the markers while $\theta(\tau)$ is computed from the sequence of discrete points $x(\tau)$, $y(\tau)$. We used Equation 3.2 to obtain the instantaneous variation of $\theta(\tau)$ replacing $\omega(\tau)$ and $\varphi(\tau)$ with $\dot{\theta}(\tau)$ and $\theta(\tau)$ respectively.

We need all these parameters to verify the geometric and the kinematic behaviors of locomotor trajectories, but also because in Chapter 4 we compare the head $\varphi_H(\tau)$, the torso $\varphi_T(\tau)$ and the pelvis $\varphi_P(\tau)$ directions (computed from the markers) with respect to the tangential direction $\theta(\tau)$ (computed from the trajectory). The aim of the comparison is to verify the differential coupling between the body position and direction in goal-directed locomotion (i.e. our hypothesis stated at the beginning of this

document).

3.3 Statistical analysis : a stereotyped behavior

For the subset of recorded trajectories executed by six subjects (i.e., for 60 targets), we validated that goal-directed locomotor trajectories are *similar* across subjects and trials both in terms of path geometry and velocity profile. To examine the geometric and kinematic features of the steering strategy, we analyzed the trajectories expressed in position and direction by three different body frames : the head, the torso and the pelvis.

To perform the analysis, we classified the subset of 60 targets in terms of the trajectory curvature induced by the final direction : HC (High Curvature), MC (Medium Curvature), LC (Low Curvature) and S (Straight) (see Figure 3.6). If the difference (angle) between the initial and the final directions is $> \frac{\pi}{2}$, then the target is labeled as HC, and consequently, the trajectories associated to the target. For MC, LC and S, the differences are $\frac{\pi}{2}$, $(\frac{2\pi}{3}, \frac{\pi}{3})$ and 0, respectively.

Then, we computed the mean trajectory to measure the deviation between the recorded and the mean trajectories corresponding to the same target (see Figure 3.7). The mean trajectory $(\bar{x}(\tau), \bar{y}(\tau))$ is computed with

$$\bar{x}(\tau) = \frac{1}{N}\sum_{i=1}^{N} x_i(\tau) \quad \textit{and} \quad \bar{y}(\tau) = \frac{1}{N}\sum_{i=1}^{N} y_i(\tau) \tag{3.4}$$

where N is the number of recorded trajectories. For a given target we performed the following steps : first the trajectories of all subjects and trials were time-rescaled by using the shortest time trajectory as the reference. After this step, the trajectories have the same final time but they contain different number of points. Then, we used a linear interpolation function to re-sample each trajectory according to the number of points contained in the reference trajectory (shortest time trajectory). After this step, the trajectories are transformed to paths (i.e. they are represented by the same number of points and with the same duration). The trajectory deviation TD is defined as

$$TD(\tau) = \sqrt{\frac{1}{N}\sum_{i=1}^{N}((x_i(\tau) - \bar{x}(\tau))^2 + (y_i(\tau) - \bar{y}(\tau))^2)} \tag{3.5}$$

The averaged and maximal deviations between the recorded and the mean trajectories are given by ATD and MTD respectively. Figure 3.8.a illustrates the path geometric stereotyped behavior for each category. We observed that ATD is less than 12 cm while MTD is less than 20 cm for the 60 targets. We also observed that TD grows when the curvature of the trajectory increases.

In addition to the path geometric variability, we performed the same procedure for the trajectory kinematic attributes. To quantify the variability of the linear velocity profile among subjects and trials we computed the mean and the maximal linear velocity profiles AV and MV respectively. Then, we calculated the averaged AVD and the maximal MVD linear velocity deviations (see Figure 3.8.b and Figure 3.8.c). We noticed that the linear velocity profile remains "reasonably" constant along the trajectories (we should keep in mind that the subjects were asked to enter the room by the starting configurations while not stopping at the goal). We observed that for all real trajectories the mean deviation from the average

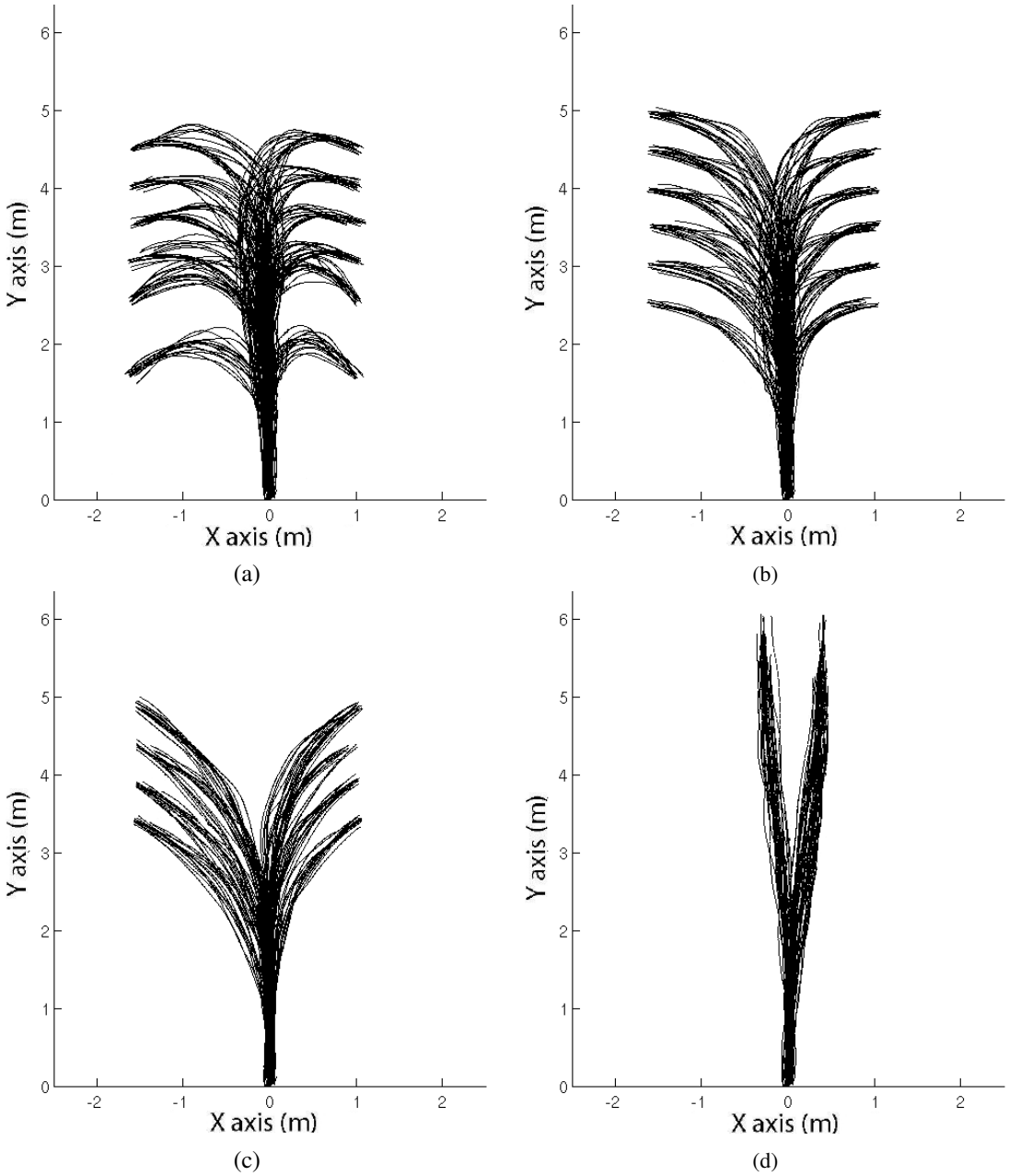

FIG. 3.6 – *Classification of recorded trajectories for a given target in terms of the curvature induced by the final direction. (a), (b), (c) and (d) show a subset of the recorded trajectories marked as HC : High Curvature, MC : Medium Curvature, LC : Low Curvature and S : Straight, respectively. The trajectories are those of the torso.*

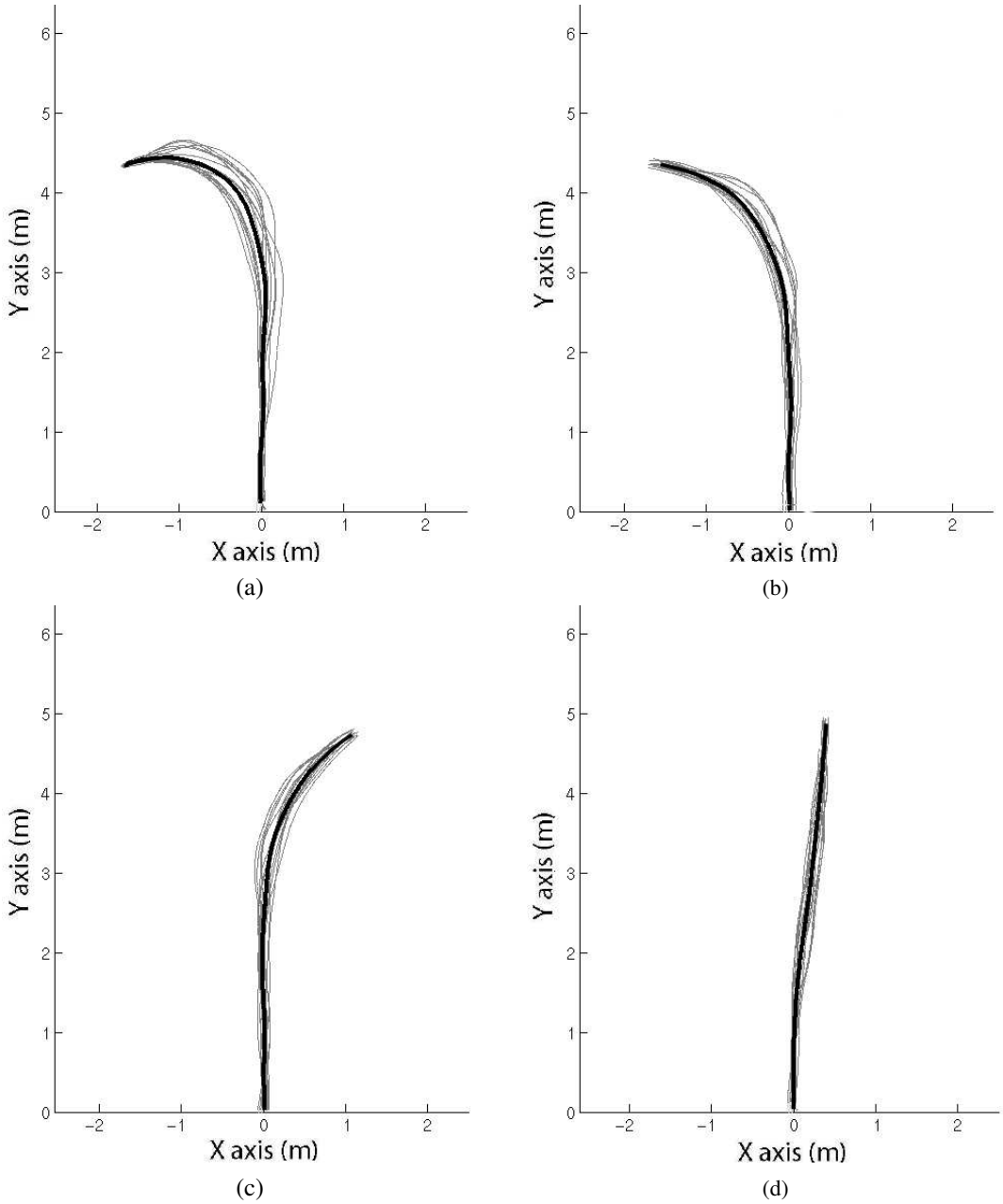

FIG. 3.7 – *The mean trajectory (black) is computed for all targets. The trajectories are those of the torso. (a) shows an example of HC : High Curvature. (b) shows an example of MC : Medium Curvature. (c) shows an example of LC : Low Curvature. (d) shows an example of S : Straight.*

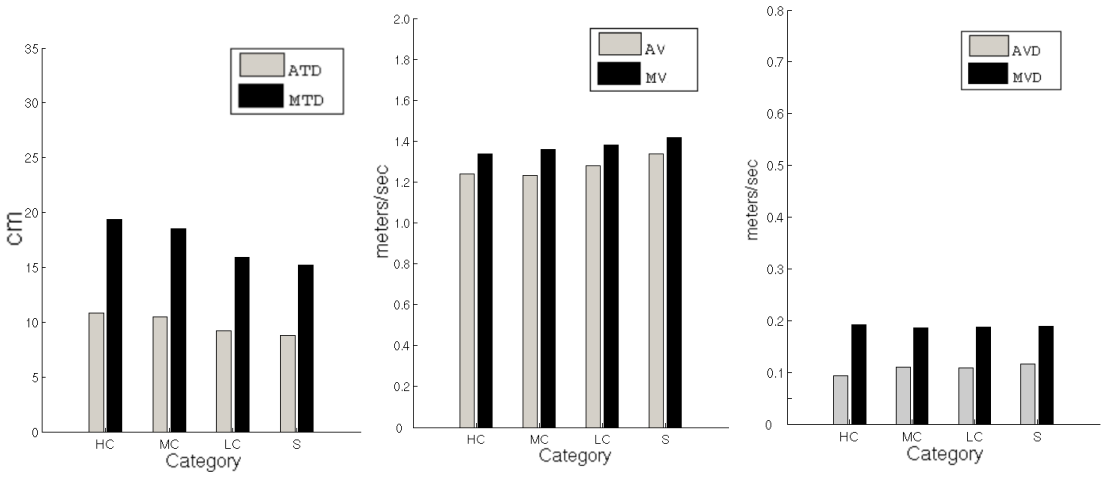

(a) (b) (c)

FIG. 3.8 – *Geometric and kinematic deviations of locomotor trajectories. (a) shows the comparison between the averaged and maximal trajectory deviations (ATD) and (MTD) for each category. The standard deviations of ATD and MTD are around 3cm for HC, MC, LC and S. (b) shows the averaged and maximal velocity profile (AV) and (MV) for each category. (c) shows the comparison between the averaged and maximal velocity deviation (AVD) and (MVD) for each category.*

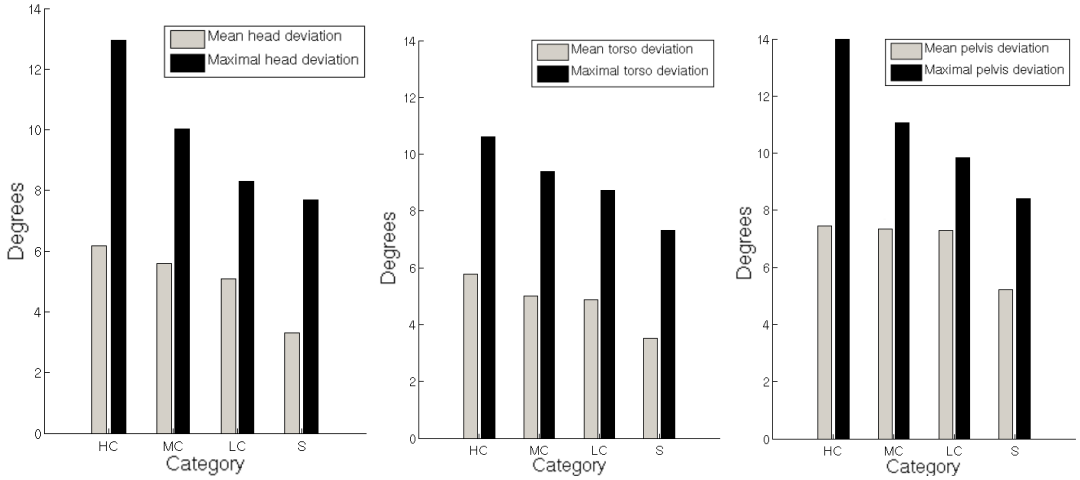

(a) (b) (c)

FIG. 3.9 – *Deviation from the mean body rotation profile for each category. (a), (b) and (c) show the comparison between the averaged and maximal head, torso and pelvis deviations respectively.*

velocity profile is around 0.10 m/s and it is not affected by the length of trajectories. The walking speed was 1.26 ± 0.3. Actually, the results obtained in [Hirasaki et al. 1999] for linear walking suggest that the optimal walking velocity lies between 1.2 and 1.8 m/s. This is also supported by the observation that the oxygen cost-speed relationship is lowest within this range (e.g., [Inman et al. 1981; Waters et al. 1988]). In addition, it has been observed that the adults prefer to walk at velocities ranged from 1.2 to 1.7 m/s during natural walking (e.g., [Finley and Cody 1970]).

The variability of the three body directions is also quantified : the head, the torso and the pelvis directions respectively. We observed that the averaged deviation is less than 8 degrees while the maximal deviation is less than 15 degrees for the head, the torso and the pelvis (see Figure 3.9). Moreover, as it is observed *in position*, we realized that the deviation grows when the curvature increases.

The comparisons of the variability of trajectory suggest that even if the length and the curvature of trajectories vary the same geometric and kinematic patterns among different subjects and trials persist. In other words it means that in goal-directed locomotion, the locomotor trajectories chosen by the subjects are stereotyped and show only little variation.

In the next chapter, we detail the analysis of each body direction in order to propose a simple differential system accounting for human forward locomotion.

3.4 Note on one-third power law

During this study we have tested the empirical observation described by a *power law*. It states that the velocity varies in proportion to the one-third power of the radius of curvature [Lacquaniti et al. 1983], and is expressed as

$$v(\tau) = kr(\tau)^{\beta} \tag{3.6}$$

or in the logarithmic form

$$logv(\tau) = logk + \beta logr(\tau) \tag{3.7}$$

where v is the linear velocity, k is a gain factor, r is the radius of curvature, and β is a constant exponent.

The studies on the power law have been validated for planar drawing patterns and elliptical patterns for pre-defined locomotor paths [Vieilledent et al. 2001]. For more complex pre-defined paths it is demonstrated that the one-third power law does not describe such relationship in locomotion [Hicheur et al. 2005].

In this study, we have tested this velocity-curvature relationship and we arrived to the same result when the path is not pre-defined : the one-third power law is not verified for the recorded locomotor trajectories.

To test this hypothesis, the locomotor trajectories were filtered using a fourth-order low pass filter with a 10 Hz cutoff frequency. After filtering, the first and the last 10 percent of data points were discarded to eliminate distortions caused by the digital filter onsets [Schaal and Sternad 2000]. Then, we performed

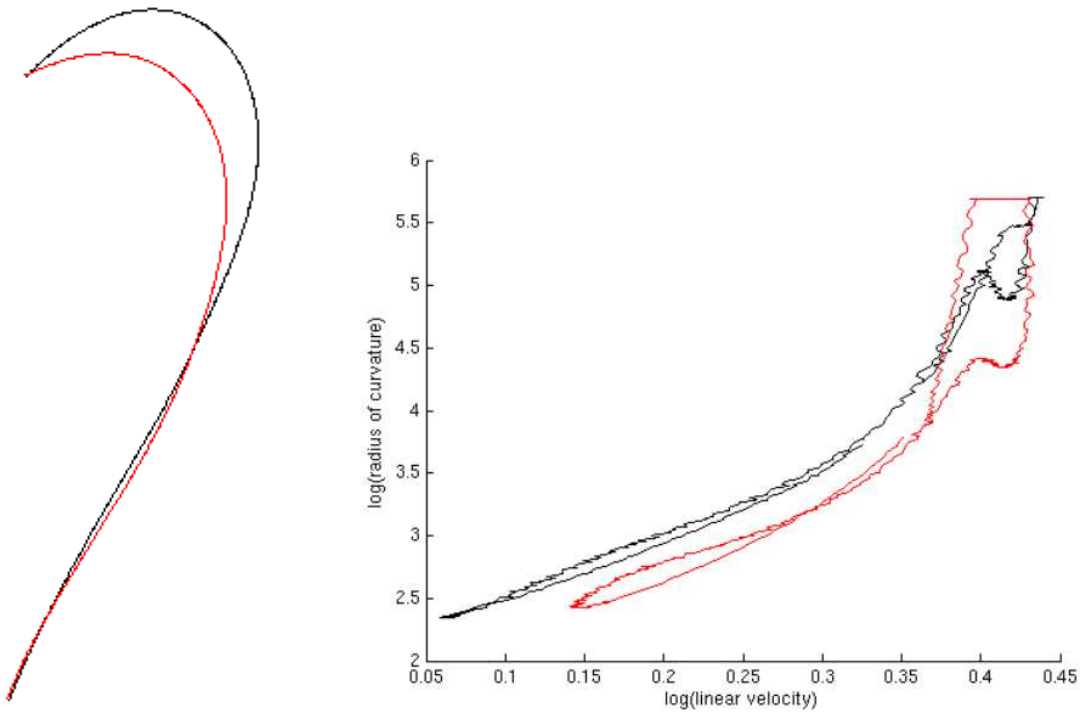

(a) (b)

FIG. 3.10 – *(a) shows two filtered locomotor trajectories (b) shows the relationship between the velocity and the radius of curvature in log-log scale. The exponents are 0.6881 (black) and 1.4160 (red). The log(velocity gain factors) are 9.9158 (black) and 8.7620 (red).*

the log-log regression to identify the power law exponent and the velocity gain factor. Figure (3.10) shows two representative trajectories and the log-log regression lines. It is noted that the velocity gain factor and the power law exponent depend on the geometric shape of the locomotor paths[1].

3.5 Discussion

Thanks to the statistical study it has been possible to show that general principles governed the motion strategy of all the seven observed subjects. While no specific constraint was provided to subjects neither at the spatial level (the path they should have followed for crossing throughout the doorway) nor at the temporal level (the velocity profile they should have produced), we observed that all subjects generated very similar trajectories both in terms of path geometry and in terms of velocity profiles. The subjects also exhibit similar turning behaviors as quantified by their body rotation in space. Based on these results, we show that the locomotor trajectories are planned according to goals which are expressed in terms of the body displacement in space, and are generated using motor coordination *patterns*.

During walking, the displacement of the limbs, body, and head are coordinated in order to reach

[1] It is important to make the distinction between a path and a trajectory. The path is a geometric curve while a trajectory is a time parametrized path.

a given target. Such coordination may reduce the dimension of the motor space associated with the number of body articulations. We can imagine the possibility that the whole body motion is mainly constructed at the step level by the influence of the leg's movements. The validity of the hypothesis that goal-directed locomotion is planned as a succession of foot steps has been recently discussed in [Hicheur et al. 2007]. The authors argued that a much greater variability was observed at the level of the successive positions of the feet than at the level of segmental and whole-body trajectories. They have done their statistical analysis using the same data basis of locomotor trajectories employed in this study. The authors concluded that goal-directed locomotion may be planned as a whole on the trajectory level rather than successive foot steps. These observations confirm the validity of the adopted top-down approach announced at the beginning of the document.

4

Human Forward Locomotion Modeling

In this chapter we propose a differential system accounting for human forward locomotion. In the previous chapter we described the spatial and temporal features of the locomotor trajectories when humans perform natural displacements. Here, we test the following simple statement : "the natural way for walking is to put one foot *in front of* the other and to repeat this actions". This basic statement is not so trivial. Indeed, "*In front of*" means that the direction of the motion is given by the direction of the body : it implies a coupling between the direction of the body and the tangent to the trajectory. In Section 4.1 we overview the motivation, the development and the results concerning the current chapter. In Section 4.2 we describe the study to find the adequate body parameters accounting for the nonholonomic nature of the human locomotion. In Section 4.3 we introduce the simplified model of a wheeled robot in the context of human walking. Then, in Section 4.4 we validate the proposed model by quantifying its accuracy in approximating the human locomotor trajectories. In Section 4.5 we comment experimental results obtained when modeling forward human locomotion.

4.1 The nonholonomic nature of the human locomotion

In the kinematics realm, wheeled robot's determining characteristic lies in its *nonholonomic* constraint. Indeed, the wheels of the robot unequivocally force the robot vehicle to move tangentially to its main axis. Here we test the hypothesis that human locomotion can also be partly described by such a nonholonomic system. This hypothesis is inspired by the trivial observation that humans do not walk sideways : some constraints of different natures (anatomical, mechanical...) may restrict the way humans generate locomotor trajectories. To model these constraints, we propose a simple differential system satisfying the so called *rolling without sliding* constraint. We validated the proposed model by

comparing simulated trajectories with recorded trajectories obtained from goal-directed locomotion of human subjects. These subjects had to start from a pre-defined position and direction in space and cross over to a distant porch so that both initial and final positions and directions were controlled. A comparative analysis was successfully undertaken by making use of numerical methods to compute the control inputs from recorded trajectories. To achieve this, three body segments were used as local reference frames : head, torso and pelvis. The best simulations were obtained using the torso body segment. We therefore suggest an analogy between the steering wheels and the torso segment, meaning that for the control of locomotion, the torso behavior is constrained in a nonholonomic manner. Our approach allowed us to successfully predict 87 percent of trajectories recorded from seven subjects. This result might be particularly relevant for future pluridisciplinary research programs dealing with modeling of biological locomotor behaviors.

4.2 The choice of the body frame

In this study the choice of the body frame we should consider has been a critical issue. We are looking for the frame that best accounts for the Equation 1.1. Three frames were considered (see Figure 3.5) : the head, the torso and the pelvis. The position and the direction of the frames are deduced from the motion capture markers located respectively above the ears, on the shoulders and on both sides of the hips.

Even though the subjects performed similar velocity profiles, the turning behavior of the head, the torso and the pelvis varies throughout the trajectory execution. In Figure 3.9, we observe that the variability of the head, the torso and the pelvis directions between four categories of trajectories (high, medium, low curvatures and straight) is less than 8 degrees with respect to the mean one. However, if we analyze the turning behavior between the head, the torso and the pelvis directions a significant statistical difference is observed as depicted in Figure 4.1. The picture shows an example of head, torso and pelvis rotation profiles computed for the same representative targets of Figure 3.7. We clearly observe that in the case of curved trajectories, the direction of the head anticipates the walking direction. In contrast, the difference between the torso and the pelvis directions seems to be almost the same. However, the pelvis direction oscillates around the torso direction which corresponds to the oscillations induced by step alternation.

Figure 4.2 shows a single trajectory represented in the three frames. Let us compare from the same trajectory the curves of the direction of the frame and the tangent to the position of the frame. Figure 4.3 illustrates the comparison of the curves. The nonholonomic hypothesis is verified if both curves coincide. The study shows that the torso frame accounts for that hypothesis much better than the head or the pelvis (see also [Arechavaleta et al. 2006a]). The shoulders behave as the front wheels of a car by anticipating the direction change of the body by a couple tenths of second.

The purpose of this section is to analyze the time course of the body turning behavior of the three different direction parameters $\varphi_H(\tau)$, $\varphi_T(\tau)$ and $\varphi_P(\tau)$ corresponding to the three different reference frames RF_H, RF_T and RF_P. These parameters correspond to the rotation of different body segments with respect to the trajectory. This quantitative and qualitative analysis is done to determine which of the frames better approximates $\theta(\tau)$.

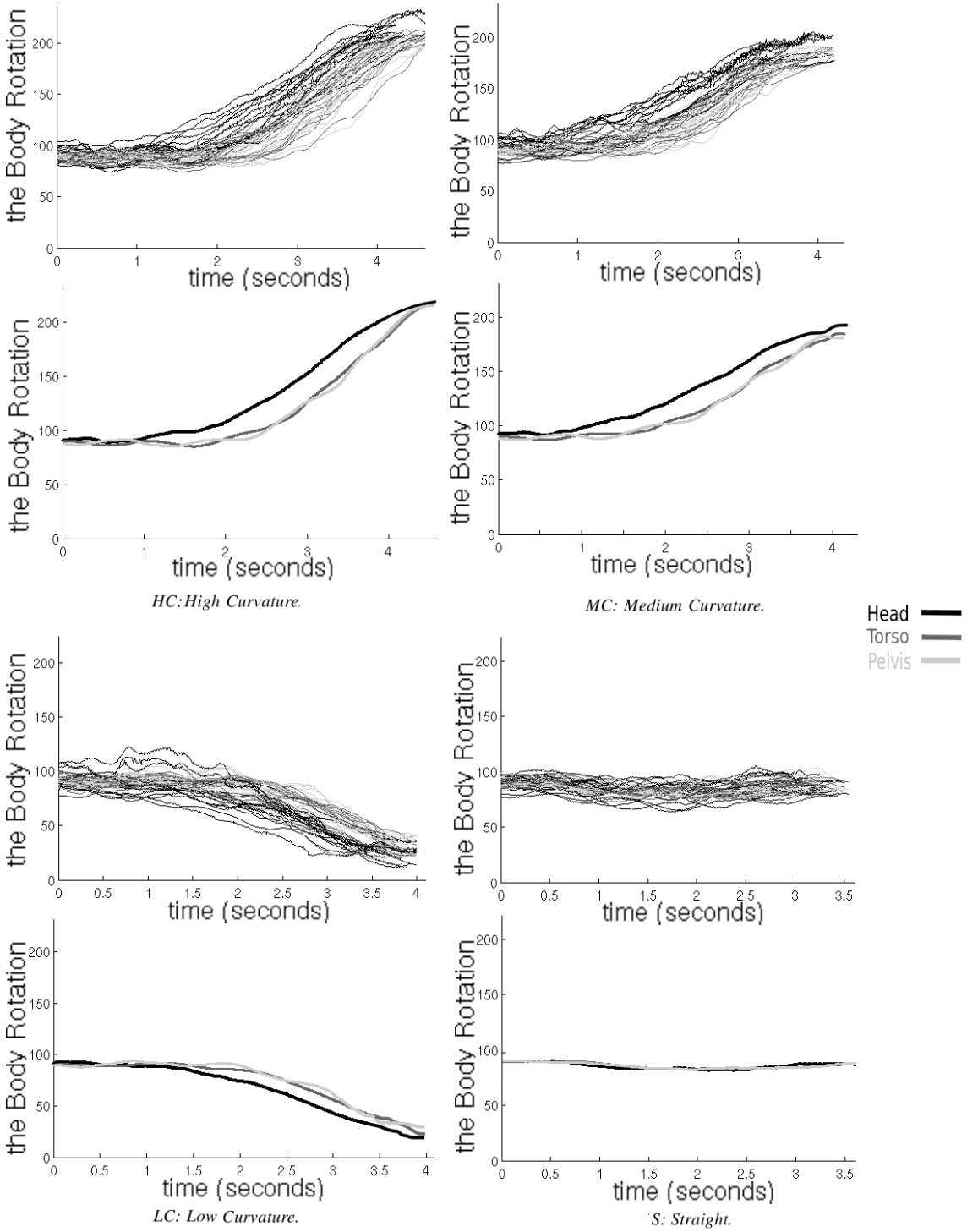

FIG. 4.1 – *Recorded (first and third rows) and mean (second and last rows) body direction profiles (head, torso and pelvis) for a given target (same targets as in Figure 3.7) in terms of the curvature induced by the final direction marked as high, medium, low curvature and straight, respectively.*

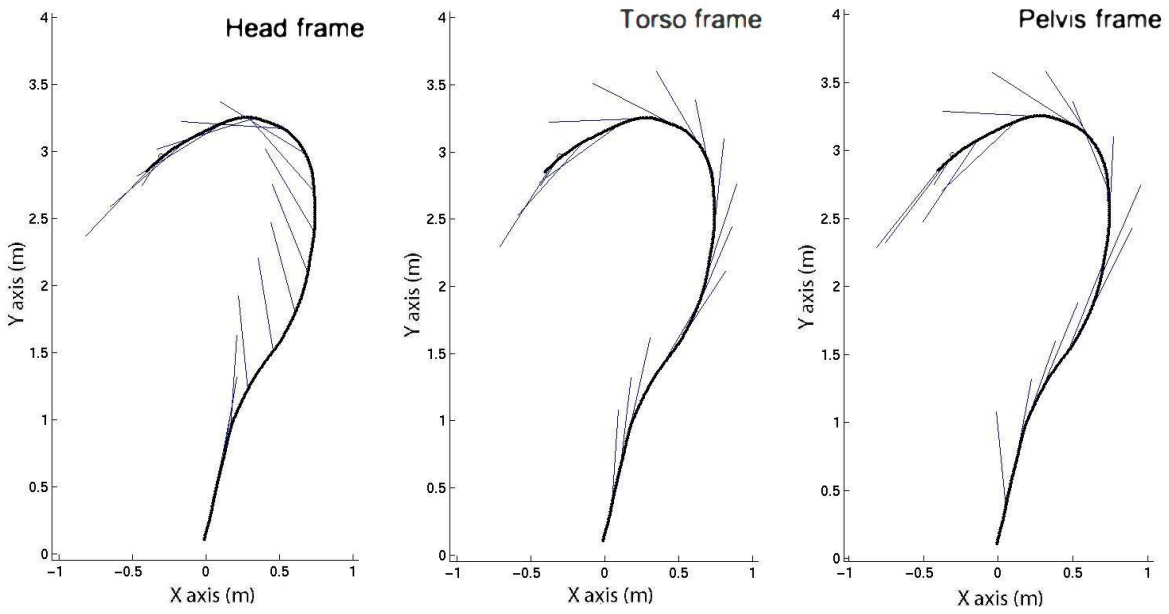

FIG. 4.2 – *The trajectories of the head, the torso and the pelvis local frames projected on the ground. All of them correspond to the same motion. (a), (b) and (c) show a single trajectory represented in the three frames. (a) shows the trajectory followed by the head reference frame and its directions. (b) shows the trajectory followed by the torso reference frame and its directions. (c) shows the trajectory followed by the pelvis reference frame and its directions.*

The deviations of the three body directions relative to $\theta(\tau)$ have been quantified as depicted in Figure 4.4. For all recorded trajectories we computed at each instant τ the angle between the tangent to the trajectory $\theta(\tau)$ and the directions $\varphi_H(\tau)$, $\varphi_T(\tau)$ and $\varphi_P(\tau)$ of each body frame. We observed that the averaged deviation of $\varphi_H(\tau)$ is large in amplitude even if in position the trajectory followed by the head is smoother than the trajectories of the torso and the pelvis for the same motion. This may be explained by the anticipatory and the stabilization role of the head in goal-directed locomotion (see [Pozzo et al. 1990; Grasso et al. 1996]). The amplitude of the deviation of the torso direction is less important in relation to the head and the pelvis directions.

4.2.1 Head direction profile

Defining RF_H as the local coordinate frame it is noted that $\varphi_H(\tau)$ points most of the time towards the direction of the target as it is illustrated in Figure 4.2.a. Furthermore, there are some cases where $\varphi_H(\tau)$ is pointing to the opposite half-plane with respect to $\theta(\tau)$. For instance, analyzing the behavior of $\varphi_H(\tau)$ and $\theta(\tau)$ in the trajectory of Figure 4.2.a, it can be shown that $\varphi_H(\tau)$ and $\theta(\tau)$ follow a similar trace until 0.55s and just after that both directions start to diverge until 1.4s (see Figure 4.3.a).

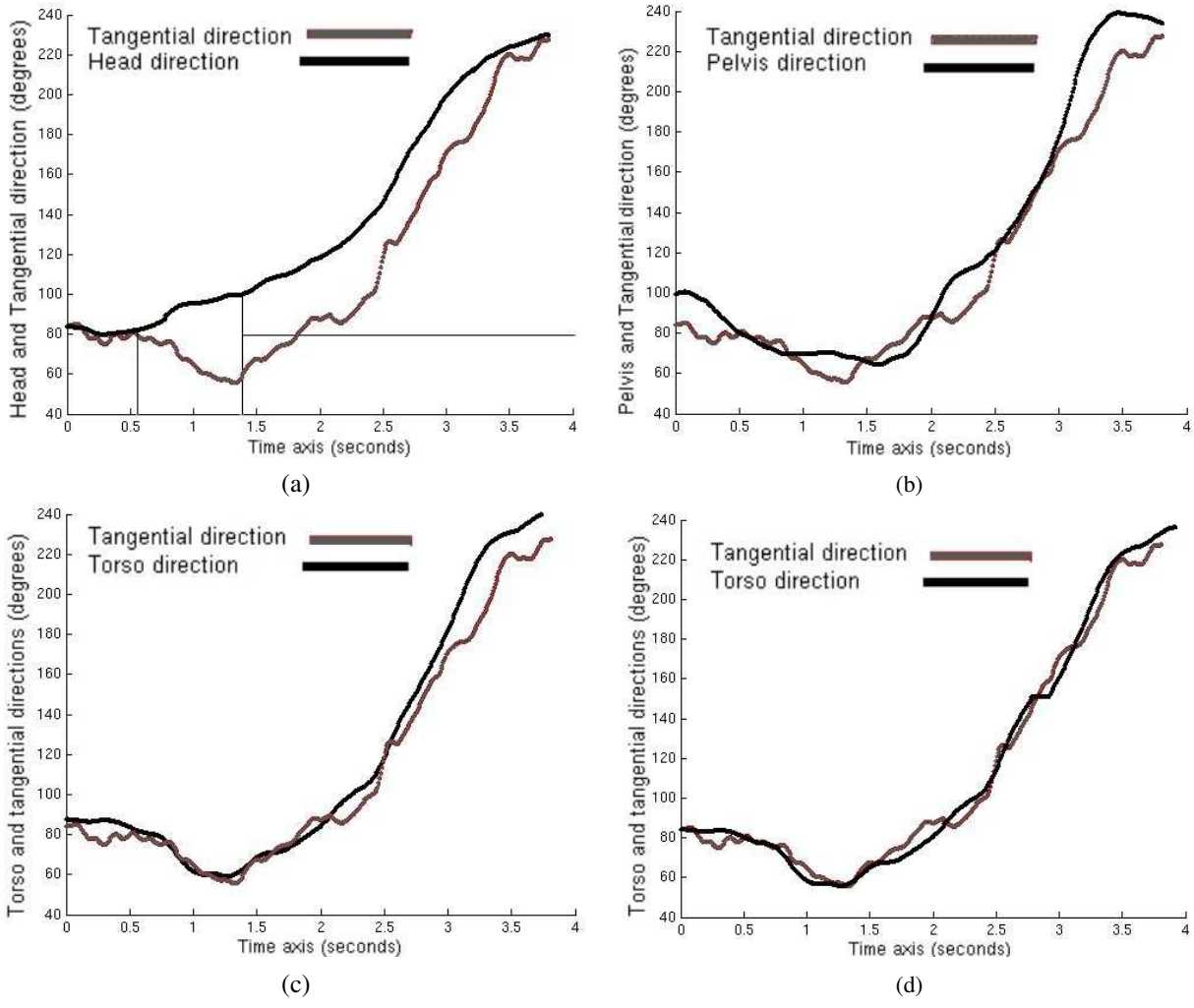

FIG. 4.3 – *Head, pelvis, torso and tangential direction profiles. All of them correspond to the same motion. (a) shows the head direction profile with respect to the tangential direction. (b) shows the pelvis direction profile with respect to the tangential direction. (c) shows the torso and the tangential directions. (d) shows the torso direction shifted* $\frac{1}{6}$*s backwards and the tangential direction.*

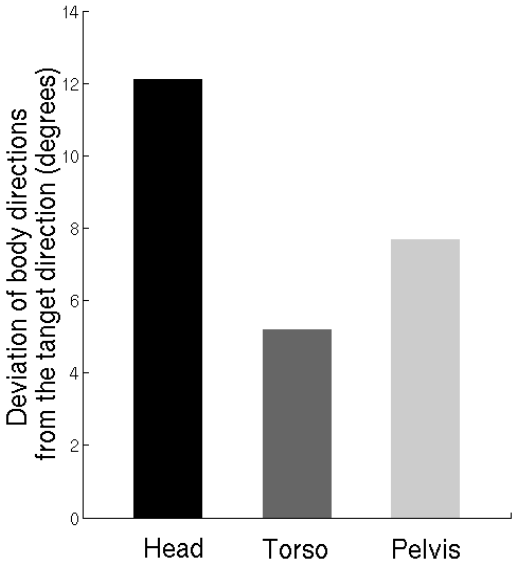

(a)

FIG. 4.4 – *The comparisons between the averaged deviations of the head, the torso and the pelvis directions with respect to the trajectory tangent direction in seven subjects.*

4.2.2 Torso direction profile

Choosing RF_T rather than RF_H, we observed that for every trajectory the curves traced by $\varphi_T(\tau)$ and $\theta(\tau)$ had a similar form. However, comparing $\varphi_T(\tau)$ and $\theta(\tau)$ in time, it is noted that $\varphi_T(\tau)$ is shifted between $\frac{1}{4}$ and $\frac{1}{8}$ s backwards (see Figure 4.3.c and Figure 4.3.d). It means that the torso as well as the head anticipate the direction relative to the current walking direction. In other terms

$$\dot{\varphi_T}(\tau+\varepsilon) \simeq \dot{\theta}(\tau) \tag{4.1}$$

where ε represents the time shifted backwards.

4.2.3 Pelvis direction profile

Examining $\varphi_P(\tau)$ relative to $\theta(\tau)$ while steering along a path, we observed that $\varphi_P(\tau)$ oscillates with an amplitude close to 15 degrees even along a curve (see Figure 4.3.b). These instantaneous variations reflect the significant influence of the gait cycle at each step. It could be possible to fit the curves of $\varphi_P(\tau)$ in agreement with the shape of $\theta(\tau)$ by filtering $\varphi_P(\tau)$ using a fourth-order low-pass filter algorithm with a cut-off frequency of 0.5 Hz. However, we did not apply any kind of filter to experimental data.

4.3 A control model of locomotion

To measure the error of the approximation expresed by Equation 4.1, we defined RF_T as the local reference frame of the body to perform numerical integration using the following control system :

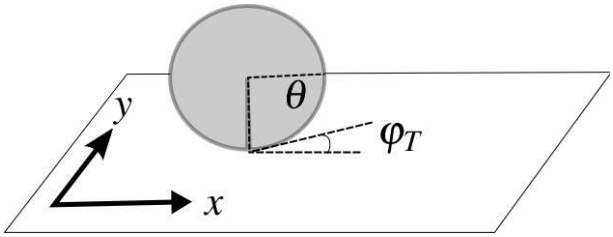

FIG. 4.5 – *The unicycle model.*

$$\begin{pmatrix} \dot{x_T} \\ \dot{y_T} \\ \dot{\varphi_T} \end{pmatrix} = \begin{pmatrix} \cos\varphi_T \\ \sin\varphi_T \\ 0 \end{pmatrix} u_1 + \begin{pmatrix} 0 \\ 0 \\ 1 \end{pmatrix} u_2 \tag{4.2}$$

The control inputs u_1 and u_2 are the linear and angular velocities respectively. The nonholonomic constraint expressed by the Equation 1.1 force the control system to move tangentially to its main axis (see Figure 4.5). We want to extract the control inputs from the trajectory followed by the torso in order to reconstruct the *same* trajectory but now by using the differential system 4.2. Thus, the integrated trajectory is determined by the choice of the initial condition which corresponds to the position and the direction of the torso. In this way, the nonholonomic hypothesis holds if the geometric shape of the recorded and the integrated trajectories is *similar*.

A parametric interpretation of the anticipation effect (delay of $\frac{1}{6}$s) can be considered within the control system. It can be seen as a bicycle as shown in Figure 4.6. Such kind of system has been used extensively in robotics [Laumond et al. 1998]. The equations describing the motion of the bicycle are given by :

$$\begin{pmatrix} \dot{x_T} \\ \dot{y_T} \\ \dot{\theta} \\ \dot{\varphi_T} \end{pmatrix} = \begin{pmatrix} \cos\theta \\ \sin\theta \\ \frac{\tan\varphi_T}{L} \\ 0 \end{pmatrix} u_1 + \begin{pmatrix} 0 \\ 0 \\ 0 \\ 1 \end{pmatrix} u_2 \tag{4.3}$$

where (x_T, y_T) denotes the position of the bicycle relative to some inertial frame, θ the angle of the bicycle relative to the horizontal axis, φ_T the angle of the front wheel relative to the bicycle, u_1 the driving speed, u_2 the steering rate and L is the length of the link between the back and the front wheel. For our purpose, L characterizes the anticipation effect represented previously by ε. We made a simple transformation from the delay ε to a distance L. Since the model is subject to rolling constraints, the Equation 1.1 must hold at every point along any achievable trajectory.

4.4 Experimental results

We observe that the trajectories performed by all subjects are similar both in geometric and kinematic terms. To validate our hypothesis, we perform several experiments on the differential system from

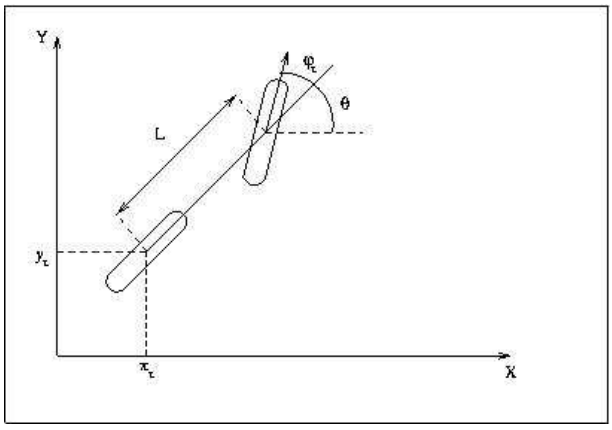

FIG. 4.6 – *Bicycle model.*

Equation 4.3.

In this section we describe the comparisons conducted to quantify, in our models, the instantaneous error of the recorded trajectory with respect to the simulated trajectory. We have defined the average and the maximal error between both trajectories.

It is important to emphasize that all the recorded trajectories have not been filtered. The data from each trial of each subject is analyzed separately (i.e., no averaging over trials is performed). Thus, for each trajectory represented by a sequence of discrete points on the plane, we use Equation 3.1 and Equation 3.2 to extract the linear $u_1(\tau)$ and angular $u_2(\tau)$ velocities. We then obtain the control inputs of the recorded locomotor trajectory expressed by RF_T.

Having the control inputs, we integrate the differential system (see Equation 4.3). Figure 4.7 shows some examples of the behavior of the recorded and integrated trajectories by translating the final position over both : the vertical and the horizontal axes with a fixed final direction. Figure 4.8 show some examples of recorded and integrated trajectories for a fixed final position. The final direction varies in intervals of $\frac{\pi}{6}$.

To measure how well the model approximates locomotor trajectories, we compute the difference between both trajectories at instant τ. To do that, we define the trajectory error TE such as

$$TE(\tau) = \sqrt{(x_i(\tau) - x_r(\tau))^2 + (y_i(\tau) - y_r(\tau))^2} \tag{4.4}$$

where $(x_i(\tau), y_i(\tau))$ and $(x_r(\tau), y_r(\tau))$ are the positions at instant τ of the integrated and recorded trajectories respectively. Then, we compute the averaged and the maximal trajectory errors

$$\begin{array}{rcl} ATE & = & \int_{\tau\in[0,T]} TE(\tau)d\tau \\ MTE & = & \max_{\tau\in[0,T]} TE(\tau) \end{array} \tag{4.5}$$

These two quantities indicate the similarity between the integrated and the recorded trajectories. Thus, small values of ATE and MTE mean that the similarity degree is high between both trajectories.

This procedure has been executed for 1,560 trajectories performed by seven subjects. The length of the paths ranged between 2 and 10 meters. The walking speed of the subjects was equal to 1.26

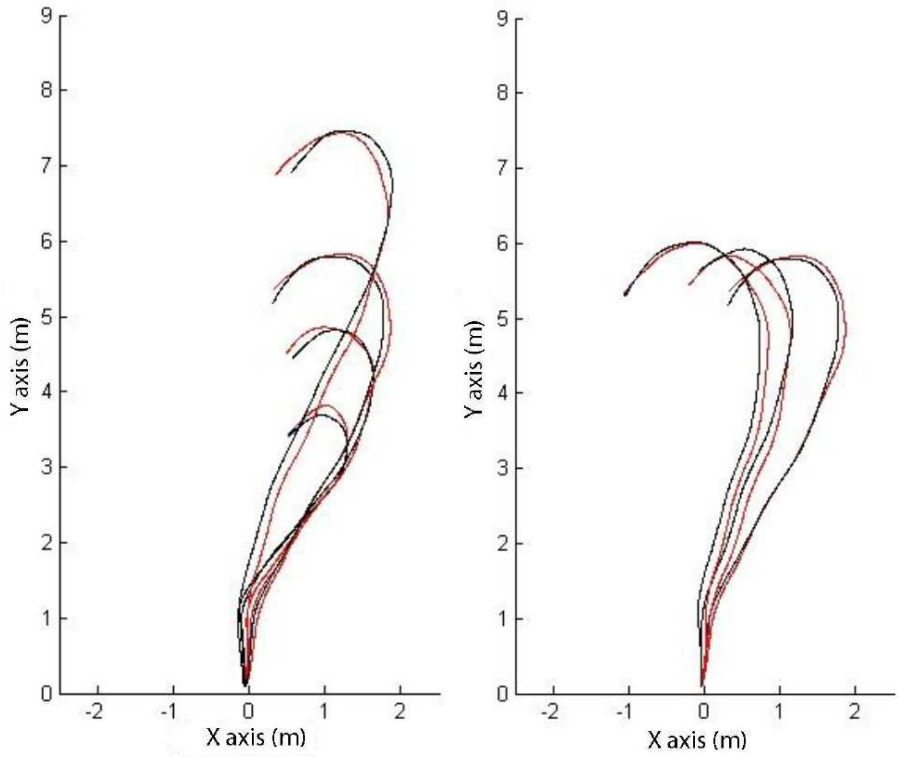

(a) (b)

FIG. 4.7 – *Representative examples of comparisons between recorded (red) and integrated (black) locomotor trajectories. (a) shows the behavior of the recorded and integrated trajectories by translating the final position in the vertical axis with a fixed final direction. (b) shows the behavior of the recorded and integrated trajectories by translating the final position in the horizontal axis with a fixed final direction.*

$\pm$0.3 meters/seconds. It is interesting to note that the model approximates 87 percent of trajectories with $ATE < 10$cm and $MTE < 20$cm.

The accuracy of the model is also supported by the fact that ATE and MTE are always lower than the averaged ATD and the maximal MTD trajectory deviations (see Figure 4.9). In other words, the integrated trajectory is always inside the area defined by the trial-to-trial variability of recorded trajectories. Consequently, locomotor trajectories represented by the position and direction of the torso reference frame are well approximated by the bicycle model.

4.5 Discussion

This model shows that human locomotion can be approximated by the motion of a nonholonomic system. Indeed, we were able to approximate more than 87 percent of the 1560 trajectories recorded from seven subjects during walking tasks with an averaged accuracy < 10cm everywhere along the paths. The path lengths ranged from 2 to 10 meters. Thus, nonholonomic constraints, similar to that described in wheeled robots, seem to be at work during human locomotion. Nevertheless, choosing different body

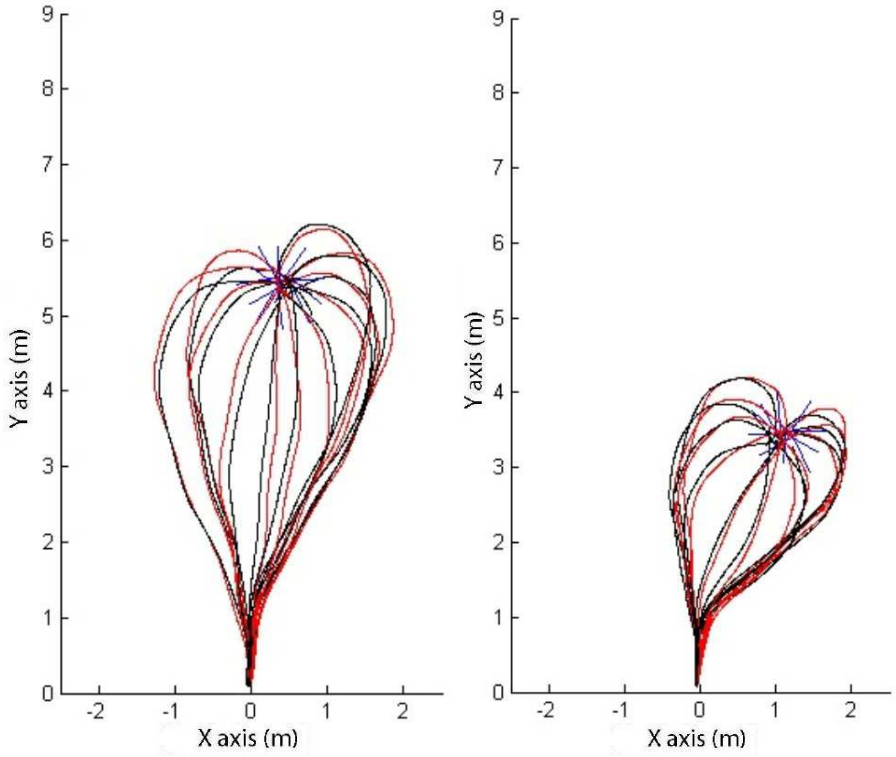

(a) (b)

FIG. 4.8 – *Representative examples of comparisons between recorded (red) and integrated (black) locomotor trajectories. (a) and (b) show the recorded and integrated trajectories for a fixed final position. The final direction varies in intervals of* $\frac{\pi}{6}$.

reference frames yields different results. We obtained the best results using the shoulder's segment. It appears that yaw oscillations induced by step alternation affect the head, torso or pelvis movements differently in such a way that only the shoulders' midpoint trajectory provided a good fit for our model's predictions. Further investigation is required to account for these differences.

In addition to the considerations relative to the geometric aspects of the trajectories, some motor aspects need to be mentioned here. Indeed, it can be argued that geometric configurations of human bodies are constrained, at the joint level, by anatomical parameters that limit a given rotation of a body segment within a certain space. For example, abduction/adduction movements of a given leg cannot cover a wide range of spatial configurations as it can be the case for the shoulders segment. Ground reaction forces also act first at the legs level and constraint indirectly the center of mass trajectory. Such a mechanical point of view has been investigated in biomechanics for the study of the human locomotion (see for instance [Winter 2004]), in computer animation (see for instance [Multon et al. 1999]) and in robotics for the study of the humanoid robots locomotion (see for instance the pioneering work [Raibert 1986] or the more recent worked out example of HRP robot [Hirukawa et al. 2005]).

Our approach differs from the previous ones since we do not consider sensory inputs or the whole complexity of mechanical system that models the human body. Our point of view is complementary and more macroscopic than the standard biomechanics approaches. Our study is devoted to analyze the

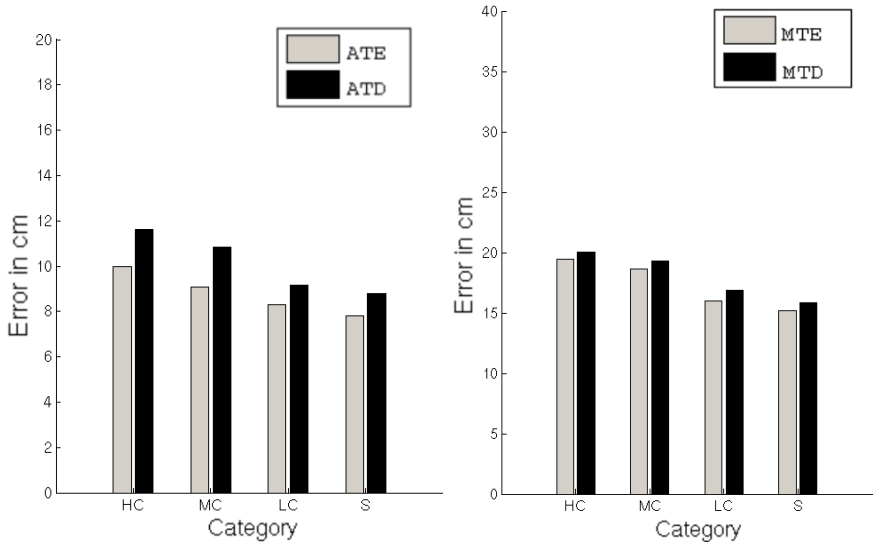

(a) (b)

FIG. 4.9 – *The accuracy of the model is also supported by the fact that the integrated trajectory is closer to the corresponding recorded trajectory than the trial-by-trial variability of recorded trajectories. (a) shows the comparison between the averaged trajectory errors (ATE) and the averaged trajectory deviations (ATD). (b) shows the comparison between the maximal trajectory errors (MTE) and the maximal trajectory deviations (MTD).*

steering of locomotion at the trajectory planning level. As a consequence of this neurophysiological perspective, appropriate experimental protocols have been defined to exhibit the behavior under study. Then, we have formalized the knowledge acquired by experimentation in terms of mathematical models already used for mobile robots [Li and Canny 1993; Laumond et al. 1998].

The present model is the starting point of the next stage of our work where we provide further evidence and details about how nonholonomic constraints are exerted during the generation of human locomotor trajectories. Our current model does not explain the geometric shape of the locomotion trajectories. Why is it that in some cases (see Figure 4.2) we are turning first on the right to finally reach a goal whose *position* is on the left of the starting configuration ? Such a difficult question is related to optimal control theory (e.g. [Sussmann 1990]) already successfully applied to mobile robotics (e.g. [Laumond et al. 1998]). Applying these tools as a way to aid in the understanding of human locomotion is the aim of the two following chapters.

5

The Geometric Shape of Locomotor Trajectories

We rely on the observation of the geometric shape of the locomotor trajectories in the simple 3-dimensional space of both the position and the direction of the body. These trajectories are the geodesics of the system that we try to identify according to some optimization principle. In Chapter 3 we presented the methodology we followed based on an experimental protocol involving seven subjects walking in a motion capture facility. The subjects were asked to pass through a fixed starting position and direction, and to cross over distant porches. Both position and direction in the room were changed over trials. Stereotyped trajectories were observed in the different subjects. In Chapter 4 we proposed a control model accounting for human locomotion. The current chapter aims at understanding the shape of the trajectories via optimal control. We investigate different possible strategies underlying the formation of human locomotor trajectories in goal-directed walking.

The central idea to understand the shape of trajectories has been to relate this problem to an optimal control scheme : the trajectory is chosen according to some optimization principle. This is our basic starting assumption (see Section 5.1). The subjects being viewed as a controlled system, we tried to identify several criteria that could be optimized. Is it the time to perform the trajectory ? the length of the path ? the minimum jerk along the path ?...

In Section 5.2 we define a dynamic extension of System 4.2. First, we apply nonlinear control tools to ensure that the system is controllable. Then, we combine existing optimal control tools for nonlinear systems. The use of a numerical algorithm is strongly justified since, for the kind of problem we address, there is no available technique providing a complete and exact analytical solution to obtain explicit information about the geometric shape of locomotor trajectories. However, there exists a difficulty in the numerical techniques associated to its sensitivity analysis. In Section 5.3 we describe the tuning of the algorithm to search a good parametrization of the algorithm.

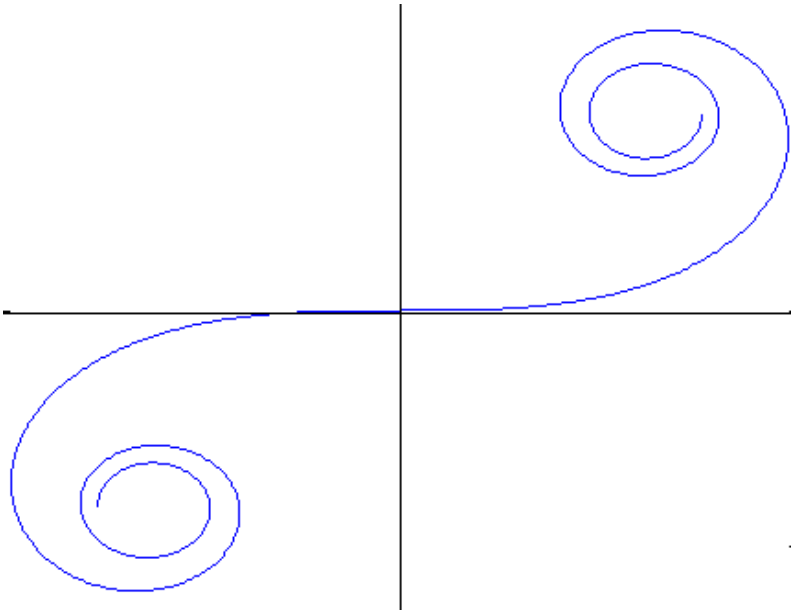

FIG. 5.1 – *Cornu spiral or clothoid is a curve whose curvature grows with the distance from the origin.*

We argue that the variation (time derivative) of the curvature of the locomotor paths is minimized. In Section 5.4, we show that the human locomotor trajectories are well approximated by the geodesics of a differential system minimizing the L_2 norm of the control. Such geodesics are made of arcs of clothoids.

Clothoids are used for trajectory smoothening in Robotics [Kanayama and Miyake 1986; Shin and Singh 1990; Fleury et al. 1993]. A clothoid, also known as a Cornu spiral, is a curve along which the curvature κ depends linearly on the arc length and varies continuously from $-\infty$ to $+\infty$ (see Figure 5.1). Its equation is $\kappa = cs + \kappa_0$ where s is the arc length, κ_0 the initial curvature and c is the sharpness or a constant characterizing the shape of the clothoid. Clothoid curves correspond to the minimum-length continuous-curvature paths under a centripetal peak-jerk constraint (i.e. the jerk is proportional to the slope of the curvature pattern). Nevertheless, other types of continuous-curvature curves for mobile robots have been proposed. A different type from the one first considered is the *cubic spiral* [Kanayama and Hartman 1989]. It is a curve along which the curvature is a cubic function on the arc length. This type of curve corresponds to minimizing the integral of the square of the centripetal jerk (i.e. it has a curvature function that is parabolic in shape). The cost function used in [Kanayama and Hartman 1989] to smooth a given path is

$$J = \int_0^T L ds = \int_0^T \dot{\kappa}^2 ds$$

where κ is the curvature. The tangent direction θ is given by

$$\theta(s) = \int_0^s \kappa(t) dt$$

Therefore, $\dot{\kappa} = \ddot{\theta}$. By calculus of variations we obtain

$$\begin{array}{rcl} \frac{\partial L}{\partial \theta} - \frac{d}{ds}\frac{\partial L}{\partial \dot{\theta}} + \frac{d^2}{ds^2}\frac{\partial L}{\partial \ddot{\theta}} & = & 0 \\ 2\frac{d^2}{ds^2}\ddot{\theta} & = & 2\frac{d^4\theta}{ds^4} \end{array}$$

By integrating four times we obtain that $\theta(s)$ is a cubic function (i.e. the curvature profile is parabolic in shape). Moreover, a generalization of the clothoid and cubic spiral curves are the *intrinsic splines* whose curvature is a polynomial function of the arc length [Delingette et al. 1991].

5.1 An optimal control approach

Our approach has been conducted as follows :

Given a control system, the reachable space and optimal trajectories, what is the optimal criterion that steers the system ? Not only is the question opposite to that of the classical optimal control problem (i.e. what are the trajectories which optimize a given criterion ?), but it also pretends to account for a "*global*" point of view while most of the theoretical results hold only locally. Our work takes advantage of both analytical and numerical approaches to optimal control. First, we apply analytical methods to characterize locally the geometric shape of the geodesics. Then we apply a numerical optimization algorithm to validate the following hypothesis : locomotor trajectories are well approximated by the optimal solutions of a dynamic extension of a simple unicycle control model. The validation method consists in comparing the optimal trajectories of the system with the trajectories of the data basis.

As a consequence of this study, we will see that it is possible to model some decision processes answering natural questions such as : should I reach a given goal by the left or by the right ?

5.2 Optimizing the derivative of the curvature

Consider a given task such as walking on the ground level in absence of obstacles from a pre-defined initial position and direction to cross over a distant door. Given all possible ways to achieve the task, it is surprising that the selected trajectory is highly stereotyped between subjects and also between repetitions of the same task. The question we address in this part of the study is to find what should be the criterion to be optimized given the experimental data and a model [Moylan and Anderson 1973; Ng and Russell 2000]. Unfortunately, it is not evident to answer this question in the context of motor control even if it could be more useful. Nevertheless, some tools of optimal control theory are still useful to characterize optimal trajectories. These tools are used to minimize different cost functions to predict locomotor trajectories that verify the nonholonomic constraints. Here we introduce a dynamic extension of System 4.2.

5.2.1 The unicycle model with inertial control law

The neuroscience approaches in modeling human motion pointed out the critical role of the curvature [Lacquaniti et al. 1983; Viviani and Flash 1995; Todorov and Jordan 1998; Vieilledent et al. 2001; Richardson and Flash 2002]. To prevent curvature discontinuities, we propose to make the curvature a

variable of the system. We then consider a dynamic extension of System 4.2 by controlling the time derivative of the curvature instead of the angular velocity.

$$\begin{pmatrix} \dot{x_T} \\ \dot{y_T} \\ \dot{\varphi_T} \\ \dot{\kappa_T} \end{pmatrix} = \begin{pmatrix} \cos\varphi_T \\ \sin\varphi_T \\ \kappa_T \\ 0 \end{pmatrix} u_1 + \begin{pmatrix} 0 \\ 0 \\ 0 \\ 1 \end{pmatrix} u_2 \tag{5.1}$$

The control inputs u_1 and u_2 are, for this system, the linear velocity and the time derivative of the curvature respectively. The nonholonomic constraint is expressed by the same Equation 1.1. By applying the lie algebra rank condition (LARC [Sussmann 1990], see Section 2.7.1) on this control system, it is proved to be controllable. First, we observe that the lie algebra of vector fields g_1 and g_2 is of dimension 4 at each point (i.e. $\forall q \in R^4$) such as

$$g_3(q) = [g_2, g_1](q) = \begin{pmatrix} 0 \\ 0 \\ 1 \\ 0 \end{pmatrix} \quad g_4(q) = [g_3, g_1](q) = \begin{pmatrix} -\sin\varphi_T \\ \cos\varphi_T \\ 0 \\ 0 \end{pmatrix}$$

and

$$det \begin{bmatrix} \cos\varphi_T & 0 & 0 & -\sin\varphi_T \\ \sin\varphi_T & 0 & 0 & \cos\varphi_T \\ \kappa_T & 0 & 1 & 0 \\ 0 & 1 & 0 & 0 \end{bmatrix} = -1$$

This means that any configuration can be reached from any other one (for an overview see [Laumond et al. 1998]). For System 5.1, the family of vector fields $\{g_1, g_2\}$ defines a 2-dimensional distribution on the $R^2 \times S^1 \times R$ manifold M. At each point $q \in M$ the vector fields $\{g_1, g_2, g_3, g_4\}$ define a basis of the tangent space T_qM (i.e. they are linearly independent). Consequently, the System 5.1 is controllable (i.e. the dimension of $LA(g_i) = n$).

5.2.2 Optimal steering of the control model : PMP analysis

Here we consider the problem of steering the System 5.1 from an initial state $q(0) = q_0$ to a final state $q(T) = q_f$ assuming $u_1 \in [a,b]$ with $a > 0$ (forward motion) and $u_2 \in [-c,c]$. The cost function is given by

$$J = \frac{1}{2}\int_0^T <(u(\tau), u(\tau))> d\tau \tag{5.2}$$

which corresponds to the least-squares optimal control problem. To find a set of control inputs, that minimizes the cost J and steers the system from q_0 to q_f, we apply the Pontryagin's maximum principle (PMP). The PMP states that if u is an admissible control then $u(\tau)$ and the trajectory $q(\tau)$ are optimal if there exists a nonzero continuous vector function ψ associated to $q(\tau)$ such that $u(\tau)$ maximizes the

Hamiltonian function for all $\tau \in [0,T]$. It should be emphasized that PMP provides a set of necessary rather than sufficient conditions for optimality (see Section 2.9.1). The Hamiltonian H is defined by

$$H = \frac{1}{2}(u_1^2 + u_2^2) + \psi_1 \cos\varphi_T u_1 + \psi_2 \sin\varphi_T u_1 + \psi_3 \kappa_T u_1 + \psi_4 u_2$$

To determine the control that minimizes H, it is necessary that

$$\frac{\partial H}{\partial u} = 0 \quad \begin{cases} u_1 + \psi_1 \cos\varphi_T + \psi_2 \sin\varphi_T + \psi_3 \kappa &= 0 \\ u_2 + \psi_4 &= 0 \end{cases}$$

So we have the adjoint system $\dot{\psi} = -\frac{\partial H}{\partial q}$ (for every $\tau \in [0,T]$) :

$$\dot{\psi} = \begin{cases} \dot{\psi}_1 &= 0 \\ \dot{\psi}_2 &= 0 \\ \dot{\psi}_3 &= \psi_1 \sin\varphi_T u_1 - \psi_2 \cos\varphi_T u_1 \\ \dot{\psi}_4 &= -\psi_3 u_1 \end{cases}$$

By differentiating the optimal controls[1] we obtain the following expressions :

$$\begin{aligned} \dot{u}_1 &= -\psi_3 u_2 \\ \dot{u}_2 &= \psi_3 u_1 \end{aligned}$$

We therefore get :

$$\begin{aligned} u_2 \dot{u}_2 &= -u_1 \dot{u}_1 \\ u_1^2 + u_2^2 &= constant \end{aligned} \tag{5.3}$$

This result is not surprising (see Section 2.9.2). The general case has been proved in [Sastry and Montgomery 1992][2] . It has not been possible to deduce more information from the maximum principle. Considering the statistical analysis performed on the trajectory data basis (see Section 3.3), it appears that the u_1 control remains "reasonably" constant along the trajectories (the subjects were asked to enter the room by the starting configurations while not stopping at the goals). Then we deduced that u_2 is a piecewise constant function. A curve followed at constant velocity while linearly increasing or decreasing the curvature is known as being a clothoid. Finally we concluded on the conjecture that locomotor trajectories are made of clothoid arcs.

The proof of that conjecture required the effective computation of the optimal trajectories for System 5.1 with the cost function 8.9. Analytical solutions are out of the scope of the current state of the art. Then, we fell back on numerical optimization algorithms. Because the System 5.1 is nonlinear, we made use of the numerical algorithm proposed in [Fernandes et al. 1994] (see Section 2.10).

[1] We suppose that u_1 and u_2 are C^2 which is a reasonable assumption.

[2] Note : However the result only holds if $u_2 \not\equiv 0$. In the numerical analysis we performed u_2 is never zero over a non empty time interval for the considered reachable space. The case $u_2 \equiv 0$ (arcs of a circle and straight line segments) may appear for long range paths.

Algorithm 5.1: A numerical optimization algorithm for optimal paths

input : 1. Initial and final configurations : q_0 and $q_f \in R^n$
2. A distribution $B(q) \in R^{n\times m}$
output: The control input $u(\tau) \in R^m$, $\tau \in [0,T]$, linking q_0 to q_f

begin
Step 0 : Choose an orthonormal basis Φ as in Equation 5.4 ;
Step 1 : Initialize $\alpha_0 \neq 0$ by some random process;
Step 2 : Choose $\rho > 0$ and $\mu > 0$;
Step 3 : Solve the set of differential equations

$$\begin{cases} \dot{q} = B(q)\Phi\alpha, & q(0) = q_0 \\ \dot{Y} = XY + B\Phi, & Y(0) = 0 \end{cases}$$

Step 4 : Set $f(\alpha) = q(T)$ and $A = Y(T)$;
Step 5 : Update α according to

$$\alpha = \alpha - \mu(\rho I + A^t A)^{-1}(\rho\alpha + A^t(f(\alpha) - q_f))$$

Step 6 : Compute $J(\alpha) = \frac{1}{2}(\alpha^2 + \gamma\|f(\alpha) - q_f\|^2)$
If $q(T) \simeq q_f$ *and* $J(\alpha)$ *ceases to decrease* **Then**
exit;
Else
repeat **Step 2;**
End
end

5.2.3 Applying the numerical optimization algorithm

The principle of the numerical method used in this study has been described in Section 2.10. Applying the optimization method to System 5.1, we have $q = (x_T, y_T, \varphi_T, \kappa_T)$, then

$$B(q) = \begin{pmatrix} \cos\varphi_T & 0 \\ \sin\varphi_T & 0 \\ \kappa_T & 0 \\ 0 & 1 \end{pmatrix}$$

And the Jacobians of the column vectors of B with respect to q are given by :

$$\frac{\partial B^1}{\partial q}(q) = \begin{pmatrix} 0 & 0 & -\sin\varphi_T & 0 \\ 0 & 0 & \cos\varphi_T & 0 \\ 0 & 0 & 0 & 1 \\ 0 & 0 & 0 & 0 \end{pmatrix} \text{ and } \frac{\partial B^2}{\partial q}(q) = 0$$

We also need to represent the control inputs u over the basis of N vectors given by the following functions :

$$\begin{array}{ll}
\mathbf{e}_1(\tau) = (1,0)^t & \mathbf{e}_2(\tau) = (0,1)^t \\
\mathbf{e}_3(\tau) = (cos(\frac{2\pi\tau}{T}),0)^t & \mathbf{e}_4(\tau) = (0,cos(\frac{2\pi\tau}{T}))^t \\
\mathbf{e}_5(\tau) = (sin(\frac{2\pi\tau}{T}),0)^t & \mathbf{e}_6(\tau) = (0,sin(\frac{2\pi\tau}{T}))^t \\
. & . \\
. & . \\
. & . \\
\mathbf{e}_{N-3}(\tau) = (cos(\frac{2N\pi\tau}{T}),0)^t & \mathbf{e}_{N-2}(\tau) = (0,cos(\frac{2N\pi\tau}{T}))^t \\
\mathbf{e}_{N-1}(\tau) = (sin(\frac{2N\pi\tau}{T}),0)^t & \mathbf{e}_N(\tau) = (0,sin(\frac{2N\pi\tau}{T}))^t
\end{array}$$

Let us define by Φ the $m \times N$ matrix whose columns are the basis elements as

$$\Phi = \begin{pmatrix} \mathbf{e}_1(\tau) & \mathbf{e}_2(\tau) & ... & \mathbf{e}_{N-1}(\tau) & \mathbf{e}_N(\tau) \end{pmatrix} \tag{5.4}$$

where $u = \Phi\alpha$. To compute a solution of the problem, a variation of the Newton's algorithm to update α is used. The Algorithm 5.1 computes a trajectory between two given configurations. Applying the optimization method 5.1 to System 5.1, the matrices $X(\tau)$ and $B(\tau)$ have the following structures :

$$X(\tau) = \begin{pmatrix} 0 & 0 & -u_1 \sin\varphi_T & 0 \\ 0 & 0 & u_1 \cos\varphi_T & 0 \\ 0 & 0 & 0 & u_1 \\ 0 & 0 & 0 & 0 \end{pmatrix} \quad B(\tau) = \begin{pmatrix} \cos\varphi_T & 0 \\ \sin\varphi_T & 0 \\ \kappa_T & 0 \\ 0 & 1 \end{pmatrix}$$

The α vector cannot be zero when initializing the algorithm. The convergence rate depends on different factors as

- the start point of the algorithm represented by α_0,
- the initial choice of ρ and μ,
- the dimension of the smooth linearly independent functions spanned by $\mathbf{e_1}(\tau), ..., \mathbf{e_1}_N(\tau)$, and
- the evaluation of ρ and μ at each iteration.

5.3 Sensitivity analysis of the numerical approach

Because we used a numerical optimization algorithm to find the optimal solutions, we had to determine the sensitivity of the optimum to a small perturbation in the parameter values. It is possible for the Algorithm 5.1 to converge to different optimal solutions α_* depending on the start point α_0. We therefore started the algorithm with an α_0 of small (non-zero) norm which is otherwise arbitrarily selected. In practice, we have tested a large range of initial solutions α_0 until we have identified some of the invariant features of unsuccessful start points α_0. During the tuning stage, we also identified a set of good α_0 regardless of the target to be reached. We observed that extracting the α_0 from the control signals of the real trajectory or the Dubins' solutions, the algorithm always converged to an optimal solution.

We obtained good results by setting the dimension $N = 20$ of the basis Φ. The other parameters in the algorithm are stepsize factor μ and penalty coefficient ρ. A typical initial value for μ is 0.1 but this can be varied at any time during the progress of the algorithm depending on the cost reduction. The

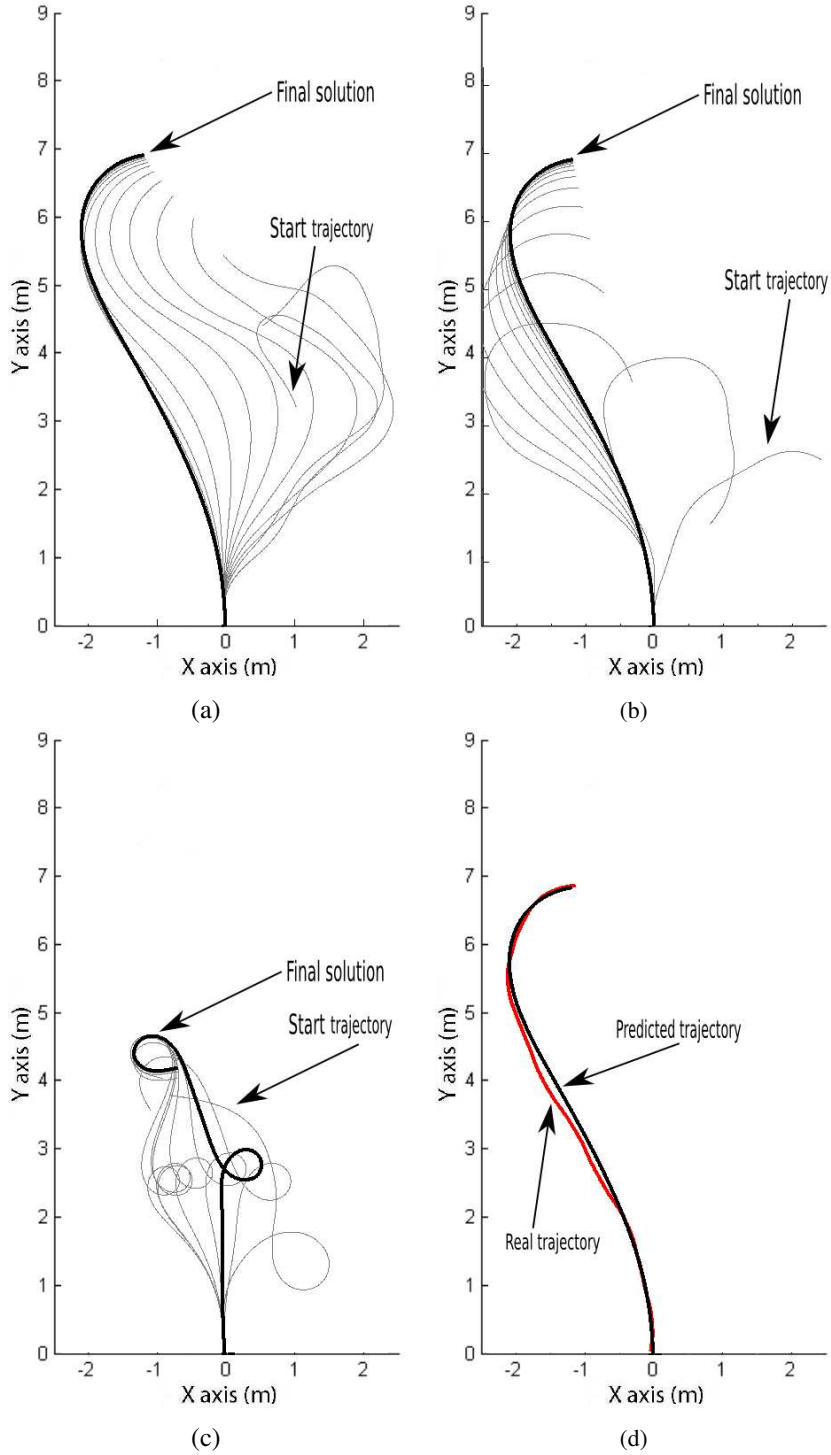

FIG. 5.2 – *Representative examples of initial solutions α_0 to start the numerical optimization algorithm. All trajectories correspond to the same initial and final configurations. (a), (b) and (c) show the iterative procedure (red trajectories) performed by the algorithm to find the optimal (black) control-effort trajectory. (a) and (b) illustrate successful cases where the algorithm converge to the same solution given two different start points α_0. (c) shows an unsuccessful case. We identified that if α_0 represents a trajectory containing spirals then the algorithm may not converge or the solution is not the correct one. (d) shows the accuracy of the predicted trajectory relative to the real one.*

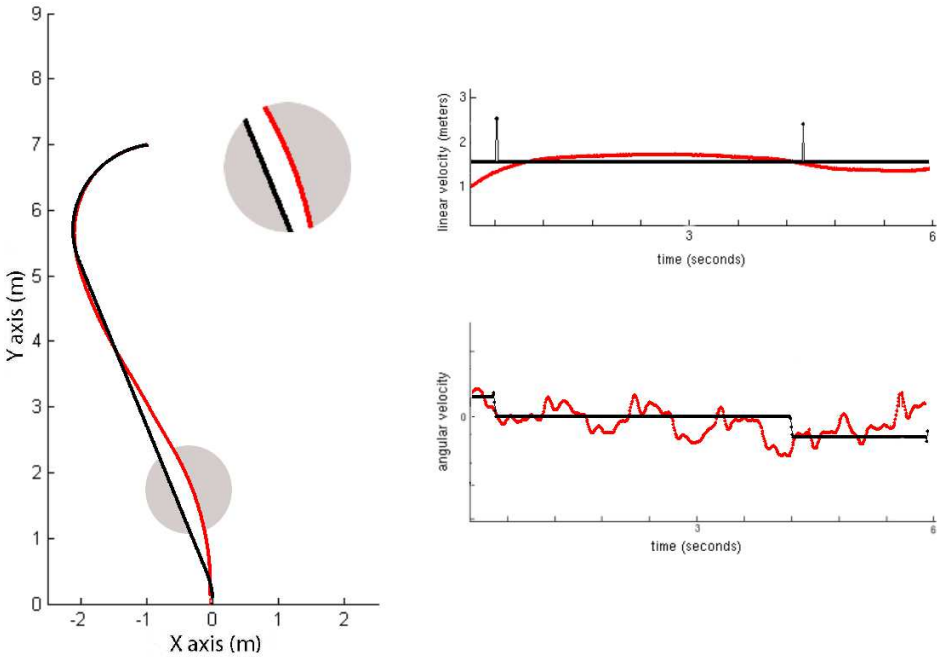

FIG. 5.3 – *Left : a representative example of a recorded trajectory performed by one subject (red) and the predicted time optimal trajectory linking the same initial and final configurations (black). Right : the comparison between the control inputs extracted from the recorded trajectory and the computed optimal control inputs.*

penalty coefficient ρ is initially set to a low value, say 0.1, and after some iterations, ρ varied until 0.5. The algorithm terminates if the $q(T) - qf$ is small and the cost function cannot decrease any more. Otherwise, the value of the penalty is increased and the algorithm continues for more iterations.

We performed exhaustive tests and we found that by using the above parameter settings the convergence of the algorithm results to be good enough both in terms of accuracy and robustness. Figure 5.2 illustrates the behavior of the algorithm using different initial values of α_0 for a representative target.

5.4 Experimental results

In this section, we show some results obtained by applying optimal control techniques to System 4.2 and System 5.1.

First, we considered the time optimal paths for System 4.2. The optimal solutions correspond to Dubins' method : at most six paths linking the given initial and final configurations are computed, and the shortest path is selected. However, the recorded trajectories are not well approximated by Dubins' solutions as we will show below.

The second cost function we tested was the control-effort expended. To compute optimal paths minimizing this criterion, we used the numerical optimization approach described in Section 5.2.3. We applied the above algorithm to find the optimal paths for System 4.2. The results were not satisfactory. This has been the motivation to envisage the differential system with inertial control law with two control

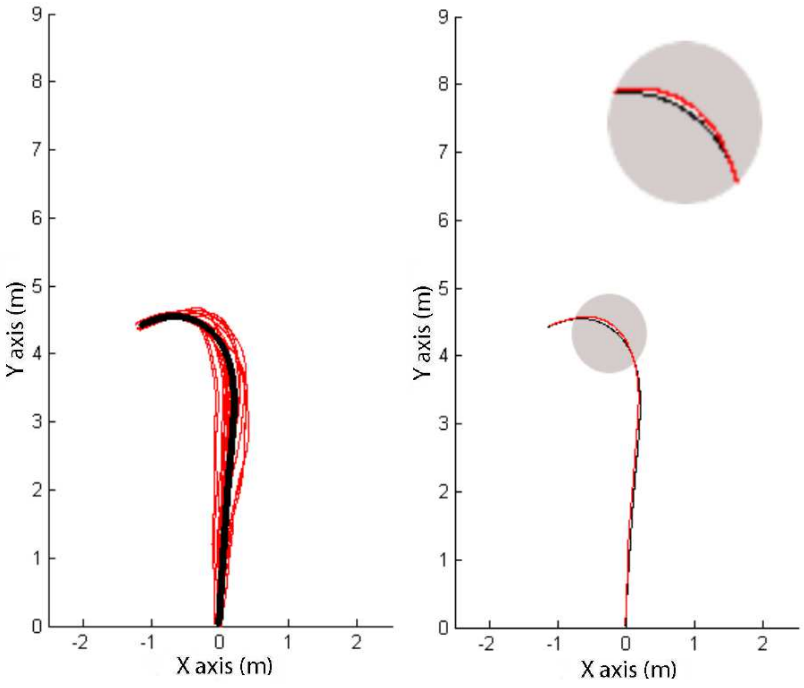

(a) (b)

FIG. 5.4 – *Representative example of statistics computed over the entire movement for the same initial and final configurations. Each subject has done 3 trials. (a) shows the real (red) trajectories performed by seven subjects with respect to predicted (black) optimal control-effort trajectory. All these trajectories correspond to the same initial and final configuration. It illustrates the variability pattern and the predicted trajectory. (b) shows the mean trajectory from real ones (red) and the predicted optimal control-effort trajectory linking the same initial and final configurations (black).*

inputs : the linear velocity and the time derivative of the curvature. The model is given by Equation 5.1. To validate these models, we compared the predicted trajectories to the recorded ones. It is important to emphasize that all the real trajectories have not been filtered.

5.4.1 Dubins' car for human locomotion

We tested the model 4.2 for all trajectories of the data basis performed by the seven subjects. The cost function to be minimized is

$$J = \int_0^T dt = T \tag{5.5}$$

The optimal paths for a car moving forward with constant velocity (i.e. $u_1 = 1$) was first addressed in [Dubins 1957]. Because the modulus of the linear velocity keeps constant, therefore, the minimum time problem becomes equivalent to the shortest path problem. The control variable is the angular velocity u_2. The problem has been revisited again by applying the PMP with geometric reasoning (see the works [Pecsvaradi 1972; Sussmann and Tang 1991; Souères and Boissonnat 1998] for the formal analysis of the solution). It has been shown that the extremal controls for this problem are not unique. Thus, the

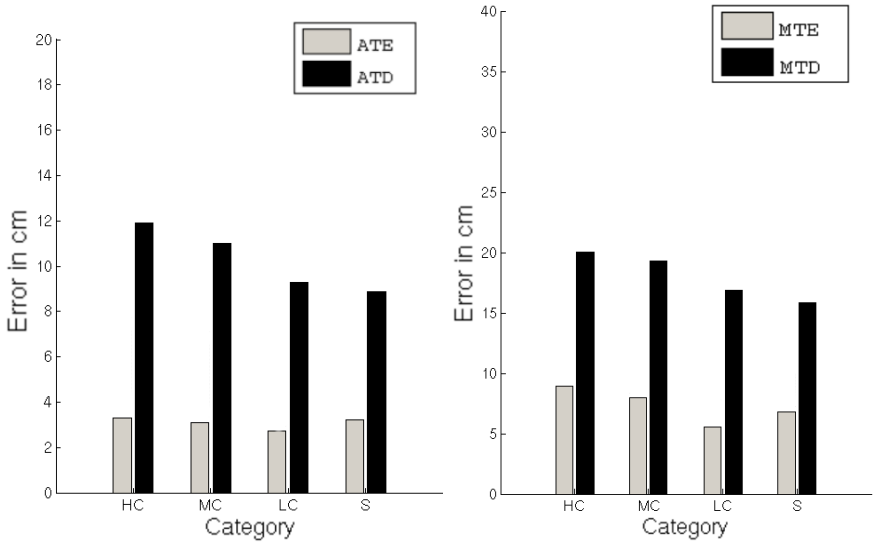

(a) (b)

FIG. 5.5 – *The accuracy of the model is also supported by the fact that the predicted trajectory is closer to the corresponding recorded trajectory than the trial-by-trial variability of recorded trajectories. (a) shows the comparison between the averaged trajectory errors (ATE) and the averaged trajectory deviations (ATD). (b) shows the comparison between the maximal trajectory errors (MTE) and the maximal trajectory deviations (MTD).*

problem becomes singular and the PMP do not give enough information concerning the extremal control function. However, it has been proved that the shortest paths are made of finite sequences of arcs of a circle with constant minimal radius C ($u_2 = \pm 1$) and straight line segments S ($u_2 = 0$). Moreover, the complete characterization of the structure of the optimal control function has been determined. There exist six types of optimal paths, each of them is composed by three parts which are either C or S. Thus, the number of switches of u_2 is at most twice in the interval $[0, T]$. Because the radius of curvature is fixed, curvature discontinuities appear at each concatenation point between two segments. From left to right Figure 2.8 illustrates the types $R_{\tau_1} S_{\tau_2} L_{\tau_3}$, $R_{\tau_1} S_{\tau_2} R_{\tau_3}$ and $L_{\tau_1} R_{\tau_2} L_{\tau_3}$ of optimal paths. An arc of a circle C can be followed in two opposite directions, either clockwise (denoted R for right arc) or counterclockwise (denoted L for left arc). For instance, the first sequence may be phrased as, "Start turning right at constant minimal radius during time τ_1, then go straight line during time τ_2 and finally turn to the left at constant minimal radius during time τ_3". These combinations generate "words" that will be revisited in the next chapter.

In order to compute the Dubins' solution for human locomotion, we had to select the appropriate radius of curvature. As a matter of fact, the selection of the radius of curvature represents a critical input of the problem. This is because *a priori* finding a constant minimal radius of the human body does not have a concrete meaning. Moreover, if the optimal solution results to be a good prediction of locomotor trajectories, then, it means that when humans turn, they turn always with a constant radius of curvature. Indeed, as we have mentioned, when constructing optimal trajectories with a fixed radius of curvature a discontinuity occurs at each concatenation point.

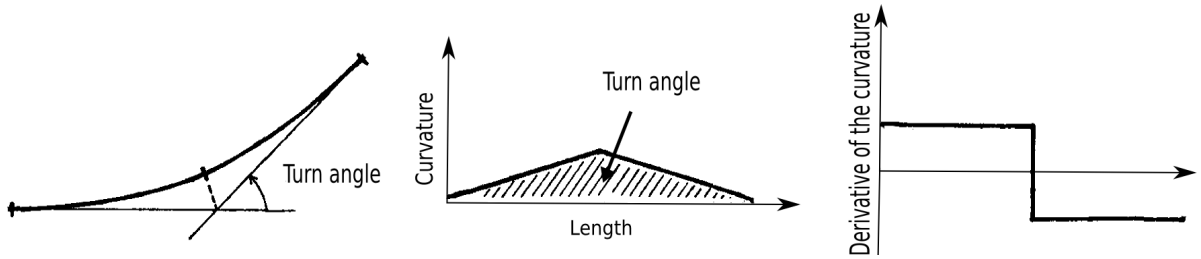

FIG. 5.6 – *Left : the concatenation of a pair of clothoid arcs. Middle : the curvature pattern. Right : the time derivative of the curvature.*

Figure 5.3 shows a representative recorded trajectory performed by one subject and the predicted time optimal trajectory linking the same initial and final configurations. The picture also illustrates the comparison between the control inputs extracted from the recorded trajectories and the optimal control inputs. We have adjusted by hand the radius of curvature until the geometric shape of both trajectories fit as closely as possible.

Comparing the optimal trajectories with respect to the recorded ones, we noted important differences both in the geometric shape of such trajectories as well as in the control signals. These discrepancies are caused by the fact that when minimizing the length the optimal trajectory must be as stretched as possible so that the curved segments (if they exist) are at the beginning and at the end of the trajectory. Whereas the trajectories performed by all the subjects tend to propagate the effort expended (energy) along the trajectory.

5.4.2 The unicycle model with inertial control law for human locomotion

We applied the numerical optimization algorithm described in Section 5.2.3 to determine the optimal control-effort trajectories for System 5.1. We proceeded to predict all trajectories performed by seven subjects given the initial and final configurations and the cost function to be minimized. In this case, the final time was an input to the problem. Then, we used the final time of the recorded trajectory for targets that only one of the subjects did. Consequently, the duration of motion between recorded and predicted trajectories was the same.

For the subset of targets that were reached by all the subjects, we computed the mean final time of recorded trajectories associated to the same target. Thus, the mean final time served as the input to compute predicted trajectories.

To examine the trial-to-trial and subject-to-subject variability for the same plan, we considered the geometric mean as the statistical measure. Because each subject did not spend the same time performing the task (even from trial to trial the duration of the motion is different), we used the duration of the predicted trajectory as the reference in order to compare all recorded trajectories with respect to the predicted one. We then computed the mean at instant $\tau \in [0, T]$ (see Figure 5.4.a). In this way, it appears that the geometric shape of the mean trajectory (from experimental data) is highly close to the optimal control-effort trajectory (predicted). It can be seen in Figure 5.4.b that the prediction gives a reasonable fit of the experimental data.

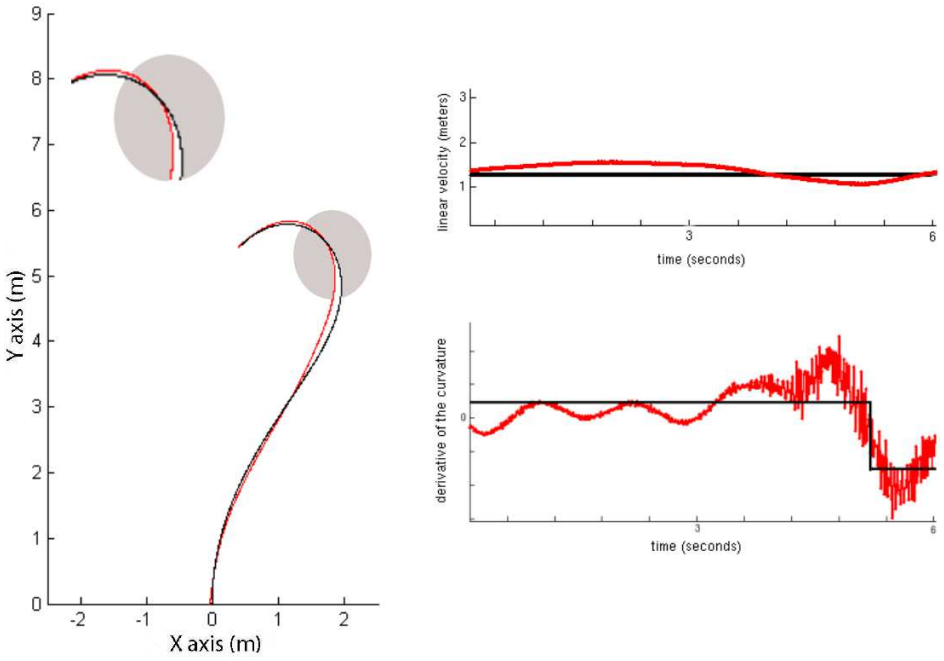

FIG. 5.7 – *Representative examples of comparisons between real (red) and predicted (black) locomotor trajectories. Left : a real trajectory performed by one subject (red) and the predicted optimal control-effort trajectory linking the same initial and final configurations (black). Right : the comparison between the control inputs extracted from the real trajectory (filtered) and the computed optimal control inputs extracted from the optimal control-effort trajectory.*

To measure how well the model predicts locomotor trajectories, we considered the position $(x_r(\tau), y_r(\tau))$ and $(x_p(\tau), y_p(\tau))$ at instant τ of the real and the predicted trajectories respectively. The distance error $TE(\tau)$ between both trajectories at instant τ is defined by Equation 4.4. Then, we computed the average ATE and the maximal MTE trajectory errors given by Equation 4.5. These two quantities indicate the similarity between the predicted and the recorded trajectories. Thus, small values of ATE and MTE mean that the similarity degree is high between both trajectories.

This procedure has been executed on the 1,560 trajectories performed by seven subjects. It is interesting to note that the model approximates 90 percent of trajectories with an averaged error < 10cm and a maximal error < 20cm.

The accuracy of the model is also supported by the fact that ATE and MTE are always lower than the averaged ATD and the maximal MTD trajectory deviations for the subset of trajectories performed by all subjects (see Figure 5.5). In other words, the predicted trajectory is always inside the area defined by the trial-to-trial variability of recorded trajectories. Consequently, this study proves that :

- **the locomotor trajectories are well approximated by the optimal solutions of a dynamic extension of a simple unicycle model, and**
- **the locomotor trajectories minimize the time derivative of the curvature.**

The statistical analysis shows that u_1 control remains "reasonably" constant over the whole interval of time. Moreover, by applying the numerical optimization algorithm we observed that the resulting

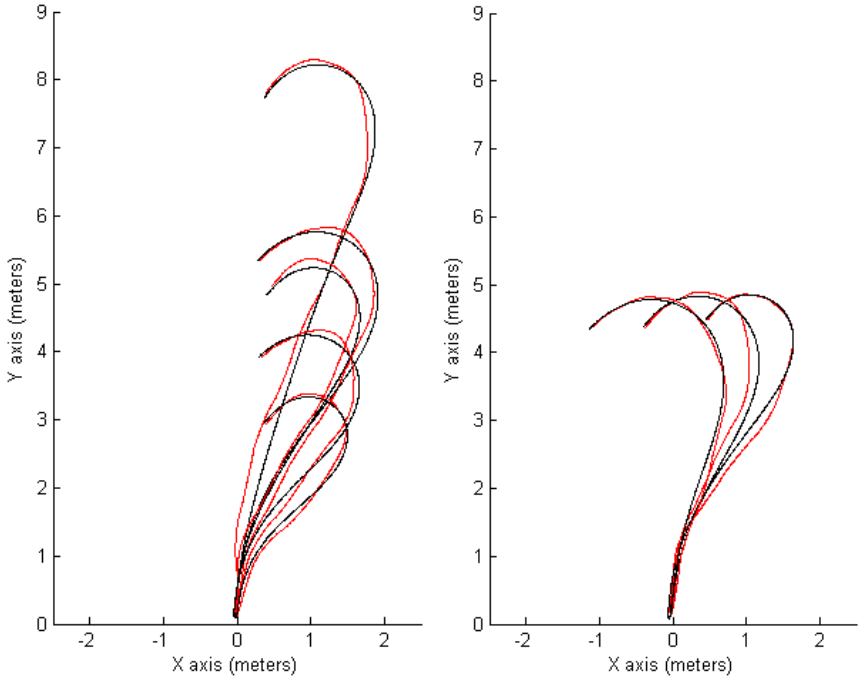

(a) (b)

FIG. 5.8 – *Representative examples of comparisons between real (red) and predicted (black) locomotor trajectories. (a) shows the behavior of the real and predicted trajectories by translating the final position in the vertical axis with a fixed final direction. (b) shows the behavior of the real and predicted trajectories by translating the final position in the horizontal axis with a fixed final direction.*

linear velocity u_1 is constant within the reachable space used in the experimental study. According to Equation 5.3 the norm of the control should be constant. Consequently, we can deduce that u_2 should be a piecewise constant function. Since $\dot{\kappa}_T = u_2$ and considering that $u_2 = cu_1$, by integration we obtain that $\kappa_T = cs + \kappa_0$ where κ_0 is the initial curvature, $s = u_1\tau$ and c a constant characterizing the shape of the clothoid, therefore :

– **clothoid arcs are a good approximation of locomotor trajectories.**

For System 5.1 moving on a curve at constant speed, the only acceleration is the centripetal acceleration given by $a_c = v^2\kappa$. The *jerk*, which is the time derivative of the acceleration, is given by

$$j_c = v^2\dot{\kappa} \quad or \quad j_c = v^3\frac{d\kappa}{ds} \tag{5.6}$$

where s is the arc length. Since a pair of clothoid arcs has a triangular curvature pattern, and the sides of the triangle have slopes equal to $\pm j_c/v^3$, it corresponds to the minimum length curve under a peak-jerk constraint (see Figure 5.6).

Figure 5.7 shows a representative real trajectory performed by one subject and the optimal control-effort trajectory linking the same initial and final configurations. The real trajectory has been filtered to illustrate the comparison between the control inputs extracted from the real (filtered) trajectory and the computed optimal control inputs. Figure 5.8 shows some examples of the behavior of the real and

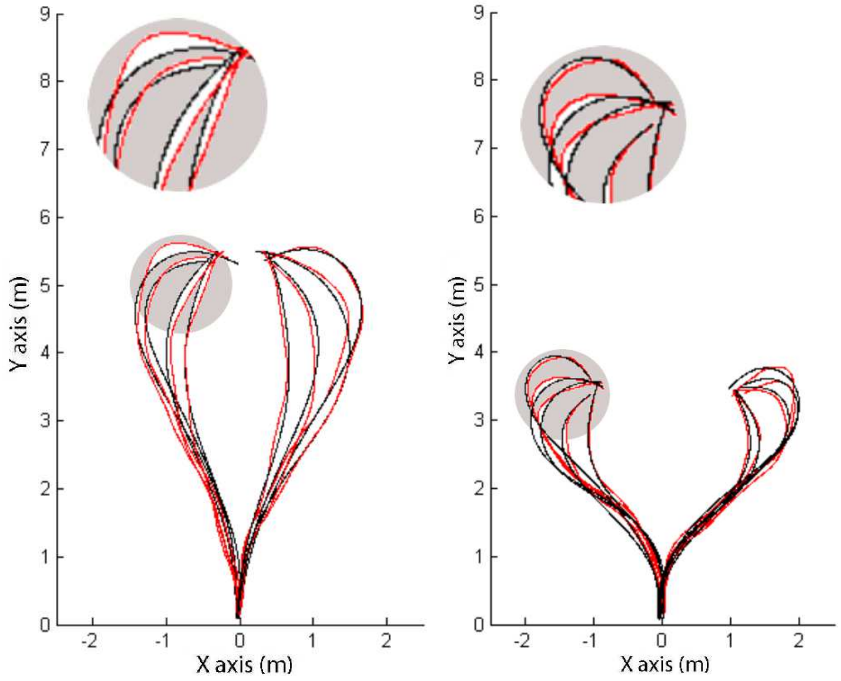

(a) (b)

FIG. 5.9 – *Representative examples of comparisons between recorded (red) and predicted (black) locomotor trajectories. (a) and (b) show the symmetric recorded and predicted trajectories. The final direction varies in intervals of* $\frac{\pi}{6}$.

predicted trajectories by translating the final position over both : the vertical and the horizontal axes with a fixed final direction. Figure 5.9 shows the symmetric recorded and predicted trajectories. The final direction varies in intervals of $\frac{\pi}{6}$. Figure 5.10.a shows some examples of real and predicted trajectories for a fixed final position.

Remark : as a consequence of this result, two corollaries may be deduced :

1. The synthesis of human walking may be computed.
2. Singular situations (known as the cut locus in SubRiemannian geometry) may exist. They explain decision processes answering natural questions such as : should I reach a given goal by the left side or by the right one ? (see Figure 5.10.b)

5.4.3 Note on the minimum jerk model for goal-directed locomotion

We have tested the minimum jerk cost function 2.1 in order to predict the locomotor trajectories used in our study. This model only considers two parameters for the placement of the human body on a 2-dimensional space. The initial and the final positions as well as the velocity constraints relative to the initial and the final directions are given by

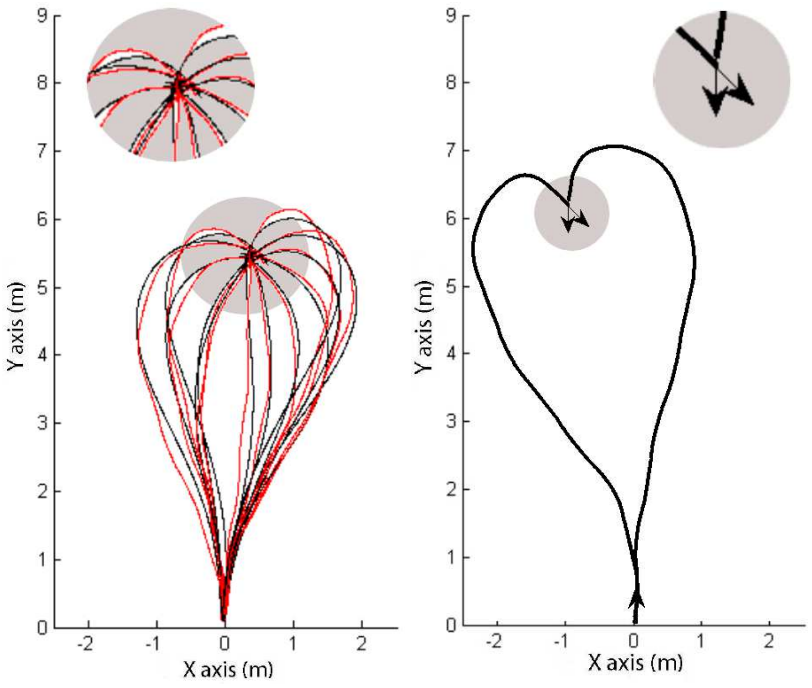

(a) (b)

FIG. 5.10 – *Representative examples of comparisons between real (red) and predicted (black) locomotor trajectories. (a) shows some examples of real and predicted trajectories for a fixed final position. The final direction varies in intervals of $\frac{\pi}{6}$ (b) illustrates the decision processes of the natural question : should I reach the goal by the left or by the right side when the final position is not in front of the initial configuration ?*

$$\begin{cases} x(0) &= x_i \\ y(0) &= y_i \\ \dot{x}(0) &= \sqrt{\dot{x}(0)^2+\dot{y}(0)^2}\cos\varphi_i \\ \dot{y}(0) &= \sqrt{\dot{x}(0)^2+\dot{y}(0)^2}\sin\varphi_i \\ x(T) &= x_f \\ y(T) &= y_f \\ \dot{x}(T) &= \sqrt{\dot{x}(T)^2+\dot{y}(T)^2}\cos\varphi_f \\ \dot{y}(T) &= \sqrt{\dot{x}(T)^2+\dot{y}(T)^2}\sin\varphi_f \end{cases}$$

It is well known that the optimal solutions for $x(\tau)$ and $y(\tau)$ are fifth order polynomials [Flash and Hogan 1985] (see Equation 2.2). We thus performed similar comparisons between the recorded and the predicted trajectories. In [Pham et al. 2007] the authors studied in detail whether the family of smoothness maximization models MSD accounts not only for hand movements but also for human locomotion. We focused here on the prediction performance of this model with respect to the trajectory predicted by our model (see Equation 5.1) for paths with more complex geometric shapes than those used in [Pham et al. 2007].

The predictions of minimum jerk model and our model are accurate for trajectories of categories HC,

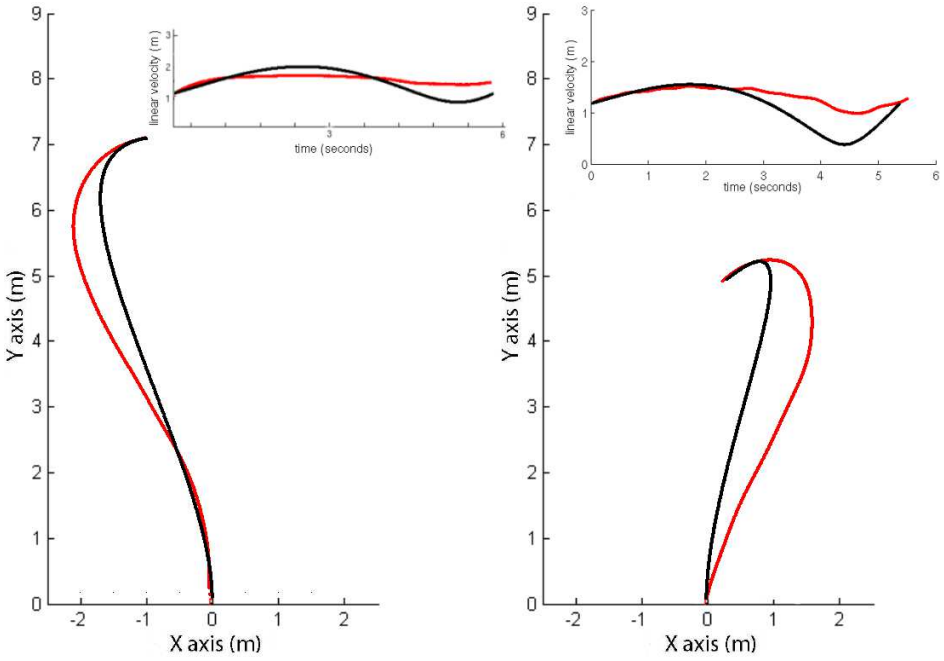

FIG. 5.11 – *Bottom : Representative examples of comparisons between real (red) and predicted (black) locomotor trajectories. The real trajectories (filtered) are performed by one subject and the predicted optimal trajectories are computed by the minimum jerk model linking the same initial and final configurations. Top : the comparisons between the linear velocity profiles extracted from the real and predicted trajectories.*

MC, LC and S plotted in Figure 3.6. However, for trajectories composed by more complex curvature profiles (e.g., changing the sign with increasing and decreasing curvatures), the minimum jerk model results to be inaccurate (see Figure 5.11). In contrast with this model, the geometric paths predicted by System 5.1 minimizing 8.9 are still accurate (see Figure 5.7). The accuracy criterion corresponds to the 10 cm of tolerance. From these results we suggest that the differential coupling (see Equation 1.1) should be considered to predict locomotor trajectories.

5.5 Discussion

In the first part of this study, we have shown that the human forward locomotion, represented by the torso position and direction, obeys the motion of a nonholonomic system with linear and angular velocity inputs. In the second part, we were able to predict more than 90 percent of the 1560 trajectories recorded from seven subjects during walking tasks with a $<$10 cm accuracy. We have implemented a numerical optimization algorithm to validate that the locomotor trajectories are well approximated by the optimal solutions of a dynamic extension of the unicycle model. The criterion to be minimized has been the time derivative of the curvature. Using an analytical optimal control approach, we have locally characterized the geometric shape of the geodesics. In the following chapter, we present the (numerical) synthesis of the proposed optimal control problem. As per the Dubins' model, the related questions are : How many

clothoid arcs the trajectories contain ? How are the sequences of arcs organized ? What is the number of the different sequences ?

Lets pinpoint an issue which opens the central theme of the next chapter. Figures 5.8 and 5.9 illustrate a natural intuition : when the goal position varies slightly (with fixed direction, Figure 5.8) and when the goal direction varies slightly (with fixed positions, Figure 5.9) the resulting trajectories are obtained by continuous reshaping. This means that close goals give rise to close trajectories. Let us consider now the case illustrated in Figure 5.10.b. The goal position of both trajectories is the same. Both goal directions differ slightly while both trajectories completely differ. This case contradicts the previous intuition. This behavior occurs only in some special cases. It arises around points reachable by two distinct trajectories with exactly the same cost. Now the question is : how does the brain identify such cases ?

The study of the geometry of nonholonomic trajectories is part of a mathematical domain of differential geometry known as SubRiemannian geometry [Bellaiche and Risler 1996; Bonnard and Chyba 2003]. For very few systems it is possible to compute exactly the locus of goal points reachable by exactly two distinct trajectories (see for instance [Souères and Laumond 1996] for the case of the car-like robot). This locus is known as the so called *cut-locus* in SubRiemannian geometry. However, methods to compute such a locus for any nonholonomic system are out of the scope of the current state of the art in differential geometry. Therefore the following chapter describes our studies to characterize the *cut-locus of the human locomotion* by numerical methods.

6

The Words of the Human Forward Locomotion

In Chapter 5, we stated that a good approximation of the geometric shape of human locomotor trajectories is the concatenation of clothoid arcs. The objective of this chapter is to provide the partition of the 3-dimensional configuration space according to the various sequences of clothoid arcs. In Section 6.1, we introduce the notions of optimal synthesis as well as some results in mobile robotics relative to our study.

The optimal paths being computed numerically, we first examine how to decompose them with a finite number of clothoid arcs (see Section 6.2). Then, we compute a partition of the 3-dimensional configuration space in cells : 2 points belong to a same cell if and only if they are reachable from the origin by a path of the same type. Such a decomposition is known as the synthesis of the optimal control problem.

The frontiers between cells are studied in Section 6.3. This study is related to the continuity of trajectory deformation. The key point of this chapter is the following one :

Most of the time when the target changes slightly the optimal trajectories change slightly. However, some singularities appear at some critical frontiers. It is noticeable that they correspond to the strategy change for the walking subjects. This fundamental result is another poof of the locomotion model we have proposed (see Section 6.4).

6.1 Related works on optimal path synthesis

Equation 1.1 is the classical differential equation governing the motions of a rolling wheel, and then the motions of mobile robots with wheels. How to steer a mobile robot from a given 3-dimensional starting configuration to a given 3-dimensional goal while the robot control space is only 2-dimensional ?

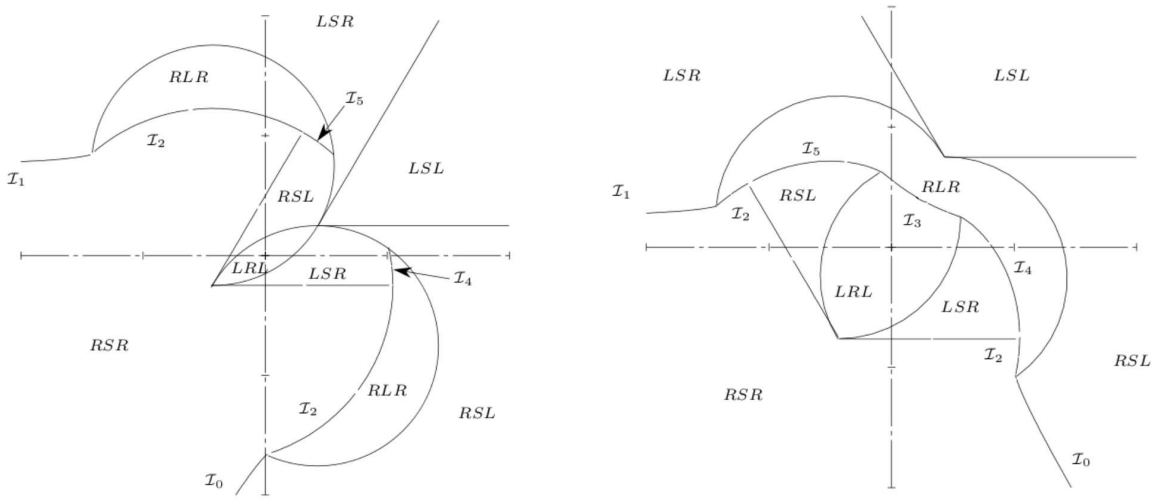

(a) (b)

FIG. 6.1 – *Partition of the slices $\theta = \frac{\pi}{3}$ and $\theta = \frac{2\pi}{3}$ induced by the Dubins' words. The pictures are borrowed from [Souères and Boissonnat 1998].*

The question gave rise to an active research topic during the past twenty years. Among the numerous steering methods (see overviews in [Laumond et al. 1998], [Choset et al. 2005] and [LaValle 2006]) optimal control based methods are certainly the most efficient ones. Unfortunately planning nonholonomic optimal motions is a difficult problem. It has been solved only for some classes of simple systems. Some of the popular include the Dubins' car [Dubins 1957] and the Reeds and Shepp's car [Reeds and Shepp 1990; Sussmann and Tang 1991] (see also [Balkcom et al. 2006; Boissonnat et al. 1992] and the overview [Souères and Boissonnat 1998]).

Let us emphasize shortly on Dubins' car since it is the closest system related to our problem. Dubins' car is a car moving only forward at a constant linear velocity. It corresponds to the following control system :

$$\begin{pmatrix} \dot{x} \\ \dot{y} \\ \dot{\theta} \end{pmatrix} = \begin{pmatrix} \cos\theta \\ \sin\theta \\ 0 \end{pmatrix} + \begin{pmatrix} 0 \\ 0 \\ 1 \end{pmatrix} u \tag{6.1}$$

where u is the steering wheel control. u is a map onto $[-1,1]$. Dubins [Dubins 1957] (and then the proof by [Sussmann and Tang 1991] using modern optimal control theory as the maximum principle of Pontryagin [Pontryagin et al. 1964]) shows that the shortest length paths of the system are made of finite sequences of straight line segments S ($u = 0$) and arcs of a circle with constant minimal radius C ($u = \pm 1$). By considering that an arc of a circle C can turn either right (R arcs when $u = 1$) or left (L arcs when $u = -1$), Dubins shown that two sufficient families of shortest paths are the following :

1. Family *CCC* includes 2 types : *RLR* and *LRL*
2. Family *CSC* includes 4 types : *RSR*, *LSL*, *RSL* and *LSR*

These sequences are what we call the "words" of the Dubins' car. From this, we can say that six words are necessary to describe all the possible optimal paths. Now another question arises dealing with the uniqueness of the shortest paths : what is the partition of the (3-dimensional) space according to the various words ? This problem has been solved in [Pecsvaradi 1972; Bui et al. 1994]. Figure 8.6 shows the partition of the slices at $\theta = \frac{\pi}{3}$ and $\theta = \frac{2\pi}{3}$ according to the Dubins' words.

Computing such a partition has been done for a few other systems [Souères and Laumond 1996; Balkcom and Mason 2002]. These contributions are based on the application of the Pontryagin principle that gives (only) necessary conditions for optimality. Necessary and sufficient conditions can be found in the works by Boltyanskii [Boltyanskii 1966]. They are related to the regular synthesis of optimal control (i.e. the computation of partitions such as the Dubins' partitions we have just sketched here). Solving the regular synthesis problem in a generic way (i.e. for any kind of nonlinear systems) remains a challenging mathematical problem.

More than that, the application of the Pontryagin principle generally does not provide enough information to describe optimal trajectories with finite words. This is why, most of the time, the optimal trajectory computation is done via numerical analysis algorithms [Nocedal and Wright 1999; Garcia 1994; Hiriart-Urruty and Lemaréchal 1996].

6.2 Computing the synthesis of human walking

In this section, we describe the numerical characterization of optimal paths by the number of concatenated clothoid arcs. First, we recall that a clothoid is the curve satisfying the following equation :

$$\kappa(\tau) = \pm c\tau, \quad \tau \in (-\infty, \infty) \tag{6.2}$$

where c is a constant and the sign $\pm$ defines the orientation of each piece. Therefore, we can determine a single clothoid by

$$\begin{aligned} u_2(\tau) &\equiv c, && \kappa(\tau) \to \infty \\ & \quad or & & \\ u_2(\tau) &\equiv -c, && \kappa(\tau) \to -\infty. \end{aligned} \tag{6.3}$$

From the results obtained in Chapter 5, we know that $u_2(\tau)$ is a piecewise constant function. The concatenation point between two clothoid arcs is called a *switching point*. At each switching point the curvature function contains a local extremum and the derivative of the curvature u_2 has a discontinuity.

From the preceding reasoning, our numerical technique consists in determining the number of switches and the order of switching points of each optimal path. The method is based on the local analysis of the curvature. To be more precise, we explore the curvature function to find the local extrema (i.e. the switching points).

A description of the regions in the configuration space is obtained by repeating the above process for all optimal trajectories spanning the reachable space. The analysis has been carried out by the following steps :

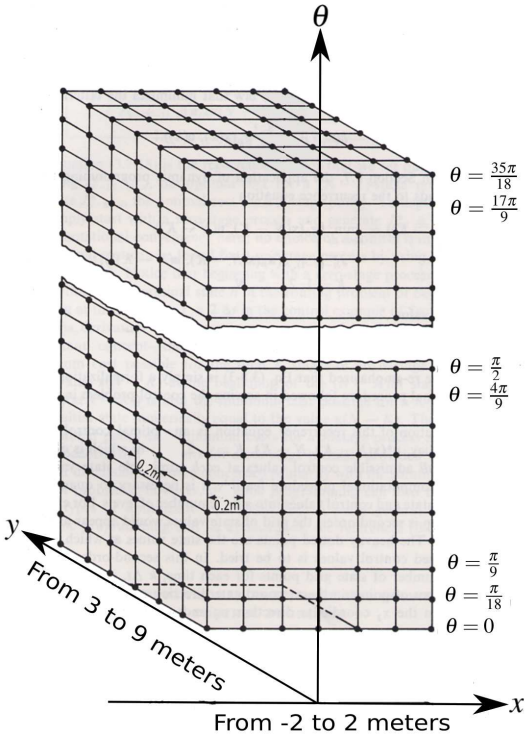

FIG. 6.2 – *We computed the approximation of the space by a grid decomposition technique. The grid resolution was* $(0.2m \times 0.2m \times \frac{\pi}{18})$ *and the grid range from* $[-2,2] \times [3,9]$ *in position.*

1. $R^2 \times S^1$ is partitioned with 36 slices according to the direction θ.
2. For each θ-slice, we computed numerically the optimal trajectories from the origin to each vertex in the grid.
3. At each θ-slice, we determined the regions mapping the types of optimal paths. Each region corresponds to a set of optimal trajectories containing the same ordered combination of clothoid arcs in terms of their orientations.

6.2.1 Sampling the reachable space

To compute the synthesis for our optimization problem, we first sampled the portion of the reachable space considered in the experimental protocol $(x,y,\theta) \in R^2 \times S^1$. Because we are interesting in human forward locomotion, we only analyzed the space in front of the starting configuration. We defined the point $(0,0,\frac{\pi}{2})$ as the origin of the configuration space. The initial and the final curvatures are equal to zero ($\kappa = 0$) at both the starting and the goal configurations. We computed the approximation of the space by a grid decomposition technique. The grid resolution was $(0.2m \times 0.2m \times \frac{\pi}{18})$ and the grid range from $[-2,2] \times [3,9]$ in position (see Figure 6.2).

We then computed the optimal paths linking the origin to each vertex in the grid. We used the Algorithm 5.1 in the implementation of the exhaustive generation of optimal paths. The input parameters for the numerical optimization algorithm were :

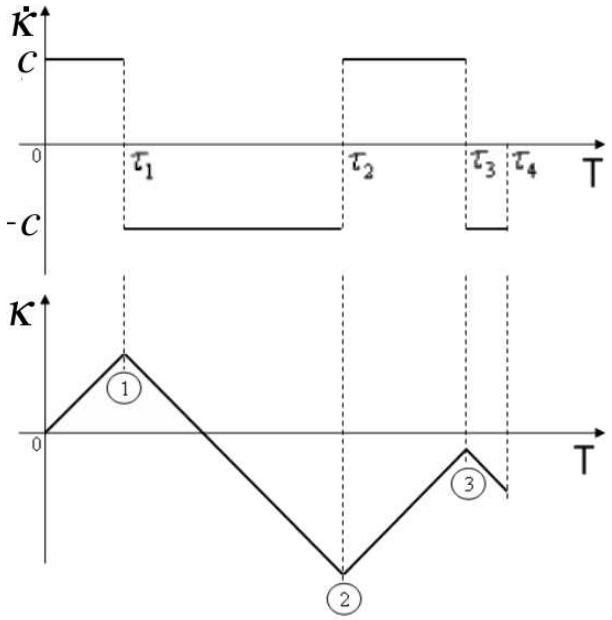

FIG. 6.3 – *The concatenation point between two clothoid arcs is called a "switching point". At each switching point the curvature function contains a local extremum and the derivative of the curvature has a discontinuity.*

1. The initial and the final configurations. In this case, they were given by the origin $(0,0,\frac{\pi}{2})$ and the corresponding vertex in the grid.
2. The final time T. This was a critical input parameter because it only exists for the subset of vertexes (targets) that were reached by all the subjects. To overcome this difficulty, we benefited from the Dubins' solution in order to find an approximation of the final time as follows : first, we set the linear velocity equals to the averaged linear velocity of the recorded locomotor trajectories. We also fixed the constant minimal radius in such a way that the final time of Dubins' paths and the final time of the recorded locomotor trajectories coincide. By using these two constants (i.e. the linear velocity and the radius of curvature) we then computed the Dubins' paths to obtain an approximation of the final time T for each vertex in the grid.
3. The initial solution represented by α_0. We used the path obtained by applying the Dubins' method to set the initial solution α_0 (see Algorithm 5.1).
4. The sampling frequency was 120 Hz. Then, the trajectory is composed by a sequence of 120 points per second.

At this stage, the grid is thus built. After this, we have generated a data basis of 22,785 optimal paths. This means that at each θ-slice, we computed 651 geodesics.

6.2.2 Finding the switching points

After the data basis is constructed, a simple algorithm is applied to recognize the local extrema of the curvature function $\kappa(\tau)$. Indeed, we are not interested to search the global extremum. We would

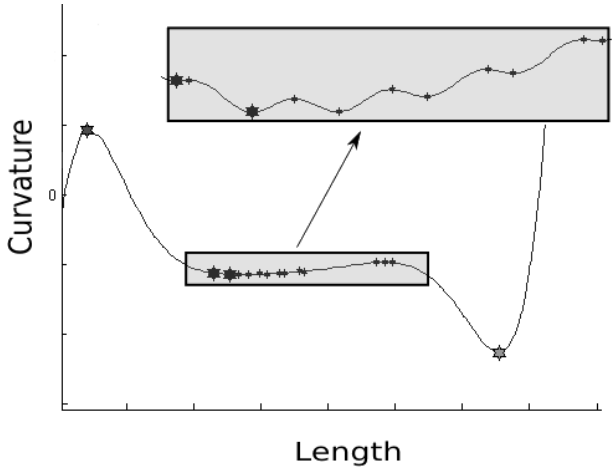

FIG. 6.4 – *The curvature profile has various local extrema. Some of them are too close each other. They are then called trivial extrema. They correspond to shaded points in the picture.*

rather find the switching points by identifying the local extrema of the curvature profile for each optimal path (see Figure 6.3). The following strategy is applied to deal with this one-dimensional optimization problem.

The procedure begin at the initial value given by $\kappa(0)$. By traveling through $\kappa(\tau)$, the algorithm find out whether a point $\kappa(\tau)^*$ is a local extremum. This is done by examining the gradient to determine the direction p_k leading to the first local extremum represented by $\kappa(\tau)^*$. The distance to move along the direction p_k is just the distance between the current and the next points. Actually, the smallest interval between two consecutive points is $\frac{1}{120}$s. This is the sampling rate used to compute the optimal trajectories.

To ensure that from the current iteration along which $\kappa(\tau)$ decrease or increase, the algorithm explore all the points in its immediate vicinity. If $\kappa(\tau)$ decrease, this means that it tends toward a minimum. While on the contrary if $\kappa(\tau)$ increase, then it tends toward a maximum.

Assuming that $\kappa(\tau)^*$ is an extremum, then the algorithm makes sure that none of the points located near to $\kappa(\tau)^*$ has a smaller (or greater) function value. Moreover, we defined a frame by using two parameters to discard trivial extrema. These parameters are defined by a curvature and a length tolerances. The constant values of the curvature and the length tolerances were $4x10^5$ radians/meters and 1.2 meters respectively. Figure 6.4 illustrates how these trivial points are discarded by passing the window through $\kappa(\tau)$. In other words, the algorithm compare $\kappa(\tau)^*$ with the previous one by using the window. The extremum $\kappa(\tau)^*$ is retained and marked either minimum or maximum if the previous extremum is outside the window. In most of the cases it is only necessary to evaluate the curvature tolerance. However, the length tolerance is used to discard extrema where the distance between two extremum candidates is too long and the curvature itself does not vary too much. This process is repeated until the end of the curvature function $\kappa(T)$. The outputs of this procedure are the ordered lists of extrema of curvature profiles, each of them is associated to an optimal path.

Remark : It turns out that the algorithm for finding the extrema requires two parameters (curvature

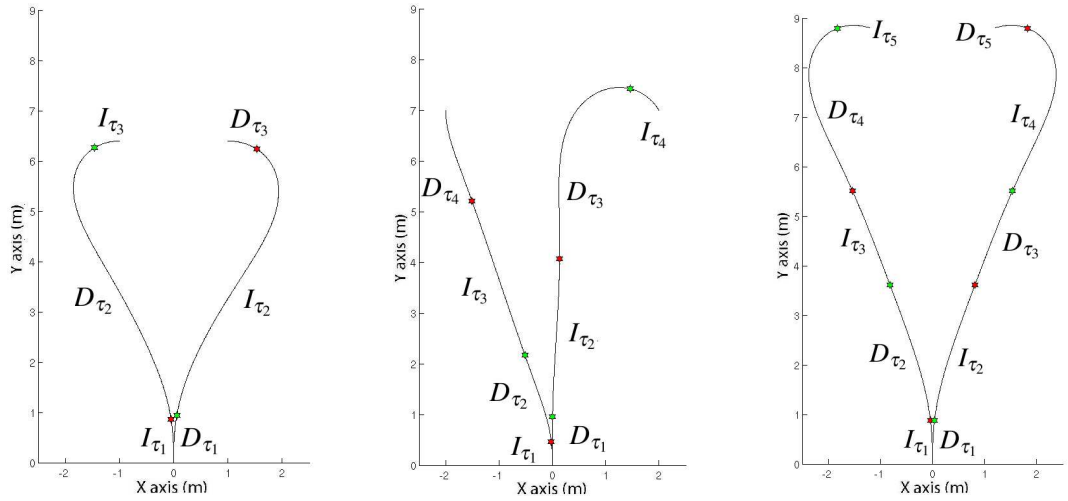

FIG. 6.5 – *We found experimentally 6 types of optimal paths to link the origin of the* 3*-dimensional configuration space to any other configuration within the reachable space we have defined.*

and length) in order to approximate the sequence of switching points. The approximation error depends mainly on the size of the window defined by the values assigned to these tolerances. As we have mentioned, we have assigned the constant values of $4x10^{-5}$ and 1.2 for the curvature and length tolerances respectively.

We noted that in the case of the curvature tolerance, if this value is smaller than $1x10^{-6}$ then the algorithm finds too many trivial extrema. If this parameter is greater than $5x10^{-4}$ then the algorithm cannot find any extremum. For choosing these parameter values we have tested different curvature profiles with complex shapes. By exploring these different cases, we have been able to estimate the size of the window.

6.2.3 Characterizing the sets of optimal paths

The purpose of this stage concerns the classification of the optimal paths according to the number of concatenated clothoid arcs. At this level, we know the number of extrema each curvature contains. Consequently, given an optimal path we can recognize its total number of clothoid arcs. Moreover, it is possible to compute a decomposition of optimal paths just following the sequence of the extrema of their curvature profiles.

By considering that the curvature κ of an arc of a clothoid can either increase (I_τ when $u_2 = c$) or decrease (D_τ when $u_2 = -c$) for a given time τ, we can find all the combinations of arcs. Actually, the combinations between I_τ and D_τ are alternated. Thus, if the first type of clothoid arc corresponds to D_τ then the next piece (if exists) must be the opposite (i.e. I_τ) and *vice versa*. Furthermore, there exist optimal paths with the same number of curves of clothoid but with different order. We have conducted the classification of optimal paths by following this strategy. We then found experimentally that only six combinations appear (see Figure 6.5) :

1. $I_{\tau_1} D_{\tau_2} I_{\tau_3}$
2. $D_{\tau_1} I_{\tau_2} D_{\tau_3}$
3. $I_{\tau_1} D_{\tau_2} I_{\tau_3} D_{\tau_4}$
4. $D_{\tau_1} I_{\tau_2} D_{\tau_3} I_{\tau_4}$
5. $I_{\tau_1} D_{\tau_2} I_{\tau_3} D_{\tau_4} I_{\tau_5}$
6. $D_{\tau_1} I_{\tau_2} D_{\tau_3} I_{\tau_4} D_{\tau_5}$

We call these sequences the words of the optimal paths. We denote by I_τ (respectively D_τ) the word "letter" corresponding to the application of control $u_2 = c$ (respectively $u_2 = -c$) during time τ. In other terms, there exist six types of optimal paths to link the origin of the 3-dimensional configuration space to any other configuration within the reachable space we have defined.

The words above induce a partition of the configuration space $R^2 \times S^1$ into cells. As we have seen, each word is described by at least three letters. Then, it follows that each cell is the image of at least three real intervals (τ_1, τ_2, τ_3) by continuous mapping.

To represent the cells, we have only considered 36 θ-slices. By fixing θ we have identified these cells in each of the θ-slices from $\theta = 0$ to $\frac{35\pi}{18}$ in intervals of $\frac{\pi}{18}$. Figures 6.6-6.8 show the partition of the reachable space for the 36 values of θ. In Figure 6.9 we show two θ-slices with their representative optimal trajectories for different regions. All these pictures have been traced by using our numerical algorithm implemented in *Matlab R2007a*.

As a result of the numerical synthesis of optimal paths in the 3-dimensional configuration space, several evidences of the structure of such paths arise. For instance, the existence of symmetric regions as depicted in Figure 6.8 when $\theta = \frac{3\pi}{2}$. From this θ-slice, we can observe that the previous and the next θ-slices are relative similar. This phenomenon is observed until $\theta = \frac{\pi}{2}$ is reached (i.e. the same direction as the origin). Notice that each θ-slice contains at least two regions. The θ-slices composed with more than four regions are those close to $\theta = \frac{\pi}{2}$. Finally, we can observe that six types of paths only appear in the slices $\theta = \frac{7\pi}{18}$, $\theta = \frac{4\pi}{9}$ and $\theta = \frac{11\pi}{18}$.

6.3 Geometric analysis of cells adjacency

Let us now consider a word, e.g. $I_{\tau_1} D_{\tau_2} I_{\tau_3}$. The mappings from R^3 onto $R^2 \times S^1$ associating the triplet (τ_1, τ_2, τ_3) to a configuration in the cell of the corresponding word is a local diffeomorphism. This means that there exists a continuous variation of the path shape. They just differ by the position of the switching points on the optimal paths. When a configuration varies continuously within a given cell, the switching times vary continuously. What happens between two adjacent cells ? Two cases may arise :

- Case 1 : Traversing the border can be done by a continuous deformation of the trajectory. For instance the cells $I_{\tau_1} D_{\tau_2} I_{\tau_3}$ and $D_{\tau_4} I_{\tau_5} D_{\tau_6}$ have common borders of respective equation $\tau_1 = 0$ and $\tau_6 = 0$. This means that there is a *continuous* reshaping of the geometric shape of the trajectories as depicted on the top of Figure 6.10.
- Case 2 : Traversing the border induces a discontinuity on the trajectory deformation. This would be the case of the same cells $I_{\tau_1} D_{\tau_2} I_{\tau_3}$ and $D_{\tau_4} I_{\tau_5} D_{\tau_6}$ if their common border is obtained respectively

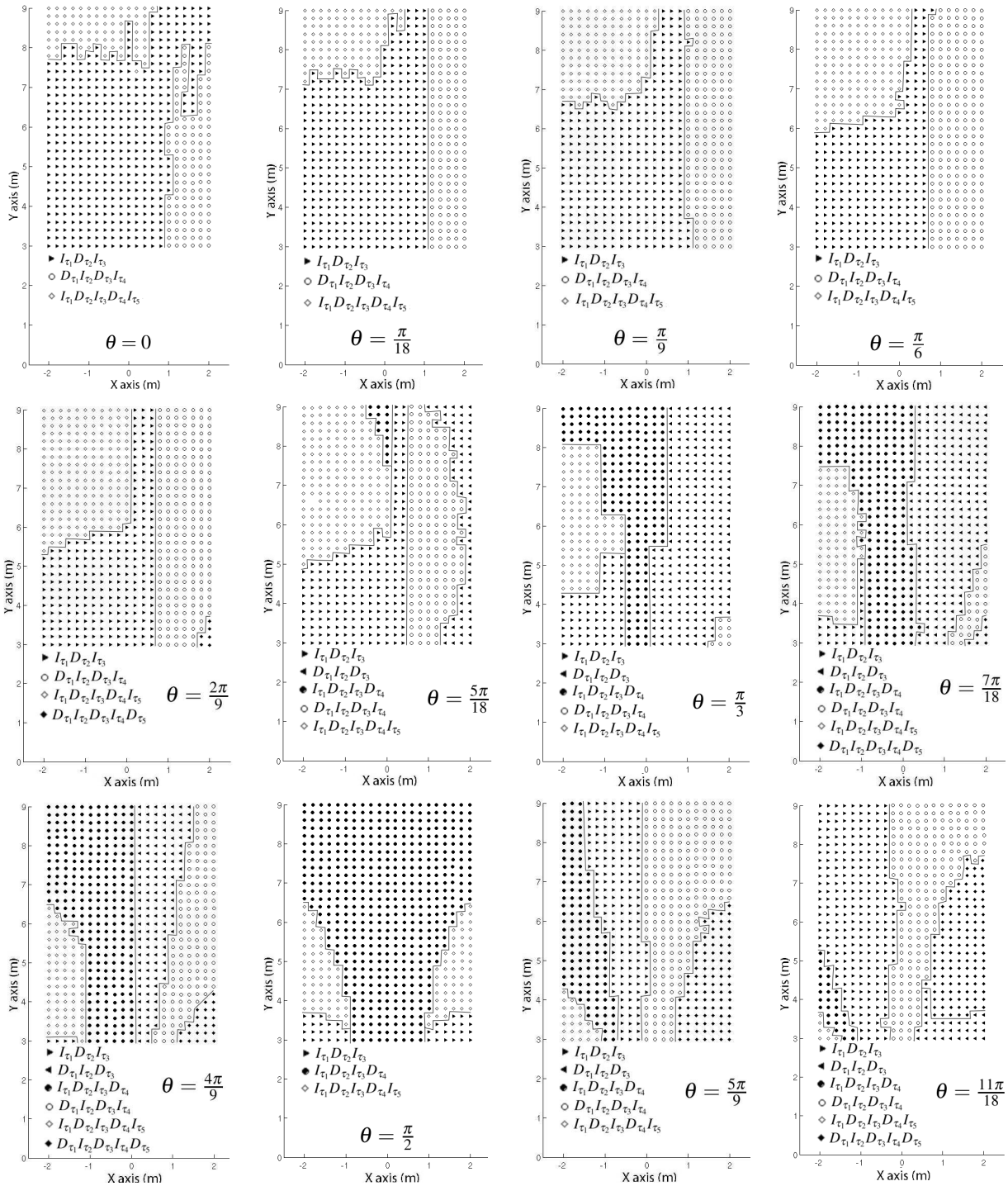

FIG. 6.6 – *At each slice the final direction is fixed. From top to bottom and from left to right, the final direction varies from* 0 *to* $\frac{11\pi}{18}$ *in intervals of* $\frac{\pi}{18}$.

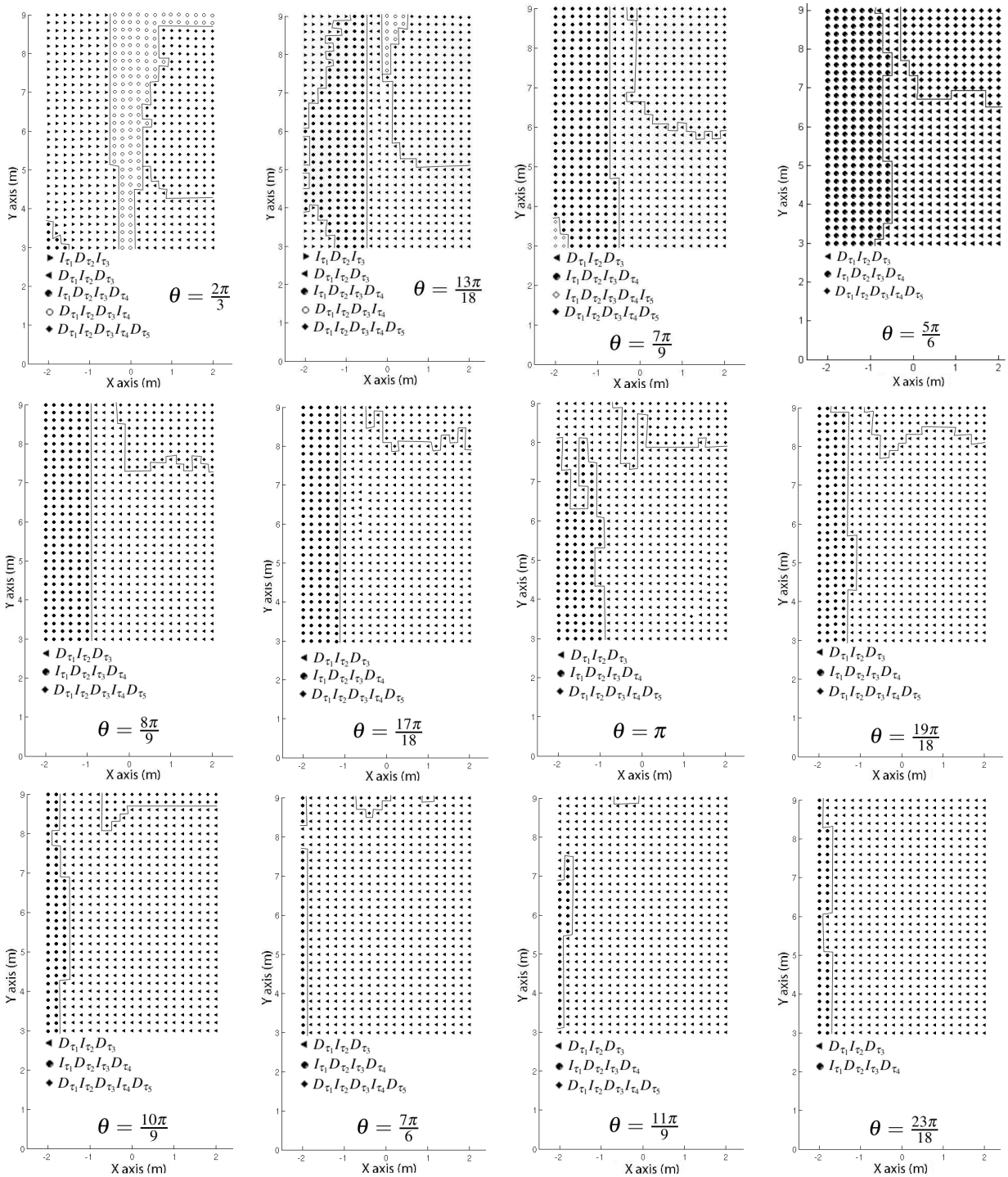

FIG. 6.7 – *At each slice the final direction is fixed. From top to bottom and from left to right, the final direction varies from* $\frac{2\pi}{3}$ *to* $\frac{23\pi}{18}$ *in intervals of* $\frac{\pi}{18}$.

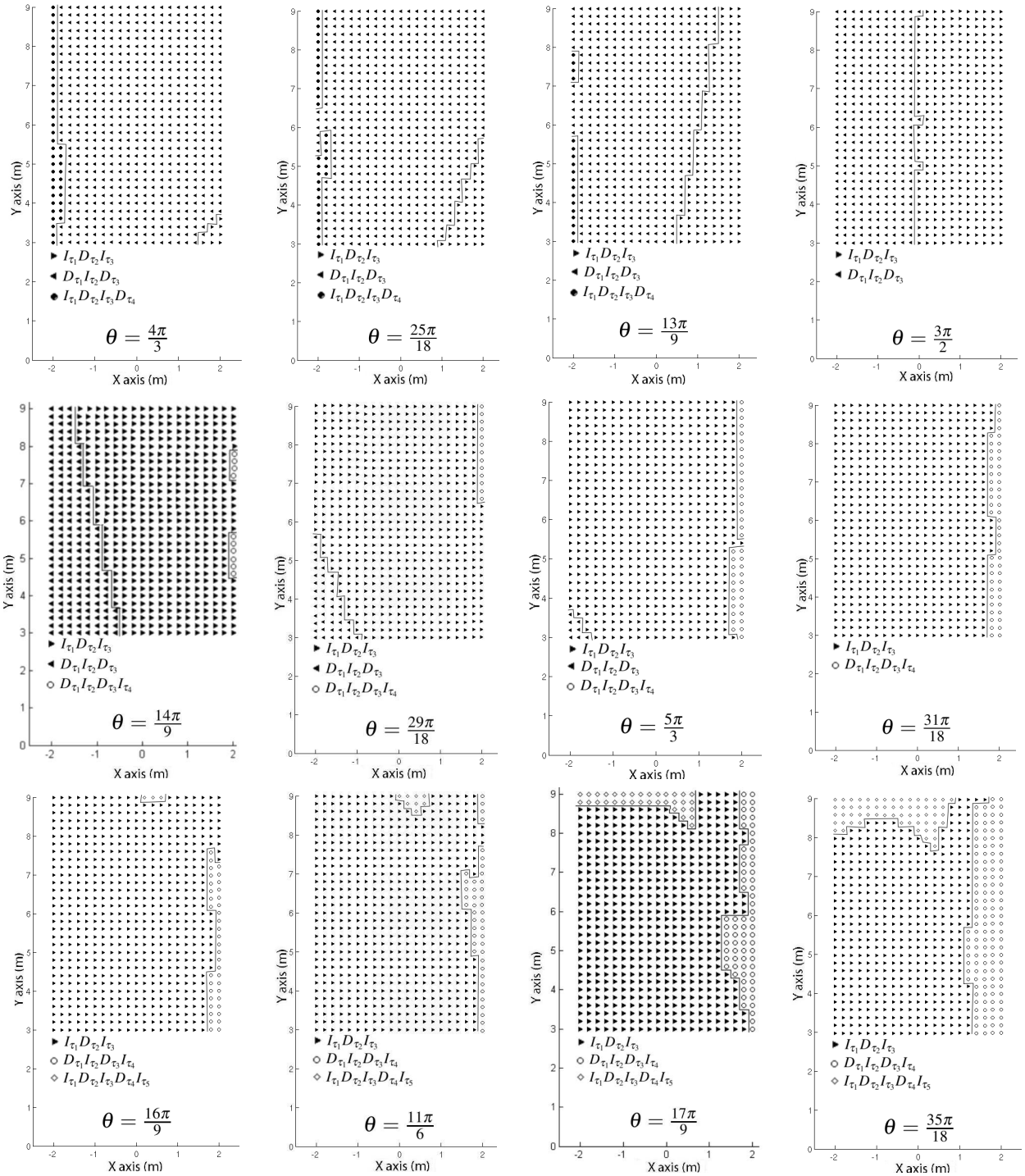

FIG. 6.8 – *At each slice the final direction is fixed. From top to bottom and from left to right, the final direction varies from* $\frac{4\pi}{3}$ *to* $\frac{35\pi}{18}$ *in intervals of* $\frac{\pi}{18}$.

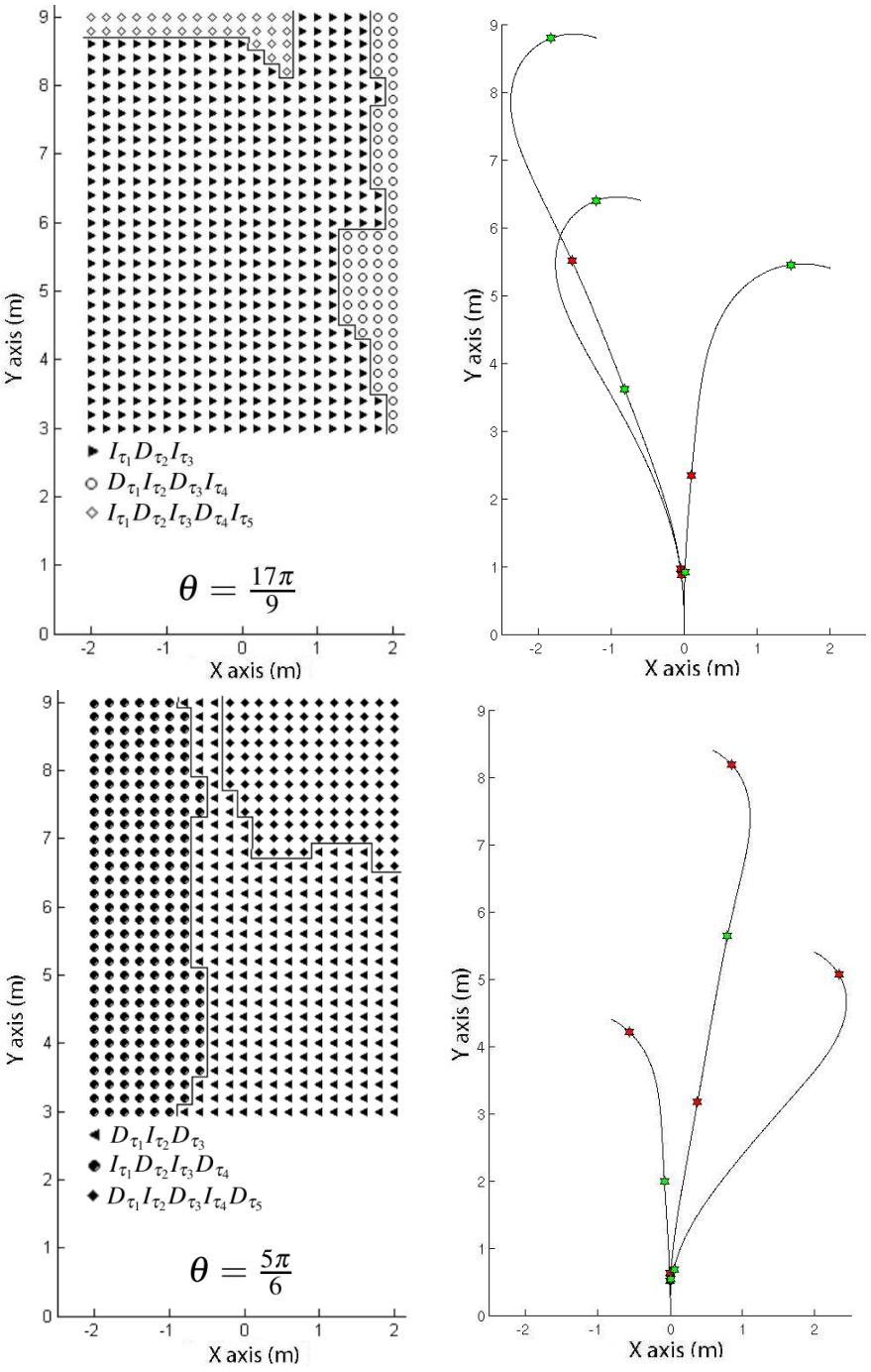

FIG. 6.9 – *Top-left : The partition of the slice* $\theta = \frac{17\pi}{9}$. *Bottom-left : The partition of the slices* $\theta = \frac{5\pi}{6}$. *Right : Some examples of representative optimal trajectories for different regions.*

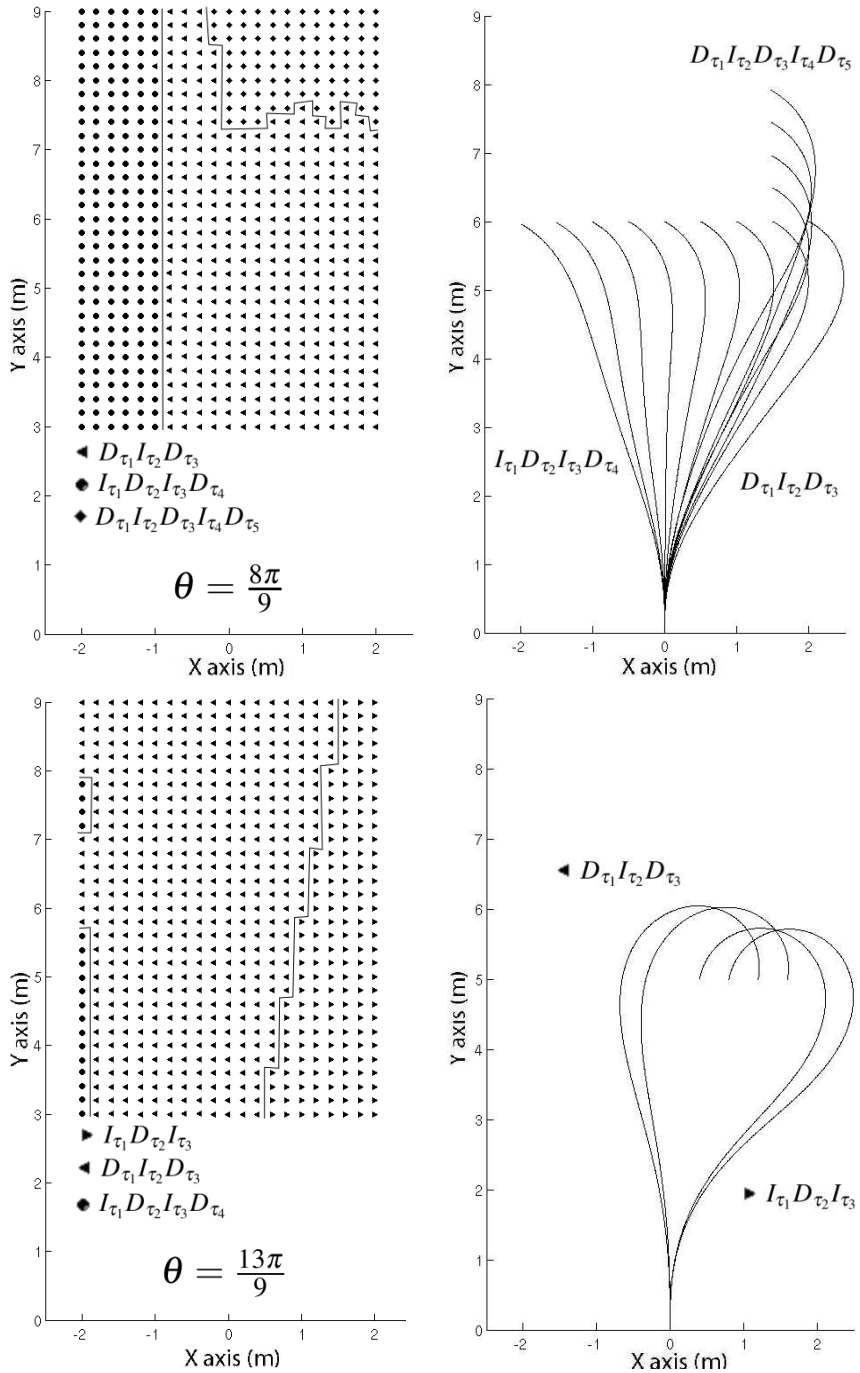

FIG. 6.10 – *Top : An example of Case 1 occurring at $\theta = \frac{8\pi}{9}$. The trajectories cross the border by a continuous deformation. Bottom : An example of Case 2 occurring at $\theta = \frac{13\pi}{9}$. A discontinuity of the geometric shape of the trajectories occurs when traversing the border.*

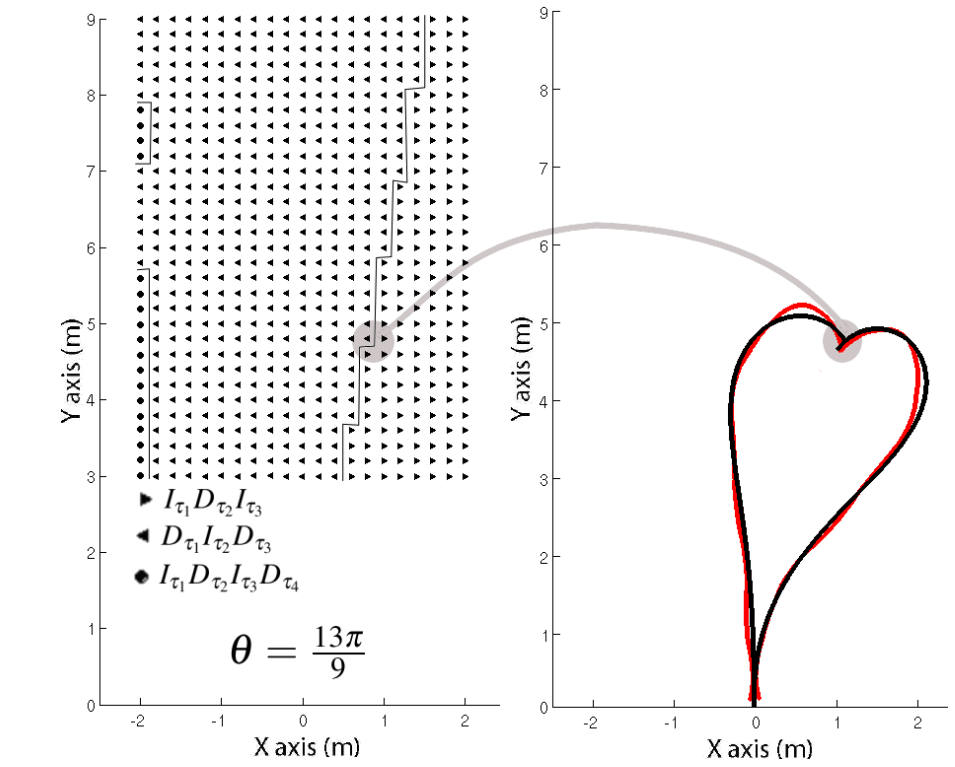

(a)

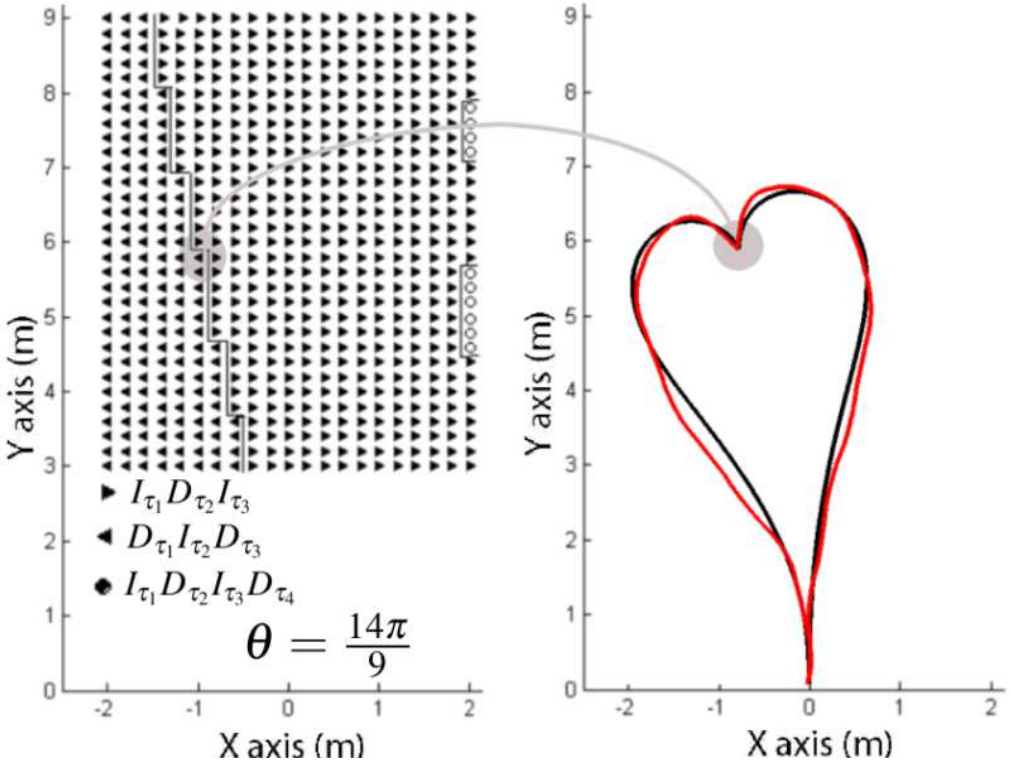

(b)

FIG. 6.11 – *Left : The partition of the slices* $\theta = \frac{14\pi}{9}$ *and* $\theta = \frac{13\pi}{9}$. *Right : Examples of two configurations belonging to two adjacent cells governed by Case 2. The real (red) trajectories performed by the same subject with respect to predicted (black) optimal trajectory. Cut-locus explains the strategy change.*

for $\tau_3 = 0$ and $\tau_6 = 0$. In that case there is a *discontinuity* of the geometric shape of the trajectories when traversing the border (see the bottom of Figure 6.10).

For most of the cells, the cell adjacency is governed by Case 1. The interesting case is Case 2. It is a subtle case : at a configuration on the common border of both cells, there exist exactly *two* optimal trajectories with the *same* cost and a completely *different* shape. Such borders arise for symmetric nonholonomic systems (e.g. a car that moves forward and backward [Souères and Laumond 1996]). In that cases they are known as the cut-locus in SubRiemannian geometry (see [Bellaiche and Risler 1996]).

For our problem, we have identified the θ-slices where Case 2 appears. This happens from $\theta = \frac{4\pi}{3}$ to $\theta = \frac{5\pi}{3}$ passing through $\theta = \frac{3\pi}{2}$ (see Figure 6.8). As it is shown in the picture, it corresponds to the frontier between regions $I_{\tau_1} D_{\tau_2} I_{\tau_3}$ and $D_{\tau_1} I_{\tau_2} D_{\tau_3}$. The shape of the frontier is represented by a "line". In the case of $\theta = \frac{3\pi}{2}$, the line is parallel with respect to the direction of the origin. Indeed, from slice $\theta = \frac{3\pi}{2}$ it is possible to identify the behavior of Case 2. Notice that the line starts to lean toward the left side if $\theta = \frac{14\pi}{9}$ or toward the right side if $\theta = \frac{13\pi}{9}$.

It is important to recall that the 3-dimensional reachable space has been partitioned according to the direction θ. This is the reason why we observe the Case 2 as a line. But the real dimension of Case 2 is 2. Actually, it represents a 2-dimensional subspace embedded in the 3-dimensional configuration space. In our particular case, it can be viewed as a sloping plane cutting the reachable space from $\theta = \frac{4\pi}{3}$ to $\theta = \frac{5\pi}{3}$ and centered at $\theta = \frac{3\pi}{2}$.

6.4 Motor control interpretation

From the above numerical analysis of the frontiers between cells, we can extract the main result of our work.

At this stage, we know that human locomotor trajectories can be approximated by at least three concatenated clothoid arcs and at most five. From this, we can deduce that human walking can be characterized by six types of paths. We call these types *the words of human locomotion*.

According to the partition of the reachable space of waking subjects, the words map different cells in the 3-dimensional configuration space. Each elementary cell consists of points that may be linked to the origin by the same kind of path. This means that *the motor controls* used to reach two different configurations in a same cell follow the same *pattern*.

By analyzing the adjacency of cells, we have determined two classes of borders. In both cases, when the goals are located in the vicinity of the frontier, *the motor control* select different *patterns* depending on the cell. However, the central difference between these two classes is the following. In the first case, the border is traversed by continuous reshaping of the locomotor trajectories. This follows the intuition that close goals give rise to close trajectories.

Considering now the second case, there exists an abrupt behavior when crossing the border. This behavior arises around points reachable by two distinct trajectories with exactly the same cost. What is worth noticing is that the cut-locus of the synthesis above accounts for the locomotion *strategy*. Figures 6.11 and 6.12 show examples of two configurations belonging to two adjacent cells governed by Case

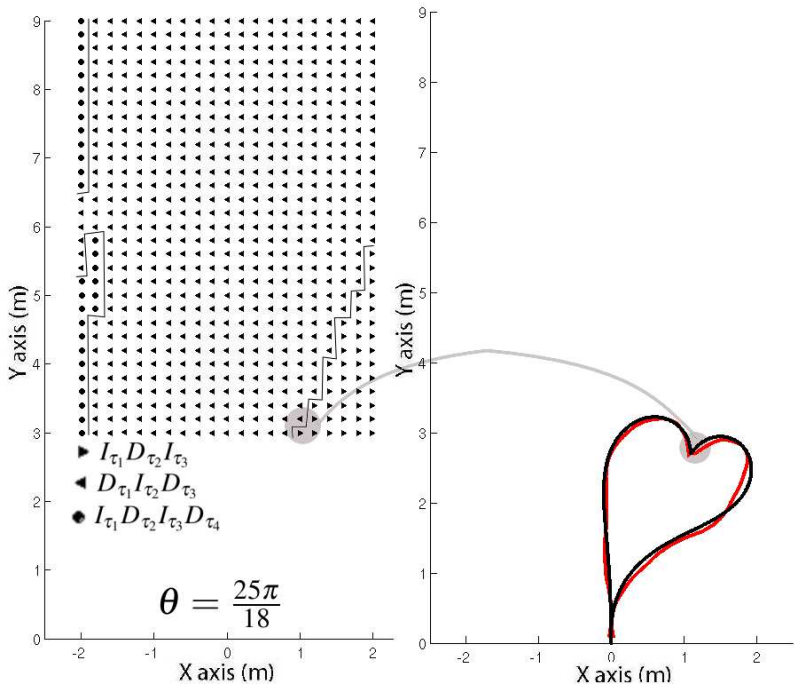

FIG. 6.12 – *Left : The partition of the slice* $\theta = \frac{25\pi}{18}$. *Right : An example of two configurations belonging to two adjacent cells governed by Case 2. The real (red) trajectories performed by the same subject with respect to predicted (black) optimal trajectory. Cut-locus explains the strategy change.*

2. *The trajectories obtained by simulating our control model fit with the observed trajectories*. This means that the *two apparently completely different strategies* used by the subject to reach two close configurations obeys *de facto* a same strategy tending to optimize the derivative of the curvature. The model we propose answers the question asked at the beginning of this document (see Figure 1.2.c).

7 Conclusion

The ability to understand and then model the fundamental principles of biological movements such as human locomotion depends primarily in having to deal with the redundancy of the human body as well as the emergence of variability in movement execution. Thus, it seems likely that optimal control theory can serve as basis to successfully describe a wide rage of motion generation strategies.

The present study has been restricted to the nominal behavior of walking subjects in a large obstacle-free room towards well-identified goals without any unexpected event. The first objective has been to study the accessibility region defined in the 3-dimensional posture space (position and direction) corresponding to nominal walking. For instance when a goal is defined only few centimeters on the left side from the starting point, reaching that goal requires just a side step that is out of the scope of a nominal walking behavior. In this document we addressed the following question : what is the reachable space of the nominal walking ?

We defined a methodology consisting in recording a data basis made of locomotor trajectories reaching 3-dimensional goals (position and direction) in empty space. By using such data basis, we performed a qualitative and quantitative analysis on the experimental data to show that the walking subjects exhibit stereotyped behavior in terms of both path geometry and trajectory kinematics. This part of our work suggests that the formation of locomotor trajectories may be governed by some underlying principles (see also [Hicheur et al. 2007]).

Recently, [Pham et al. 2007] proposed a computational model for the generation of locomotor trajectories. Such model is an extension of the smoothness maximization models that have been studied in the context of hand trajectory formation [Richardson and Flash 2002]. These models do not take into account the body direction. However, they predict accurately the locomotor trajectories for a limited turning amplitudes.

In the present study, we have shown that the coupling between body position and body direction follows differential equations similar to nonholonomic mobile robots which has given rise to well defined control models. Synthesizing optimal motions for wheeled robots has been a major research area in robotics. By considering the effect of the differential constraint in the context of human locomotion we were able to propose a model accounting for the generation of locomotor trajectories involving narrow turns (i.e. trajectories with complex geometric shapes). Consequently, by using the optimal control tools already applied in mobile robots, the preceding chapters of this thesis have presented a research effort aimed at explaining the geometric shape of human locomotor trajectories.

We tested three optimization models by comparing how well they fit the experimental data. First we tested the minimum jerk model already studied in the context of hand trajectory formation [Flash and Hogan 1985]. Then we tested the Dubins' car model already studied in the context of wheeled robots [Laumond et al. 1998]. Finally, we proposed a dynamic extension of the unicycle as the model and the minimization of the L_2 norm of the control as the cost function. To determine the validity of the models, we compared predicted trajectories with all recorded locomotor trajectories composed of various lengths and curvatures. We have obtained predictions close to the real trajectories, at the geometric and kinematic levels, by applying the dynamic extension of the unicycle minimizing the derivative of the curvature.

In [Todorov and Jordan 1998] is stated that to measure how well a model predicts experimental data, it is not sufficient to evaluate the integrity of the fit. At least there exist two other criteria to take into consideration. One of them is the quantity of extracted information from experimental data. In our case we need a small number of parameters with respect to other models in the literature (e.g., for hand movement prediction [Viviani and Flash 1995; Todorov and Jordan 1998] among others). Actually we need the initial and final positions and directions as well as the movement duration of real trajectories. The issue of speed-accuracy tradeoff in our experimental protocol of human locomotion has not been investigated (we mention this aspect in the perspectives). The second criterion for estimating the veracity of a model prediction is the number of parameters to be tuned in order to fit the data. In our case, because we used a numerical optimization method we have to tune the parameters related to the convergence rate of the algorithm (see Section 5.2.3).

For the dynamic extension of the unicycle model and optimizing the L_2 norm of the control as the cost function, the optimal control synthesis has been done by numerical computation. The numerical algorithms as well as an analysis of their robustness in capturing singularities as the *cut-locus* have been described in the last part of this study.

More precisely, we have generated optimal trajectories within the reachable space considered in the experimental protocol in order to cover the 3-dimensional space of human walking. For that, we have defined an origin of the space. Then we computed the optimal trajectories from the origin to each point in the discrete 3-dimensional space. After that, we have identified the combinations of basic geometric elements composing the family of optimal trajectories. Thus, we provide a vocabulary of the human walking composed by a finite number of words. The words of the vocabulary represent *motor patterns*. Each word maps a cell in the human walking reachable space. This means that for a given cell the walking subjects use the same pattern of motion. At the frontiers between cells either a continuous or a discontinuous transition of motor patterns occurs (i.e. a switch between two words).

The formulation of a vocabulary of actions has been reported in various movement neuroscience studies. For instance, [Mussa-Ivaldi and Bizzi 2000] have performed an experimental study on the spinal cord of frogs and rats suggests that the words of a vocabulary are represented by neuronal populations, each of which specifies a given motor act.

7.1 Perspectives

The study presented in this document deserves comments and opens questions :

- The reachable space of the control system 8.10 covers the entire $R^2 \times S^1$ configuration space of the position and the direction of the human body. However our model accounts only for a part of a human locomotion strategies. Indeed when the configuration to be reached is just behind you, you will certainly perform a *backward* step motion. If the configuration is just on your left, then you will perform a *sideway* step. Both backward and sideway motions are not accounted by our model. We just focus on forward natural locomotion when the goal is defined *in front* of the starting configuration. The scope of our model remains to be defined in terms of the shape of the reachable space it accounts for.
- Applying the maximum principle we found that the optimal trajectories verify locally $u_1^2 + u_2^2$ should be constant. The result is not surprising (see[Sastry and Montgomery 1992]). However the result only holds if $u_2 \not\equiv 0$. In the numerical analysis we performed u_2 is never zero over a non empty time interval for the considered reachable space. The case $u_2 \equiv 0$ (arcs of a circle and straight line segments) may appear for long range paths. This theoretical issue is the subject of ongoing research.
- The current study opens intriguing mathematical questions. Usually, in optimal control, the considered costs induce metrics in the state space. Here the cost of a trajectory does *not* induce any metric : for instance, as for Dubins' model, the considered cost is not symmetric at all. We can say that the locomotion space is not a metric space. What special geometry accounts for the locomotion space ? We have seen that the presence of special structures as the observed cut-locus is related to SubRiemannian geometry. However the space is not equipped with a SubRiemannian metric.
- From a pure neuroscience point of view, our study validates the top-down methodology approach. It appears that decisional problems, such as the problem to decide *before moving* what strategy the subject selects (Figure 1.2.c), is accounted by the *same* model explaining how the trajectories are reshaped locally with respect to the goal to be reached (Figure 1.2.b). As a consequence the brain *plans* its actions. It has a *global* point of view of the task to be performed. A reasonable conjecture to explain the shape of the locomotor trajectories could have be a simple *local* sensory feedback control assumption : the gaze seems to be the only sensor used by the subjects in our experiments ; we have checked that the gaze is always directed towards the goal ; then it would have been possible to conclude that the body *follows* the gaze (as the rear wheels of a car follow the front wheels). This conjecture is not true : as depicted in the study case of Figure 3.5 (see Chapter 3 for details) it may appear that the body is turning right while the head is turning left. As

a consequence locomotion does not obey such a simple sensory feedback control model tending to reduce locally some sensory distance to the goal. Our study shows that *planning* (i.e. open-loop control) gives an explanation that pure *feedback control* (i.e. close-loop control) cannot give. The open question is now this one : how are planning and feedback control related ? This is the next step of our current research.

– A natural extension of the present study is the definition of a similar experimental protocol but in this case the width of the doorway may vary as well as the subjects walking speeds. Optimal control and filtering techniques can be used to describe and to model the locomotor behaviors.
– We can apply the trajectory deformation tools developed for mobile robots to address the problem of human navigation in presence of a single obstacle. If we consider a static obstacle, the idea is to identify whether the trajectory deformation occurs early during the task execution (leading to slight deformation distributed among the whole trajectory) or it occurs at a specific part of the trajectory, where it leads to a local deformation with a larger curvature around the obstacle. The question is to understand what criteria the subjects are optimizing (length versus smoothness). In the case of a moving obstacle, the main difference with the static obstacle case is that the subject does not have the a priori knowledge of the potential collision position. Assuming that the subject is able to predict the crossing point between the moving object and him, then we may consider the case in which the subject decreases its speed without modifying its direction to reach the crossing point after the moving obstacle with a sufficient safety delay. But there may exist the case in which the subject modifies its direction but not its speed in order to pass behind the obstacle with a sufficient safety distance. The last case may be a combination of these two behaviors. To address this problem we may analyze the dynamic balance of the subject during his collision-avoidance tasks.

8

Résumé

Introduction

L'objectif de ce travail est d'étudier la locomotion humaine. Nous partons d'une observation simple : quand les humains marchent, ils marchent vers l'avant et la direction instantanée du corps est tangente à la trajectoire qu'ils réalisent (sans prendre en compte les oscillations dues au cycle de marche). Ce couplage entre la direction θ et la position (x,y) du corps peut être exprimée par l'équation différentielle : $tan\theta = \frac{\dot{y}}{\dot{x}}$. Nous savons que cette équation différentielle définit une distribution non-intégrable de dimension 2 : le couplage entre θ et (x,y) impose une contrainte non holonome parce qu'elle ne restreint pas la dimension de l'espace accessible à partir d'une configuration quelconque. Une base de la distribution peut être obtenue par les champs de vecteurs suivants :

$$\begin{pmatrix} \cos\theta \\ \sin\theta \\ 0 \end{pmatrix} \text{et} \begin{pmatrix} 0 \\ 0 \\ 1 \end{pmatrix} \tag{8.1}$$

De récentes recherches conduites en neurosciences sur les mouvements intentionnels dans la fonction locomotrice se sont focalisées principalement sur l'intégration dynamique de différents capteurs afin de faciliter l'élaboration des commandes locomotrices pour atteindre une posture du corps désirée [Berthoz and Viaud-Delmon 1999]. La locomotion utilise simultanément plusieurs capteurs pendant nos déplacements : vestibulaires, proprioceptifs et visuels. Les entrées de ces capteurs ont été analysées pendant la marche normale et la marche en l'absence de vision afin d'étudier comment les humains peuvent d'une manière continue contrôler leurs trajectoires [Glasauer et al. 2002; Hicheur et al. 2005]. Cependant, la question de savoir quels sont les critères qui gouvernent la génération (ou la planification)

de trajectoires pour le corps entier n'a pas reçu beaucoup d'intérêt. Récemment, il a été montré dans le cas de trajectoires dessinées au sol qu'il existe des principes communs qui gouvernent la génération de trajectoires des mains et du corps entier [Vieilledent et al. 2001; Hicheur et al. 2005]. En particulier, il a été observé un fort couplage entre le profil de la courbure et la vitesse linéaire avec une certaine différence quantitative entre deux types de mouvements [Hicheur et al. 2005].

On peut constater que les configurations géométriques possibles de chaque partie du corps sont restreintes par les limites articulaires [Winter 2004]. Ce point de vue biomécanique de la locomotion humaine a été abordé dans le domaine de l'animation graphique [Multon et al. 1999] et dans le domaine de la robotique humanoïde [Raibert 1986; Hirukawa et al. 2005]. Nous ne considérons ici ni les capteurs ni la complexité d'un modèle mécanique du corps humain. Le point de vue abordé est plutôt complémentaire. Nous nous intéressons en effet à la forme des trajectoires locomotrices dans un espace de dimension 3 qui comprend la position et la direction du corps. Nous montrons que les trajectoires locomotrices peuvent être modélisées par un système différentiel.

Un des systèmes non holonomes les plus populaires est celui de la voiture [Li and Canny 1993; Laumond et al. 1998]. Ce système est soumis à une contrainte de roulement sans glissement qui se traduit par l'équation différentielle 8.1. Du point de vue du conducteur, une voiture possède deux commandes : l'accélérateur et le volant. La première question abordée ici pourrait être formulée de la manière suivante : où se trouve le "volant" du corps humain ? Plusieurs repères ont été associés aux différents parties du squelette (tête, tronc et bassin). Dans cette partie de notre étude expérimentale nous montrons qu'il existe un repère qui prend en compte la nature non holonome de la locomotion humaine et que c'est le tronc qui joue le rôle du "volant".

La deuxième question abordée dans ce travail est la suivante : parmi toutes les trajectoires possibles qui existent pour atteindre une position avec une orientation données, pourquoi l'humain effectue une trajectoire plutôt d'une autre ? Afin de donner une réponse à cette question, nous avons fait appel à la commande optimale : les trajectoires ont été choisies selon un critère à optimiser.

Dans cette perspective, le sujet est vu comme un système de commande et la question devient : quel est le critère à optimiser ? Est-ce la longueur de la trajectoire ? Ou le temps parcouru ? Ou la secousse minimale ?... Dans cette étude nous montrons que les trajectoires locomotrices peuvent être approchées par les géodésiques d'un système différentiel minimisant la norme L_2 de la commande. Ces géodésiques sont composées de morceaux de clothoides. Une clothoide, ou spirale de Cornu, est une courbe dont la courbure varie linéairement en fonction de l'abscisse curviligne. Nous montrons que 90 % des trajectoires faites par les 7 sujets de nos expérimentations ont été approchées avec une erreur moyenne de moins de 10cm.

Dans la dernière partie de ce travail nous réalisons la synthèse numérique de trajectoires optimales dans l'espace atteignable. Il s'agit de partitionner l'espace des configurations par rapport aux différents types de trajectoires optimales qui peuvent relier l'origine à un point dans cet espace. Deux points appartiennent à une même cellule si les trajectoires parcourues sont de même type. Dans la plupart des cas le passage entre deux cellules adjacentes se fait par une déformation continue des trajectoires. Il est remarquable de noter que les rares cas de discontinuités du modèle proposé correspondent précisément aux changements de stratégies observées chez les sujets.

La section suivante présente le protocole expérimental pour enregistrer les trajectoires à partir de la capture de mouvement. Ensuite, nous présentons le matériel et l'analyse de données. Puis, l'étude comparative entre le repère de la tête, du tronc et du bassin est présentée. Après, nous proposons un modèle pour la marche humaine. Ensuite, nous étudions la forme géométrique des trajectoires locomotrices et finalement nous présentons la synthèse numérique de la marche humaine.

Matériel et protocole expérimental

Nous avons utilisé la technologie de capture du mouvement afin d'enregistrer les trajectoires des corps en trois dimensions. Les sujet ont été équipés de 34 marqueurs passifs et fonctionnant à une fréquence d'échantillonage de 120 Hz (système Vicon V8, Oxford metrics).

Placé dans un gymnase, ce système était composé de 24 caméras. Les marqueurs étaient des sphères recouvertes de papier adhésif réfléchissant la lumière infrarouge des caméras. Il est important de noter que nous n'avons utilisé aucun filtre pour faire l'analyse de données (voir Figure 8.1).

Afin d'expliquer les propriétés géométriques des trajectoires locomotrices, nous avons enregistré les trajectoires de 7 sujets dans un gymnase. Afin de mesurer la position du sujet au sol, nous avons fait le rapport entre le repère global placé dans le gymnase et le repère de la trajectoire à partir de marqueurs attachés à la tête, au tronc et au bassin. Le calcul de (x, y) et θ à partir des marqueurs est expliqué après.

Nous avons demandé aux sujets de marcher d'une configuration initiale (x_i, y_i, θ_i) à une configuration finale (x_f, y_f, θ_f) choisie de manière aléatoire. La configuration initiale était toujours la même tandis que la configuration finale était représentée par un portique en rotation par rapport une position fixée (voir Figures 8.2.a et 8.2.b). Les sujets ont choisi leur vitesse sans aucune contrainte spatiale. L'angle θ variait de $-\pi$ à π par intervalles de $\frac{\pi}{6}$ en chaque configuration finale. Afin de supprimer les effets causés par l'accélération initiale et finale, les sujets ont commencé à marcher deux mètres avant (x_i, y_i, θ_i) et ils se sont arrêtés deux mètres après (x_f, y_f, θ_f). Les premiers et derniers pas ne sont donc pas considérés dans cette étude (voir Figure 8.3).

L'expérience a été faite pendant 7 sessions. Le premier sujet a réalisé 480 trajectoires différentes en 2 sessions. Les 6 autres sujets ont réalisé en 6 sessions 180 trajectoires avec 60 configurations finales différentes.

Repères et analyse des données

Afin de décrire les trajectoires du mouvement du corps pendant la marche, nous avons défini des repères locaux par rapport au repère global placé dans le gymnase. Trois repères ont été considérés, au niveau de la tête (RF_H), du tronc (RF_T) et du bassin (RF_P), respectivement. L'origine et la direction de RF_H, RF_T et RF_P ont été déterminés à partir de marqueurs.

Afin de représenter l'origine (x_H, y_H) de RF_H, nous avons utilisé les marqueurs qui se trouvent à l'avant et l'arrière de la tête. La direction φ_H a été identifiée facilement à partir du segment qui va du marqueur de l'avant au marqueur de l'arrière.

Pour le tronc RF_T, nous avons calculé le point (x_T, y_T) comme barycentre des marqueurs au niveau

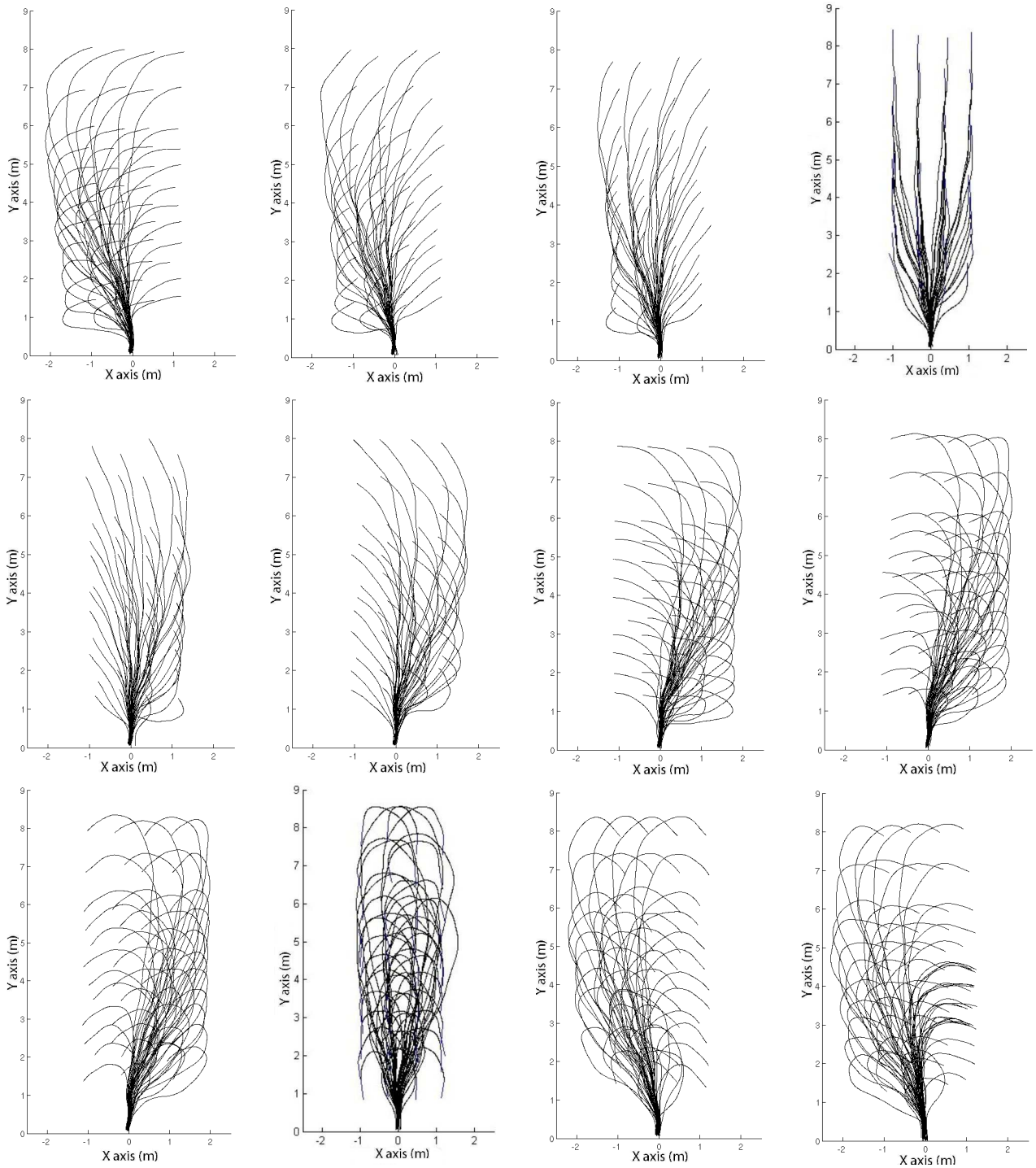

FIG. 8.1 – *Quelques exemples de trajectoires enregistrées avec une même direction finale. De haut en bas et de gauche à droite, la direction finale varie de -π à π par intervalles de* $\frac{\pi}{6}$.

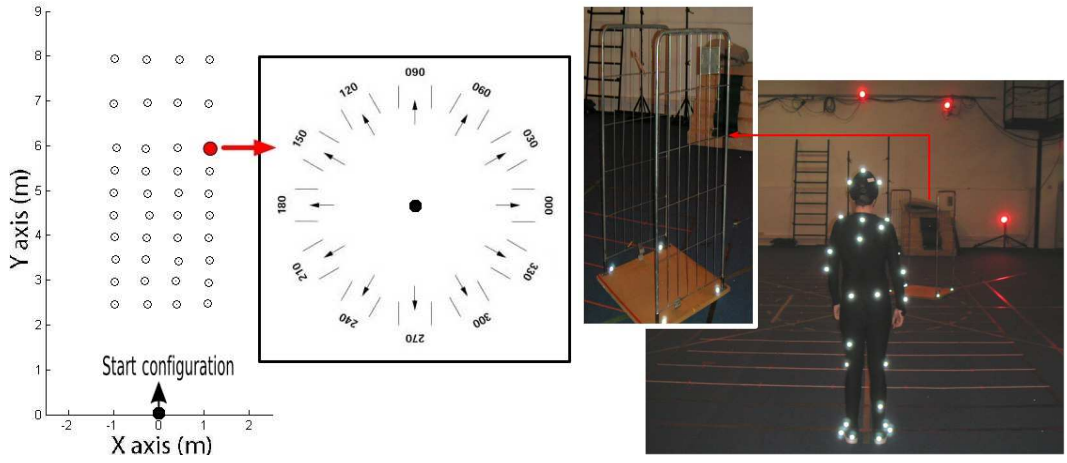

(a) (b)

FIG. 8.2 – *(a) Nous avons ici échantillonné une zone d'un gymnase par 480 points définis en 40 positions au sol (dans un espace de 5mpar 9m) et 12 directions en chaque position. La configuration initiale a été toujours la même alors que la cible a été sélectionnée aléatoirement. Un sujet a fait les 480 trajectoires tandis que les autres 6 ont fait un sous-ensemble des trajectoires. (b) Le portique et le gymnase utilisés dans l'expérience.*

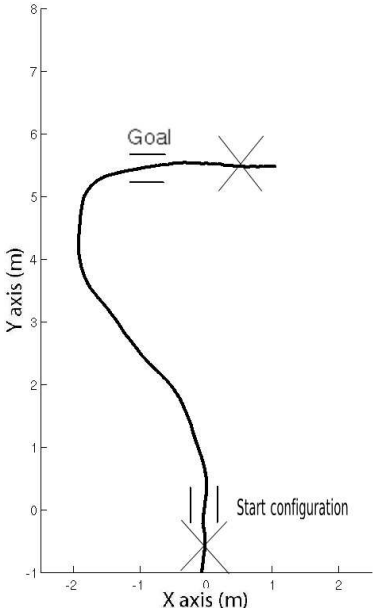

FIG. 8.3 – *Afin de supprimer les effets causés par les accélérations initiale et finale, les sujets ont commencé à marcher deux mètres avant* (x_i, y_i, θ_i) *et ils se sont arrêtés deux mètres après* (x_f, y_f, θ_f).

des épaules et comme direction φ_T nous avons pris la direction orthogonale à l'axe des épaules. Enfin, pour trouver l'origine (x_P, y_P) de RF_P et la direction φ_P, nous avons utilisé quatre marqueurs qui entourent le bassin du sujet.

Afin d'obtenir le profil de vitesse, nous avons fait appel au calcul numérique. Chaque trajectoire est représentée comme une séquence de points dans le plan. Nous avons calculé la vitesse linéaire v et angulaire ω en chaque point :

$$\begin{aligned} \dot{x}(\tau) &\leftarrow \tfrac{x(\tau+\Delta\tau)-x(\tau-\Delta\tau)}{2\Delta\tau} \\ \dot{y}(\tau) &\leftarrow \tfrac{y(\tau+\Delta\tau)-y(\tau-\Delta\tau)}{2\Delta\tau} \\ v(\tau) &\leftarrow \sqrt{\dot{x}^2(\tau)+\dot{y}^2(\tau)} \end{aligned} \tag{8.2}$$

$$\omega(\tau) \leftarrow \frac{\varphi(\tau+\Delta\tau)-\varphi(\tau-\Delta\tau)}{2\Delta\tau} \tag{8.3}$$

où $x(\tau)$, $y(\tau)$ et $\varphi(\tau)$ sont les paramètres de la configuration du corps le long de la trajectoire. Afin de calculer la tangente à la trajectoire à chaque instant, nous avons utilisé la relation :

$$\theta(\tau) \leftarrow tan^{-1}\left(\frac{\dot{y}(\tau)}{\dot{x}(\tau)}\right) \tag{8.4}$$

Il faut remarquer que $\varphi(\tau)$ est calculé à partir de marqueurs tandis que $\theta(\tau)$ est calculé à partir de la séquence de points $x(t), y(t)$. Pour obtenir la variation instantanée de $\theta(\tau)$, nous avons remplacé $\omega(\tau)$ et $\varphi(\tau)$ par $\dot{\theta}(\tau)$ et $\theta(\tau)$, respectivement.

Comparaison de la direction de la tête, du tronc et du bassin

Nous allons maintenant décrire l'analyse temporelle de trois différents paramètres de direction mesurés $\varphi_H(\tau)$, $\varphi_T(\tau)$ et $\varphi_P(\tau)$. L'analyse que nous avons faite est qualitative et quantitative, afin de déterminer, parmi les différentes directions mesurées, quelle est celle qui se rapproche au mieux de $\theta(\tau)$.

Afin de faire l'évaluation, nous avons comparé le profil de $\varphi_H(\tau)$, $\varphi_T(\tau)$ et $\varphi_P(\tau)$ par rapport à celui de $\theta(\tau)$, le long des trajectoires. Nous nous sommes aperçu que la direction de $\theta(\tau)$ est presque tout le temps vers le but. En effet, dans certains cas, $\varphi_H(\tau)$ pointe du côté opposé par rapport à $\theta(\tau)$. Pour le tronc, nous avons observé que les traces de $\varphi_P(\tau)$ et $\theta(\tau)$ étaient très similaires. Pourtant, la comparaison en temps nous a indiqué qu'il existe un décalage d'entre $\frac{1}{4}$ et $\frac{1}{8}$s. à l'arrière. Autrement dit :

$$\dot{\varphi_T}(\tau+\varepsilon) \simeq \dot{\theta}(\tau) \tag{8.5}$$

où ε représente la durée du décalage à l'arrière. Après avoir examiné $\varphi_P(\tau)$ par rapport à $\theta(\tau)$, nous avons observé que $\varphi_P(\tau)$ oscille avec une amplitude de près de 15 degrés même dans une courbe (voir Figure 8.4). Ces variations sont causées par le cycle de marche.

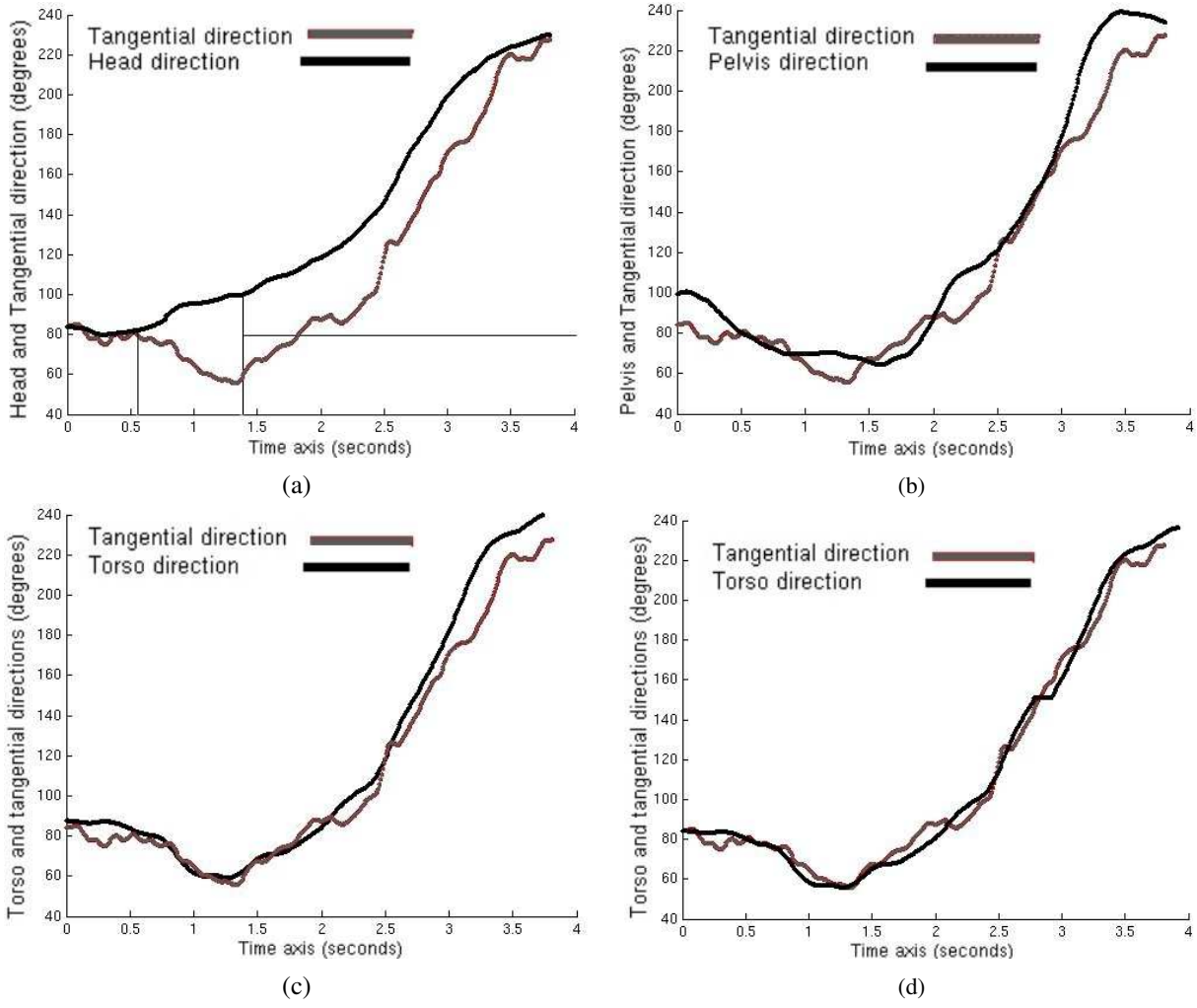

FIG. 8.4 – *Le profil de la direction de la tête, du tronc et du bassin par rapport à la tangente à la trajectoire, respectivement. (a) montre le profil de la tête vis-à-vis de la tangente. (b) montre le profil du bassin vis-à-vis de la tangente. (c) montre le profile du tronc décalé de* $\frac{1}{6}s$ *à l'arrière vis-à-vis de la tangente. Toutes correspondent au même mouvement.*

Un modèle pour la marche humaine

Afin de mesurer l'erreur de l'approximation $\dot{\varphi}_T(\tau+\varepsilon) \simeq \dot{\theta}(\tau)$, nous avons défini RF_T comme le repère local du corps afin de faire l'intégration numérique du système cinématique suivant :

$$\begin{pmatrix} \dot{x_T} \\ \dot{y_T} \\ \dot{\varphi_T} \end{pmatrix} = \begin{pmatrix} \cos\varphi_T \\ \sin\varphi_T \\ 0 \end{pmatrix} v + \begin{pmatrix} 0 \\ 0 \\ 1 \end{pmatrix} \omega \tag{8.6}$$

La contrainte de non holonomie de ce système est représentée par :

$$\dot{y}\cos\varphi_T - \dot{x}\sin\varphi_T = 0. \tag{8.7}$$

Pour valider le modèle, nous avons calculé $v(t)$ et $\omega(t)$ en utilisant les Équations 8.2 et 8.3 afin d'obtenir les entrées du système à partir de trajectoires enregistrées par rapport au RF_T. Ensuite, nous avons intégré le système différentiel (voir Équation 8.6) en utilisant ces entrées et en considérant ε.

Par la suite, nous avons calculé la distance en chaque point entre la trajectoire intégrée et la trajectoire enregistrée (réelle). Finalement, nous avons calculé l'erreur moyenne de la distance en divisant la somme des erreurs par le nombre de points.

Cette procédure a été réalisée pour 1560 trajectoires effectuées par 7 sujets. La longueur des trajectoires allait de 3 à 9 mètres. La vitesse était de $1,26\pm$ mètres/seconde (m/s). Nous avons constaté que l'approximation de ce modèle a une erreur de précision $<$ 10cm pour 87% des trajectoires satisfaisant le modèle de la voiture.

Le modèle présenté précédemment est le point de départ pour commencer l'étape suivante de notre travail. Cette dernière consiste à expliquer la forme géométrique des trajectoires locomotrices par la théorie de la commande optimale.

La forme géométrique des trajectoires locomotrices

Les études réalisées en neurosciences sur la modélisation du mouvement humain ont souligné l'importance de la courbure des trajectoires [Lacquaniti et al. 1983; Viviani and Flash 1995; Todorov and Jordan 1998; Vieilledent et al. 2001; Richardson and Flash 2002]. Afin d'éviter d'éventuelles discontinuités de la courbure, nous avons considéré celle-ci comme une variable du système. Par conséquent, une extension dynamique du Modèle 8.6 est considérée en commandant cette fois la dérivée de la courbure au lieu de la vitesse angulaire.

$$\begin{pmatrix} \dot{x_T} \\ \dot{y_T} \\ \dot{\varphi_T} \\ \dot{\kappa_T} \end{pmatrix} = \begin{pmatrix} \cos\varphi_T \\ \sin\varphi_T \\ \kappa_T \\ 0 \end{pmatrix} u_1 + \begin{pmatrix} 0 \\ 0 \\ 0 \\ 1 \end{pmatrix} u_2 \tag{8.8}$$

Les commandes u_1 et u_2 sont, pour ce système, la vitesse linéaire et la dérivée de la courbure, respectivement.

Dans cette section, nous considérons le problème de déplacement optimal du Système 8.8 depuis une configuration initiale donnée par $q(0) = q_0$ à une configuration finale $q(T) = q_f$, en supposant que $u_1 \in [a,b]$ avec $a > 0$ (mouvement en avant) et $u_2 \in [-c,c]$. Le coût à optimiser est donné par

$$J = \frac{1}{2}\int_0^T <(u(\tau),u(\tau))> d\tau \tag{8.9}$$

En appliquant le principe du maximum de Pontryagin [Pontryagin et al. 1964] (PMP) nous avons obtenu que les trajectoires optimales vérifient, localement, que $u_1^2 + u_2^2$ doit être constant (voir [Sastry and Montgomery 1992] pour le cas général). Nous n'avons pas pu extraire plus d'information du PMP. Par conséquent, nous avons utilisé un algorithme numérique afin de trouver la solution optimale (voir Algorithme 5.1). Nous avons constaté que u_1 devient toujours constante dans l'espace qui a été considéré dans le protocole expérimental. Les solutions optimales ont été comparées au niveau géométrique avec les trajectoires réelles pour les mêmes configurations initiales et finales afin de mesurer l'erreur de prédiction. Nous avons constaté que l'erreur de prédiction de ce modèle est $<$ 10cm pour 90% des trajectoires. Ainsi, les trajectoires locomotrices sont bien approximées par les solutions optimales de l'extension dynamique du modèle de l'unicycle, et les trajectoires locomotrices minimisent la dérivée de la courbure.

Selon l'analyse du PMP pour notre problème d'optimisation, $u_1^2 + u_2^2$ doit être constant. Ainsi, nous pouvons déduire que u_2 devrait être une fonction constante par morceaux. Si $\dot{\kappa}_T = u_2$ et en considérant que $u_2 = cu_1$, par intégration nous obtenons que $\kappa_T = cs + \kappa_0$ où κ_0 est la courbure initiale, $s = u_1\tau$ et c est une constante. Une courbe parcourue à vitesse constante où la courbure augmente ou diminue linéairement en fonction de l'abscisse curviligne est une clothoide. Donc, les arcs de clothoides sont une bonne approximation des trajectoires locomotrices.

La Figure 8.5 montre une trajectoire réelle qui a été effectuée par un sujet et la trajectoire optimale qui a été calculée pour relier les mêmes configurations initiales et finales.

Synthèse : les mots de la marche humaine

Introduction

L'équation 8.7 est l'équation différentielle classique qui gouverne *les mouvements d'une roue qui roule*, et donc les mouvements des robots mobiles à roues. Comment déplacer un robot mobile d'une configuration initiale à une configuration finale données en position et en direction (i.e. dans un espace à trois dimensions) tandis que l'espace de commande du robot est à deux dimensions ? La question a motivé une activité de recherche importante pendant ces vingt dernières années. Parmi les nombreuses méthodes développées dans cet axe de recherche (voir un résumé général [Laumond et al. 1998], [Choset et al. 2005] et [LaValle 2006]), les méthodes qui se basent sur la commande optimale sont certainement les plus efficaces. Malheureusement, la contrainte de nonholonomie rend le problème difficile à résoudre. Le problème a été résolu seulement pour des systèmes simples. Un des plus populaires est la voiture de Dubins [Dubins 1957] et la voiture de Reeds et Shepp [Reeds and Shepp 1990; Sussmann and Tang 1991] (voir également [Balkcom et al. 2006; Boissonnat et al. 1992] et le résumé général [Souères and

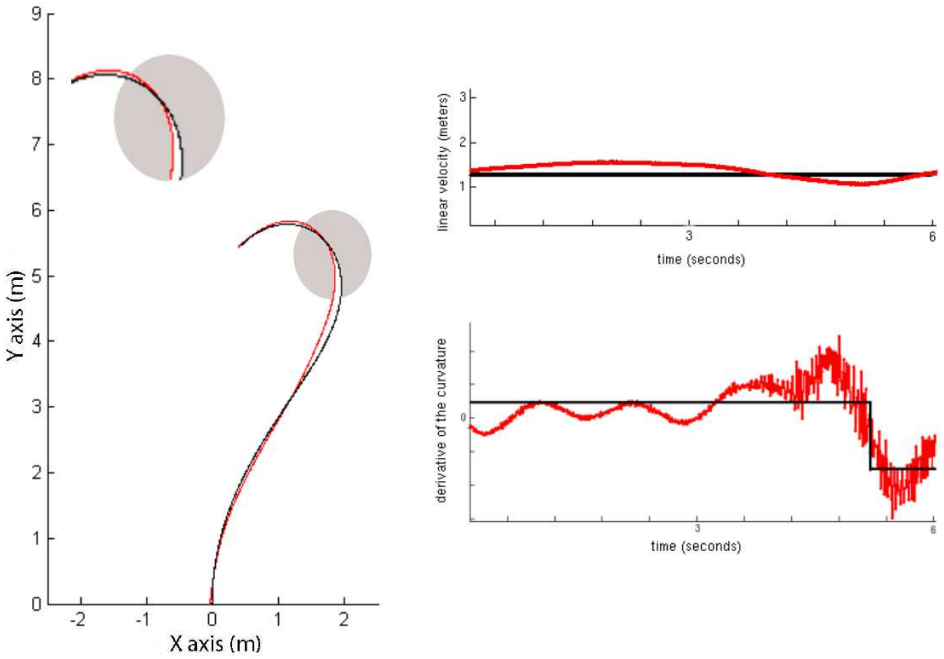

FIG. 8.5 – *À gauche : superposition d'une trajectoire réelle (rouge) et d'une trajectoire optimale (noir) reliant les mêmes configurations initiales et finales. À droite : superposition de la commande qui correspond à la trajectoire réelle (rouge) et de la commande qui correspond à la trajectoire optimale (noir).*

Boissonnat 1998]).

Nous allons expliquer la synthèse analytique de la voiture de Dubins puisque c'est le système le plus proche de notre problème. La voiture de Dubins est une voiture qui se déplace seulement vers l'avant à vitesse linéaire constante. Elle correspond au système de commande suivant :

$$\begin{pmatrix} \dot{x} \\ \dot{y} \\ \dot{\theta} \end{pmatrix} = \begin{pmatrix} \cos\theta \\ \sin\theta \\ 0 \end{pmatrix} + \begin{pmatrix} 0 \\ 0 \\ 1 \end{pmatrix} u \tag{8.10}$$

où u est la vitesse angulaire bornée dans l'intervalle $(-1,1)$. Dubins [Dubins 1957] (et puis Sussmann et autres [Sussmann and Tang 1991] prouve, en utilisant la théorie de la commande optimale moderne comme le principe du maximum de Pontryagin [Pontryagin et al. 1964]), que les plus courts chemins du système sont composés par une séquence ordonnée de segments de ligne droite S $(u = 0)$ et d'arcs de cercle de rayon minimal constant C $(u = \pm 1)$.

En considérant qu'un arc de cercle C peut tourner à droite R (quand $u = 1$) ou à gauche L (quand $u = -1$), Dubins a montré qu'une famille suffisante des plus courts chemins est la suivante : $RSR, RSL, LSR, LSL, LRL, RLR$. Ces séquences, nous les appelons les "mots" de la voiture du Dubins. De ceci, nous pouvons conclure que six mots sont nécessaires pour décrire les chemins optimaux. Une autre question se pose : quelle est la partition de l'espace (à trois dimensions) selon les divers mots ? Ce problème a été résolu dans [Pecsvaradi 1972; Bui et al. 1994]. La Figure 8.6 montre deux tranches de la

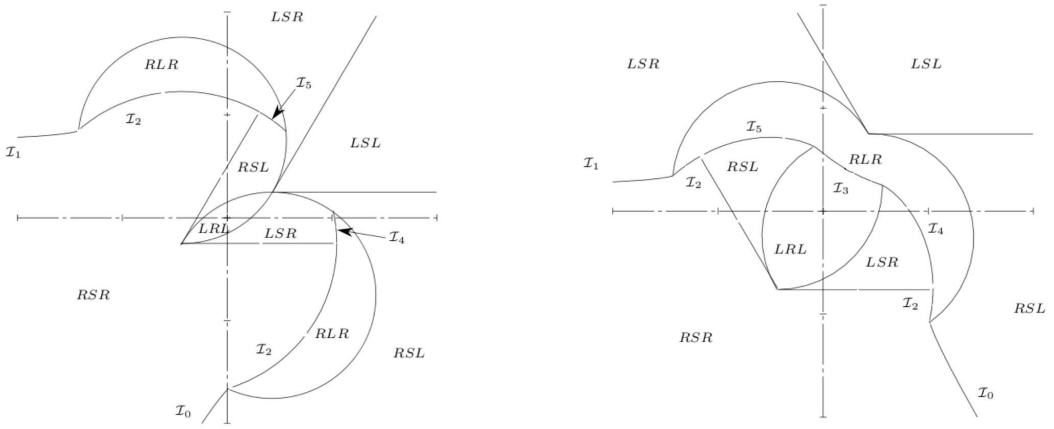

(a) (b)

FIG. 8.6 – *La partition des tranches $\theta = \frac{\pi}{3}$ et $\theta = \frac{2\pi}{3}$ induite par les mots de Dubins. Les images sont tirées de [Souères et Boissonnat 1998].*

partition de l'espace selon les mots de Dubins quand la direction donnée par $\theta = \frac{\pi}{3}$ et $\theta = \frac{2\pi}{3}$ est fixée.

Le calcul d'une telle partition a été fait pour d'autres systèmes [Souères and Laumond 1996; Balkcom and Mason 2002]. Ces contributions sont basées sur l'application du principe de Pontryagin qui donne (seulement) des conditions nécessaires d'optimalité. Des conditions nécessaires et suffisantes peuvent être trouvées dans les travaux de Boltyanskii [Boltyanskii 1966]. Elles sont liées à la synthèse régulière de la commande optimale. La solution générale du problème de la synthèse régulière (i.e. pour tout type de système non linéaire) reste un problème mathématique extrêmement difficile.

De plus, l'application du principe de Pontryagin ne fournit pas assez d'information pour décrire les trajectoires optimales par une séquence finie de mots. C'est pour cela que la plupart du temps, le calcul optimal de trajectoires est mené en utilisant des algorithmes d'analyse numérique [Nocedal and Wright 1999; Garcia 1994; Hiriart-Urruty and Lemaréchal 1996]. L'objectif ici est de fournir la synthèse numérique de la marche humaine.

Synthèse

Dans cette section, nous caractérisons numériquement les chemins optimaux par le nombre d'arcs enchaînés de clothoides. Nous pouvons définir une clothoide comme une courbe satisfaisant l'équation suivante :

$$\kappa(\tau) = \pm c\tau, \quad \tau \in (-\infty, \infty) \tag{8.11}$$

où c est une constante et le signe $(\pm)$ définie l'orientation de chaque morceau de clothoide. Donc, nous pouvons déterminer une seule clothoide par

$$\begin{aligned} u_2(\tau) &\equiv c, \qquad \kappa(\tau) \to \infty \\ &\textit{ou} \\ u_2(\tau) &\equiv -c, \qquad \kappa(\tau) \to -\infty. \end{aligned} \tag{8.12}$$

Depuis les résultats obtenus précédemment, nous savons que $u_2(\tau)$ est une fonction constante par morceaux. Le point qui se trouve à la conjonction deux morceaux de clothoides est appelé *point de commutation*. À chaque point de commutation, la fonction de courbure a un extremum local et la dérivée de la courbure u_2 a une discontinuité.

Notre approche consiste à déterminer le nombre et l'ordre des points de commutation pour chaque chemin optimal. La méthode est basée sur l'analyse locale de la courbure. Pour être plus précis, en chaque extremum local de la courbure, il existe un point de commutation. Donc, une description des régions dans l'espace de configuration est obtenue en répétant le processus ci-dessus pour toutes les trajectoires optimales possibles. En effet, nous avons identifié les ensembles de trajectoires optimales qui sont définies par l'orientation de chaque morceau de clothoide et par le nombre d'arcs de clothoides.

Pour calculer la synthèse numérique de nôtre problème d'optimisation, nous avons pris en compte la partie de l'espace d'accessibilité considéré dans le protocole expérimental $(x,y,\theta) \in R^2 \times S^1$. En conséquence, nous avons seulement considéré l'espace devant la configuration initiale (la marche vers l'avant). Nous avons défini le point $(0,0,\frac{\pi}{2})$ comme l'origine de l'espace de configuration ($\kappa = 0$ au début et à la fin). Nous avons calculé une approximation de l'espace par une grille de $[-2,2] \times [3,9]$ en position. La résolution de la grille est $(0.2m \times 0.2m \times \frac{\pi}{18})$. L'analyse a été effectuée selon les étapes suivantes :

1. $R^2 \times S^1$ est représenté par 36 tranches avec la direction finale θ fixée.
2. Pour chaque θ-tranche, nous avons calculé numériquement toutes les trajectoires optimales reliant l'origine à chaque sommet de la grille.
3. À chaque θ-tranche, nous avons déterminé les régions données par les types de chemins optimaux. Chaque région correspond à un ensemble de trajectoires optimales contenant la même combinaison d'arcs de clothoides en fonction de leurs orientations.

En considérant que la courbure κ d'un arc de clothoide peut augmenter I_τ (quand $u_2 = c$) ou diminué D_τ (quand $u_2 = -c$) pendant un temps donné τ, alors nous avons trouvé numériquement que seulement 6 types de chemins optimaux apparaissent :

1. $I_{\tau_1} D_{\tau_2} I_{\tau_3}$
2. $D_{\tau_1} I_{\tau_2} D_{\tau_3}$
3. $I_{\tau_1} D_{\tau_2} I_{\tau_3} D_{\tau_4}$
4. $D_{\tau_1} I_{\tau_2} D_{\tau_3} I_{\tau_4}$
5. $I_{\tau_1} D_{\tau_2} I_{\tau_3} D_{\tau_4} I_{\tau_5}$
6. $D_{\tau_1} I_{\tau_2} D_{\tau_3} I_{\tau_4} D_{\tau_5}$.

Nous appelons ces combinaisons les mots de la marche humaine.

Analyse géométrique et interprétation par la commande motrice

Les mots ci-dessus induisent une partition en cellules de l'espace de configuration $R^2 \times S^1$. Considérons un mot, e.g. $I_{\tau_1} D_{\tau_2} I_{\tau_3}$. Notons la projection $R^3 \to R^2 \times S^1$ qui associe (τ_1, τ_2, τ_3) à une configuration dans la cellule du mot correspondant. Ceci signifie que les commandes motrices employées pour atteindre deux configurations différentes dans une même cellule suivent le même modèle. Elles diffèrent juste par la position des points de commutation. Quand une configuration change de manière continue dans une cellule donnée, les temps de commutations changent de manière continue. Que se produit-il entre deux cellules adjacentes ? Deux cas peuvent se présenter :

- Cas 1 : Traverser la frontière peut se faire par un changement continu de la commande motrice. Par exemple, les cellules $I_{\tau_1} D_{\tau_2} I_{\tau_3}$ et $D_{\tau_4} I_{\tau_5} D_{\tau_6}$ ont des frontières communes données par l'équation $\tau_1 = 0$ et $\tau_6 = 0$. Ceci signifie qu'il y a une déformation continue de la forme géométrique de la trajectoire (voir la partie supérieure de la Figure 8.7).
- Cas 2 : Traverser la frontière induite une discontinuité dans la commande motrice. En considérant les mêmes cellules $I_{\tau_1} D_{\tau_2} I_{\tau_3}$ et $D_{\tau_4} I_{\tau_5} D_{\tau_6}$, si leur frontière commune était respectivement $\tau_3 = 0$ et $\tau_6 = 0$, il y aurait une discontinuité de la forme géométrique de la trajectoire en traversant la frontière (voir la partie basse de la Figure 8.7).

Pour la plupart des cellules, leurs frontières sont gouvernées par le Cas 1. Le cas intéressant est le Cas 2. C'est un cas subtile : à la frontière commune entre deux cellules, il existe exactement deux trajectoires optimales avec le même coût, même si leurs formes sont complètement différentes. Le Cas 2 apparaît avec les systèmes nonholonomiques qui sont symétriques (par exemple une voiture qui se déplace en avant et vers l'arrière [Souères and Laumond 1996]). Ce cas singulier est appelé *cut-locus* dans le langage de la géométrie sub-Riemannian (voir [Bellaiche and Risler 1996]).

Il faut noter que le *cut-locus* de la synthèse ci-dessus reflète le changement de stratégie pendant la marche chez les sujets analysés (voir la Figure 8.8). Ceci signifie que les deux stratégies employées par les sujets obéissent *de facto* une même stratégie tendant à optimiser la dérivée de la courbure.

Conclusion

Nous avons présenté une étude sur la marche humaine en utilisant la commande optimale. Nous avons défini un protocole expérimental rigoureux afin d'enregistrer des trajectoires locomotrices de 7 sujets. Puis, nous avons trouvé une stéréotypie au niveau géométrique et cinématique. Cela nous a permis de montrer que les sujets utilisent une même stratégie pour marcher d'une configuration initiale à une configuration finale données en position et en direction. Après, nous avons proposé un modèle cinématique très simple qui vérifie l´hypothèse du couplage différentiel entre la position et la direction du corps pendant la marche.

Afin d'étudier la forme géométrique des trajectoires locomotrices, nous avons fait appel à la commande optimale : les trajectoires ont été choisies selon un critère à optimiser. Donc, en utilisant le modèle cinématique précédant et un critère énergétique, nous avons calculé la synthèse numérique. Cela nous a permis de trouver la partition de l'espace atteignable que nous avons considéré dans cet étude. De cette manière, nous avons calculé les différentes cellules qui correspondent aux différent

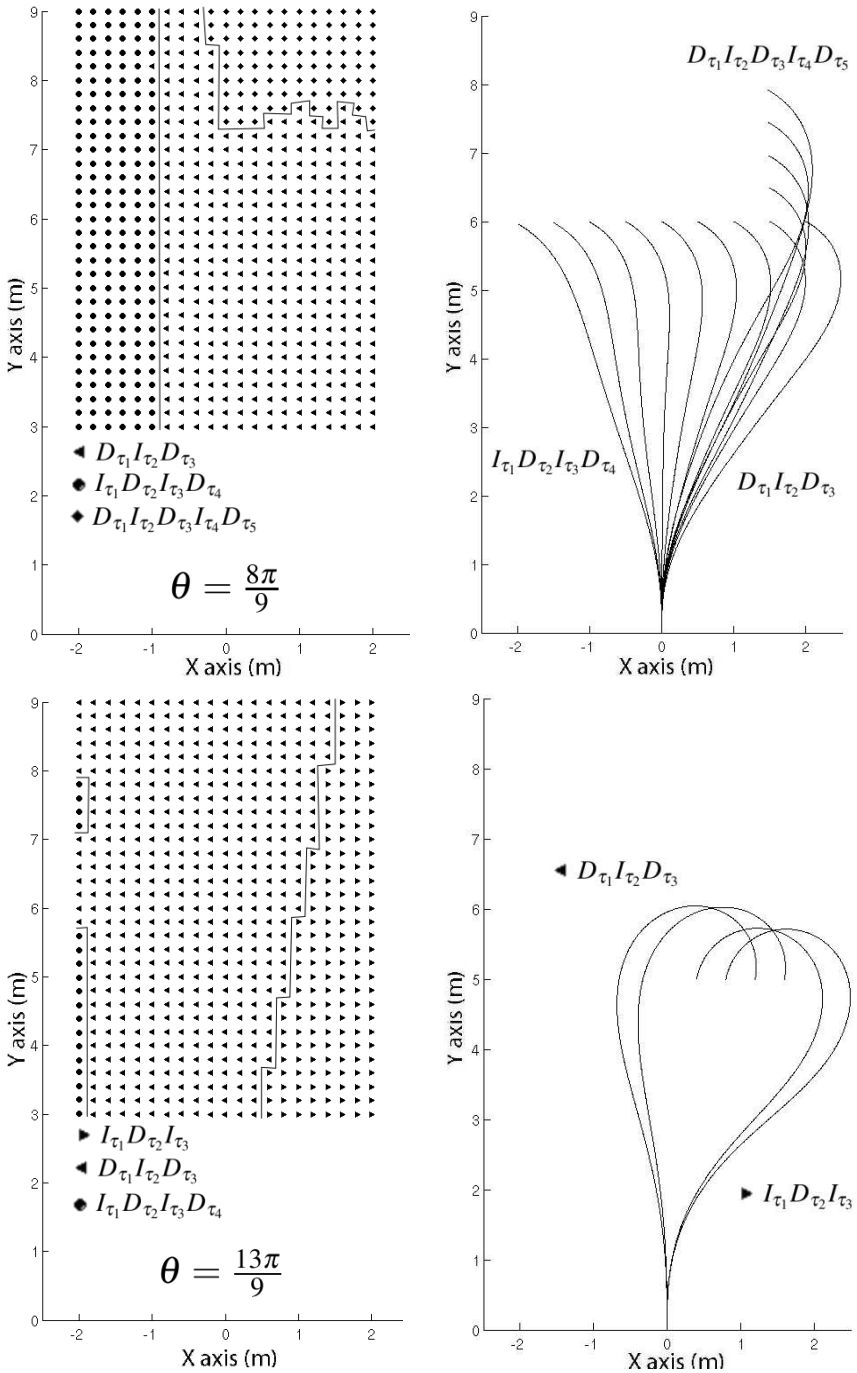

FIG. 8.7 – *En haut : Un exemple du Cas 1 pour $\theta = \frac{8\pi}{9}$. Les trajectoires traversent la frontière par une déformation continue. En bas : Un exemple du Cas 2 pour $\theta = \frac{13\pi}{9}$. Une discontinuité de la forme géométrique des trajectoires est apparue à la frontière entre deux cellules.*

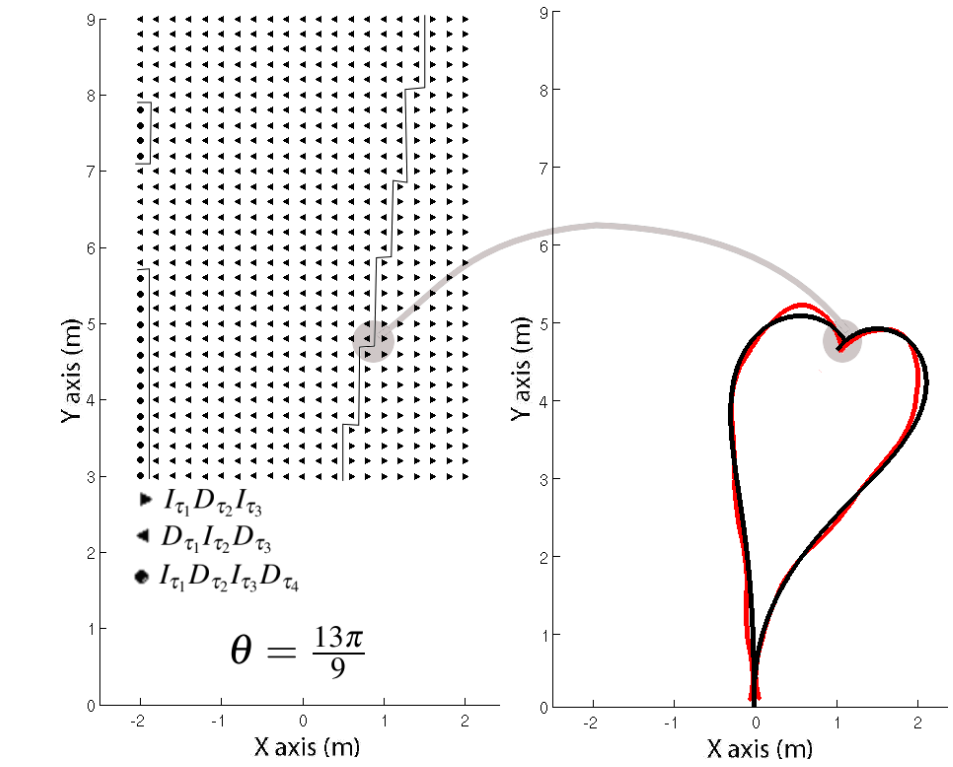

(a)

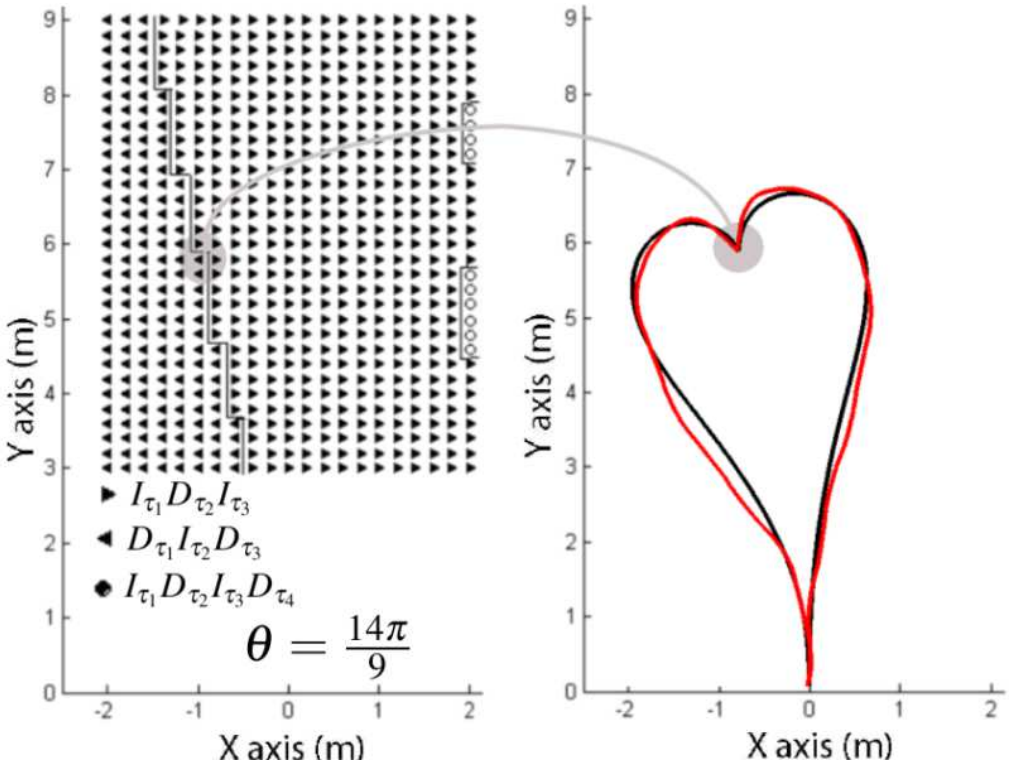

(b)

FIG. 8.8 – *À gauche : La partition des tranches $\theta = \frac{14\pi}{9}$ et $\theta = \frac{13\pi}{9}$. À droite : Exemples de deux configurations appartenant à deux cellules adjacents qui sont gouvernées par le Cas 2. La trajectoire réelle (rouge) correspond à la trajectoire optimale (noir).*

types des trajectoires optimales. Puis, nous avons vérifié que les trajectoires optimales de ce problème correspondent aux trajectoires locomotrices. En conséquence, nous avons proposé une famille de trajectoires optimales que nous l'appelons *les mots de la marche humaine* où un mot correspond à un type de trajectoires optimales. Pour cela, nous avons développé des algorithmes numériques arrivant à capturer des singularités qui correspondent aux changements de stratégies observées chez les sujets. Cependant, les singularités du problème méritent une analyse beaucoup plus détaillée qui n'est pas développée dans ce travail. En plus, l'espace atteignable ne couvre toute l'espace $R^2 \times S^1$. En effet quand la configuration à atteindre est juste derrière le sujet, il vas effectuer certainement un mouvement vers l'arrière. Si la configuration est juste à côte du sujet, il vas effectuer certainement un mouvement du côte. Ces deux stratégies ne sont pas considéré dans nôtre modèle. Nous avons étudié ici juste la locomotion *normale* vers l'avant quand le but est défini devant la configuration initial.

References

ABEND, W.-K., BIZZI, E., AND MORASSO, P. 1982. Human arm trajectory formation. *Brain 105*, 331–348.

ARECHAVALETA, G., LAUMOND, J.-P., HICHEUR, H., AND BERTHOZ, A. 2006a. The nonholonomic nature of human locomotion : a modeling study. In *1st IEEE/RAS-EMBS Int. Conf. on Biomedical Robotics and Biomechatronics*. Pisa, Italy.

ARECHAVALETA, G., LAUMOND, J.-P., HICHEUR, H., AND BERTHOZ, A. 2006b. Optimizing principles underlying the shape of trajectories in goal oriented locomotion for humans. In *IEEE / RAS Int. Conf. on Humanoid Robots*. Genoa, Italy.

BALKCOM, D., KAVATHEKAR, P.-A., AND MASON, M. New York, July 16-18, 2006. Fastest trajectories for an omni-directional vehicle. *International Workshop on Algorithmic Foundations of Robotics*.

BALKCOM, D. AND MASON, M. 2002. Time optimal trajectories for bounded velocity differential drive vehicles. *International Journal of Robotics Research 21(3)*, 199–217.

BAYS, P.-M. AND WOLPERT, D.-M. 2007. Computational principles of sensorimotor control that minimize uncertainty and variability. *Journal of Physiology 578(2)*, 387–396.

BELLAICHE, A. AND RISLER, J.-J. 1996. *SubRiemannian Geometry*. Progress in Math. 144, Birkhauser, Basel.

BERNSTEIN, N.-I. 1967. *The Coordination and Regulation of Movements*. Pergamon Press.

BERTHOZ, A. 1997. *Le sens du mouvement*. Editions Odile Jacob.

BERTHOZ, A. AND VIAUD-DELMON, I. 1999. Multisensory integration in spatial orientation. *Current Opinion in Neurobiology 9*, 708–712.

BIZZI, E., HOGAN, N., MUSSA-IVALDI, F.-A., AND GISZTER, S. 1992. Does the nervous system use equilibrium-point control to guide single and multiple joint movements ? *Behavioral and Brain Sciences 15*, 603–613.

BOISSONNAT, J.-D., CEREZO, A., AND LEBLONG, J. 1992. Shortest paths of bounded curvature in the plane. In *IEEE Int. Conf. on Robotics and Automation*. Nice, France.

BOISSONNAT, J.-D., CEREZO, A., AND LEBLONG, J. 1994. A note on shortest paths in the plane subject to a constraint on the derivative of the curvature. *INRIA, Nice-Sophia-Antipolis, Research Report 2160*.

BOLTYANSKII, V.-G. 1966. Sufficient conditions for optimality and the justification of the dynamic programming method. *Journal Siam Control 4(2)*.

BONNARD, B. AND CHYBA, M. 2003. *Singular Trajectories and Their Role in Control Theory*. New York, Springer-Verlag.

BROCKETT, R.-W. 1976. Nonlinear systems and differential geometry. *Proceedings of the IEEE 64(1)*, 61–72.

BUI, X.-N., SOUÈRES, P., BOISSONNAT, J.-D., AND LAUMOND, J.-P. 1994. Shortest path synthesis for dubins nonholonomic robot. In *IEEE International Conference on Robotics and Automation*. San Diego, California.

BULLOCK, D. AND GROSSBERG, S. 1988. Neural dynamics of planned arm movements : emergent invariants and speed-accuracy properties during trajectory formation. *Psychological Review 95(1)*, 49–90.

CESARI, L. 1983. *Optimization, theory and applications*. Springer-Verlag.

CHATILA, R. 1995. Mobile robot natigation algorithms. In *Workshop in Algorithmic Foundations of Robotics*. San Francisco, California, 97–108.

CHOSET, H., LYNCH, K., HUTCHINSON, S., KANTOR, G., BURGARD, W., KAVRAK, L.-E., AND THRUN, S. 2005. *Principles of Robot Motion : Theory, Algorithms, and Implementations*. MIT Press, Boston.

DELINGETTE, M., HERBERT, M., AND IKEUCHI, K. 1991. Trajectory generation with curvature contraint based on energy minimization. In *IEEE Int. Workshop on Intell. Robots and Syst.*

DESMURGET, M. AND GRAFTON, S. 2000. Forward modeling allows feedback control for fast reaching movements. *Trends in Cognitive Sciences 4*, 423–431.

DUBINS, L.-E. 1957. On curves of minimal length with a constraint on average curvature and with prescribed initial and terminal positions and tangents. *American Journal of Mathematics 79*, 497–516.

ESTEVES, C., ARECHAVALETA, G., PETTRE, J., AND LAUMOND, J.-P. 2006. Animation planning for virtual character cooperation. *ACM Transactions on Graphics 25*.

FELDMAN, A.-G. AND LATASH, M.-A. 2005. Testing hypotheses and the advancement of science : recent attempts to falsify the equilibrium point hypothesis. *Experimental Brain Research 161(1)*, 91–103.

FERNANDES, C., GURVITS, L., AND LI, Z. 1994. Near-optimal nonholonomic motion planning for a system of coupled rigid bodies. *IEEE Transactions on Automatic Control 39(3)*, 450–463.

FINLEY, F.-R. AND CODY, K.-A. 1970. Locomotive characteristics of urban pedestrians. *Archives of Physical Medicine Rehabilitation 51(7)*, 423–426.

FITTS, P.-M. 1954. Journal exp. psychol. *The information capacity of the human motor system in controlling the amplitude of movements 47*, 381–391.

FLASH, T. AND HANDZEL, A.-A. 1996. Affine differential geometry of human arm trajectories. *Abstracts of the Society for Neuroscience (in press)*.

FLASH, T. AND HANDZEL, A.-A. 2007. Affine differential geometry analysis of human arm movements. *Biological Cybernetics 96*, 577–601.

FLASH, T. AND HOGAN, N. 1985. The coordination of arm movements : an experimentally confirmed mathematical model. *Journal of Neuroscience 5*, 1688–1703.

FLEURY, S., SOUERES, P., LAUMOND, J.-P., AND CHATILA, R. 1993. Primitives for snoothing mobile robot trajectories. In *IEEE Int. Conf. on Robotics and Automation*. 832–839.

GARCIA, A.-L. 1994. *Numerical Methods for Physics*. Prentice Hall.

GLASAUER, S., AMORIM, M.-A., VIAUD-DELMON, I., AND BERTHOZ, A. 2002. Differential effects of labyrinthine dysfunction on distance and direction during blindfolded walking of a triangular path. *Experimental Brain Research 145(4)*, 489–497.

GRASSO, R., GLASAUER, S., TAKEI, Y., AND BERTHOZ, A. 1996. The predictive brain : anticipatory control of head direction for the steering of locomotion. *Neuroreport 7(6)*, 1170–1174.

GRASSO, R., PREVOST, P., IVANENKO, Y.-P., AND BERTHOZ, A. 1998. Eye-head coordination for the steering of locomotion in humans : an anticipatory strategy. *Neuroscience Letters 253*, 115–118.

GRIBBLE, P.-L. AND OSTRY, D.-J. 1996. Origins of the power law relation between movement velocity and curvature : modeling the effects of muscle mechanics and limb dynamics. *Journal of Neurophysiology 76*, 2853–2860.

GRILLNER, S., KOZLOV, A., AND KOTALESKI, J.-H. 2005. Integrative neuroscience : linking levels of analyses. *Current Opinion in Neurobiology 15*, 614–621.

GUIGON, E., BARADUC, P., AND DESMURGET, M. 2007. Computational motor control : Redundancy and invariance. *Journal of Neurophysiology 97*, 331–347.

HAKEN, H., KELSO, J.-A.-S., AND BUNZ, H. 1985. A theoretical model of phase transitions in human hand movements. *Biological Cybernetics 51*, 347–356.

HARRIS, C.-M. AND WOLPERT, D.-M. 1998. Signal-dependent noise determines motor planning. *Nature 394*, 780–784.

HICHEUR, H. AND BERTHOZ, A. 2005. How do humans turn ? head and body movements for the steering of locomotion. In *IEEE / RAS Int. Conf. on Humanoid Robots*. Tsukuba, Japan.

HICHEUR, H., GLASAUER, S., VIEILLEDENT, S., AND BERTHOZ, A. 2005. *Head direction control during active locomotion in humans*. MIT Pres, Cambridge.

HICHEUR, H., PHAM, Q.-C., ARECHAVALETA, G., LAUMOND, J.-P., AND BERTHOZ, A. 2007. The formation of trajectories during goal-oriented locomotion in humans I. *In European Journal of Neuroscience 26*.

HICHEUR, H., VIEILLEDENT, S., RICHARDSON, M.-J.-E., FLASH, T., AND BERTHOZ, A. 2005. Velocity and curvature in human locomotion along complex curved paths : A comparison with hand movements. *Experimental Brain Research 162(2)*, 145–154.

HIRASAKI, E., MOORE, S.-T., RAPHAN, T.-R., AND COHEN, B. 1999. Effects of walking velocity on vertical head and body movements during locomotion. *Experimental Brain Research 127*, 117–130.

HIRIART-URRUTY, J.-B. AND LEMARÉCHAL, C. 1996. *Convex Analysis and Minimization Algorithms I.* Springer-Verlag.

HIRUKAWA, H., KAJITA, S., KANEHIRO, F., KANEKO, K., AND ISOZUMI, T. 2005. The human-size humanoid robot that can walk, lie down and get up. *The International Journal of Robotics Research 24(9)*, 755–769.

HOLLERBACH, J.-M. AND FLASH, T. 1982. Dynamic interactions between limb segments during planar arm movements. *Biological Cybernetics 44*, 67–77.

IMAI, T., MOORE, S.-T., AND RAPHAN, T. 2000. Interation of the body, head, and eyes during walking and turning. *Experimental Brain Reseach 136*, 1–18.

INMAN, V.-T., RALSTON, H.-J., AND TODD, F. 1981. *Human walking*. Williams & Wilkins, Baltimore.

JORDAN, M.-I. AND WOLPERT, D.-M. 1999. *Computational motor control*. Gazzaniga, (Ed.), MIT Press, Cambridge, MA.

KANAYAMA, Y. AND HARTMAN, B. 1989. Smooth local planning for autonomous vehicles. In *IEEE Int. Conf. on Robotics and Automation*.

KANAYAMA, Y. AND MIYAKE, N. 1986. Trajectory generation for mobile robots. In *Robotics Research 3*. Giralt G., and Faugeras O., MIT Press, Boston.

KAWATO, M., FURUKAWA, K., AND SUZUKI, R. 1987. A hierarchical neural-network model for control and learning of voluntary movement. *Biological Cybernetics 57(3)*, 169–185.

KELSO, J.-A.-S. 1997. *Dynamic Patterns : The Self-Organization of Brain and Behavior*. MIT Press, Cambridge.

KENNEDY, P.-M., CARLSEN, A.-N., INGLIS, J.-T., CHOW, R., FRANKS, I.-M., AND CHUA, R. 2003. Relative contributions of visual and vestibular information on the trajectory of human gait. *Experimental Brain Research 153*, 113–117.

KHATIB, O. 1987. A unified approach to motion and force control of robot manipulators : The operational space formulation. *IEEE Journal on Robotics and Automation 3(1)*, 43–53.

KOSTOV, V.-P. AND DEGTIARIOVA-KOSTOVA, E.-V. 1995. The planar motion with bounded derivative of the curvature and its suboptimal paths. *Acta Mathematica Universitatis Comeianae 64*, 185–226.

LACQUANITI, F., TERZUOLO, C., AND VIVIANI, P. 1983. The law relating the kinematic and figural aspects of drawing movements. *Acta Psychol. 54*, 115–130.

LAUMOND, J.-P., S., S. S., AND LAMIRAUX, F. 1998. *Robot Motion Planning and Control*. Lectures Notes in Control and Information Sciences 229, Springer, Chapter Guidelines in Nonholonomic Motion Planning for Mobile Robots.

LAVALLE, S.-M. 2006. *Planning Algorithms*. Cambridge University Press.

LI, Z. AND CANNY, J. 1993. *Nonholonomic Motion Planning*. Kluwer, Boston.

MORASSO, P. 1981. Spatial control of arm movements. *Experimental Brain Research 42*, 223–227.

MOYLAN, P. AND ANDERSON, B. 1973. Nonlinear regulator theory and an inverse optimal control problem. *IEEE Transactions on Automatic Control 18*, 460–465.

MULTON, F., FRANCE, L., CANI-GASCUEL, M.-P., AND DEBUNNE, G. 1999. Computer animation of human walking : a survey. *Journal of Visualization and Computer Animation 10*, 39–54.

MUSSA-IVALDI, F. AND BIZZI, E. 2000. Motor learning through the combination of primitives. *Philosophical Transactions of the Royal Society of London 355*, 1755–1769.

NAKAMURA, Y. 1991. *Advanced Robotics : Redundancy and Optimization*. Addison Wesley.

NELSON, W.-L. 1983. Physical principles for economies of skilled movements. *Biological Cybernetics 46*, 135–147.

NG, A. AND RUSSELL, S. 2000. Algorithms for inverse reinforcement learning. In *Proceedings of the 17th Int. Conf. on Machine Learning*. San Francisco.

NOCEDAL, J. AND WRIGHT, S.-J. 1999. *Numerical Optimization*. Springer-Verlag.

PAPAXANTHIS, C., POZZO, T., VINTER, A., AND GRISHIN, A. 1998. The representation of gravitational force during drawing movements of the arm. *Experimental Brain Research 120*, 233–242.

PECSVARADI, T. 1972. Optimal horizontal guidance law for aircraft in the terminal area. *IEEE Transactions on Automatic Control 17(6)*, 763–772.

PHAM, Q.-C., HICHEUR, H., ARECHAVALETA, G., LAUMOND, J.-P., AND BERTHOZ, A. 2007. The formation of trajectories during goal-oriented locomotion in humans II. *In European Journal of Neuroscience 26*.

POLLICK, F.-E. AND SAPIRO, G. 1997. Constant affine velocity predicts the 1/3 power law of planar motion perception and generation. *Vision Research 37*, 347–353.

PONTRYAGIN, L.-S., BOLTYANSKII, V.-G., GAMKRELIDZE, R.-V., AND MISHCHENKO, E.-F. 1964. *The Mathematical Theory of Optimal Processes*. Pergamon Press.

POZZO, T., BERTHOZ, A., AND LEFORT, L. 1990. Head stabilization during various tasks in humans. *Experimental Brain Reseach 82*, 97–106.

POZZO, T., LEVIK, Y., AND BERTHOZ, A. 1995. Head and trunck movements in the frontal plane during complex dynamic equilibrium tasks in humans. *Experimental Brain Reseach 106*, 327–338.

RAIBERT, M.-H. 1986. *Legged Robots That Balance*. MIT Press, Cambridge.

REEDS, J.-A. AND SHEPP, R.-A. 1990. Optimal paths for a car that goes both forward and backwards. *Pacific Journal of Mathematics 145 (2)*, 367–393.

RICHARDSON, M.-J.-E. AND FLASH, T. 2002. Comparing smooth arm movements with the two-thirds power law and the related segmented-control hypothesis. *Journal of Neuroscience 22(18)*, 8201–8211.

SASTRY, S.-S. AND MONTGOMERY, R. 1992. The structure of optimal controls for a steering problem. In *IFAC Workshop on Nonlinear Control*. 385–390.

SCHAAL, S. AND SCHWEIGHOFER, N. 2005. Computational motor control in humans and robots. *Current Opinion in Neurobiology 15*, 675–682.

SCHAAL, S. AND STERNAD, D. 2000. Origins ans violations of the 2/3 power law in rhythmic three-dimensional movements. *Experimental Brain Research 136*, 60–72.

SCHAAL, S., STERNAD, D., OSU, R., AND KAWATO, M. 2004. Rhythmic arm movement is not discret. *Nature Neuroscience 7*, 1136–1143.

SHIN, D. AND SINGH, S. 1990. Path generation for robot vehicles using composite clothoid segments. In *Technical Report CMU-RI-TR-90-31*. Robotics Institute, Carnegie Mellon University.

SICILIANO, B. AND SLOTINE, J.-J. 1991. A general framework for managing multiple tasks in highly redundant robotic systems. In *5th International Conference on Advanced Robotics*. Pisa, Italy.

SOECHTING, J.-F. AND FLANDERS, M. 1994. Moving in three-dimensional space : frames of reference, vectors and coordinate systems. *Annu. Rev. Neurosci. 15*, 167–191.

SOUÈRES, P. AND BOISSONNAT, J.-D. 1998. *Optimal Trajectories for Nonholonomic Mobile Robots, in Robot Motion Planning and Control*. Laumond J.P. (ed.) LNCIS 229, Springer.

SOUÈRES, P. AND LAUMOND, J.-P. 1996. Shortest path synthesis for a car-like robot. *IEEE Transanctions on Automatic Control 41(5)*, 672–688.

SUSSMANN, H.-J. 1990. *Nonlinear Controllability and Optimal Control*. Marcel Dekker, Inc., New York.

SUSSMANN, H.-J. AND TANG, W. 1991. Shortest paths for reeds-shepp car : a worked out example of the use of geometric techniques in nonlinear control. *Report SYCON-91-10, Rutgers University*.

SUSSMANN, H.-J. AND WILLEMS, J.-C. 1997. 300 years of optimal control : From the brachystochrone to the maximum principle. *IEEE Control Systems*.

TODOROV, E. 2004. Optimality principles in sensorimotor control. *Nature Neuroscience 7(9)*, 907–915.

TODOROV, E. AND JORDAN, M.-I. 1998. Smoothness maximization along a predefined path acccurately predicts the speed profile of complex arm movements. *Journal of Neurophysiology 80*, 696–714.

TODOROV, E. AND JORDAN, M.-I. 2002. Optimal feedback control as a theory of motor coordination. *Nature Neuroscience 5*, 1226–1235.

UNO, Y., KAWATO, M., AND SUZUKI, R. 1989. Formation and control of optimal trajectory in human multijoint arm movement : Minimum torque-change model. *Biological Cybernetics 61*, 89–101.

VARADARAJAN, V.-S. 1984. *Lie Groups, Lie Algebra and their Representations*. Springer-Verlag.

VIEILLEDENT, S., KERLIRZIN, Y., DALBERA, S., AND BERTHOZ, A. 2001. Relationship between velocity and curvature of a locomotor trajectory in human. *Neuroscience Letters 305*, 65–69.

VIVIANI, P. AND CENZATO, M. 1985. Segmentation and coupling in complex movements. *J. Exp. Psychol. Hum. Percept. Perform 6*, 828–845.

VIVIANI, P. AND FLASH, T. 1995. Minimun-jerk model, two-thirds power law, and isochrony : converging approaches to movement planning. *J. Exp. Psychol. Hum. Percept. Perform 21*, 32–53.

WATERS, R.-L., LUNSFORD, B.-R., PERRY, J., AND BYRD, R. 1988. Energy-speed relationship of walking : standard tables. *Journal of Orthopaedic Research 6*, 215–222.

WINTER, D.-A. 2004. *Biomechanics and Motor Control of Human Movement*. Wiley Press.

WISE, S.-P. AND SHADMEHR, R. 2002. *Motor Control*. Vol. 3. V.-S. Ramachandran, (Ed.), Academic Press, San Diego, CA.

WOLPERT, D.-M. 1995. An internal model for sensorimotor integration. *Sciences 269*, 1880–1882.

WOLPERT, D.-M. 1997. Computational approaches to motor control. *Trends in Cognitive Sciences 1*, 209–216.

WOLPERT, D.-M. AND GHAHRAMANI, Z. 2000. Computational principles of movement neuroscience. *Nature Neuroscience supplement 3*, 112–117.

YOSHIDA, E., BELOUSOV, I., ESTEVES, C., AND LAUMOND, J.-P. 2005. Humanoid motion planning for dynamic tasks. In *IEEE / RAS Int. Conf. on Humanoid Robots*. Tsukuba, Japan.

YOSHIKAWA, T. 1984. Analysis and control of robot manipulators with redundancy. In *1st. International Symposium of Robotics Research eds. M. Brady and R. Paul*. M. Brady and R. Paul Eds., MIT Press, Cambridge, 735–747.